

NAT'L INST. OF STAND & TECH



5

A11107 263811

A UNITED STATES
DEPARTMENT OF
COMMERCE
PUBLICATION



NBS SPECIAL PUBLICATION 353

NBS
PUBLICATIONS

The Menzel Symposium on Solar Physics, Atomic Spectra, and Gaseous Nebulae

U.S.
DEPARTMENT
OF
COMMERCE
National
Bureau
of
Standards

20-
100
157
353
1971
copy 2

OCT 6 1971

UNITED STATES DEPARTMENT OF COMMERCE • Maurice H. Stans, *Secretary*NATIONAL BUREAU OF STANDARDS • Lewis M. Branscomb, *Director*

The Menzel Symposium
on
Solar Physics, Atomic Spectra,
and
Gaseous Nebulae

in Honor of the Contributions
Made by Donald H. Menzel

Proceedings of a Symposium held
at the Harvard College Observatory,
Cambridge, Massachusetts
April 8-9, 1971

Edited by

Katharine B. Gebbie

Joint Institute for Laboratory Astrophysics
Institute for Basic Standards
National Bureau of Standards
Boulder, Colorado 80302



U.S. National Bureau of Standards Special Publication 353

Nat. Bur. Stand.(U.S.), Spec. Publ. 353, 213 pages (Aug. 1971)
CODEN: XNBSA

Issued August 1971

ABSTRACT

A symposium in honor of Donald H. Menzel's contributions to astrophysics was held on his 70th birthday at the Harvard College Observatory, Cambridge, Massachusetts, 8-9 April 1971. Menzel and his school have made distinguished contributions to the theory of atomic physics, solar physics, and gaseous nebulae. The work on planetary nebulae represented the first investigations of non-equilibrium thermodynamic conditions in astronomy; the solar work extended these investigations to stellar atmospheres. The applied atomic physics laid the basis for what we now call laboratory astrophysics and, together with work on non-equilibrium thermodynamics, inspired the founding of the Joint Institute for Laboratory Astrophysics. Menzel has served as a distinguished consultant to the National Bureau of Standards, and publication of this volume represents a grateful acknowledgment of his service to the Bureau. The papers summarize the current status of work in the three fields he pioneered.

Key words: atomic energy levels, transition probabilities, solar physics, gaseous nebulae, non-LTE thermodynamics.

THE MENZEL SYMPOSIUM
ON
SOLAR PHYSICS, ATOMIC SPECTRA
AND GASEOUS NEBULAE

CONTENTS

Preface	vii
Foreword	ix

PART I

ATOMIC ENERGY LEVELS AND TRANSITION PROBABILITIES 1

<i>W. R. S. Garton</i>	
Experimental Studies of Atomic Spectra and Transition Probabilities	3

<i>David Layzer</i>	
Towards an Elementary Theory of the Periodic Table	20

<i>Hugh P. Kelly</i>	
Many-body Calculations of Energies and Transition Probabilities	37

<i>Alexander Dalgarno</i>	
Radioactive Transitions in the Helium Isoelectronic Sequence	47

PART II

SOLAR ASTRONOMY 59

<i>John W. Evans</i>	
Solar Instrumentation (Part I)	61

<i>Richard B. Dunn</i>	
Solar Instrumentation (Part II)	71

<i>Richard N. Thomas and Katharine B. Gebbie</i>	
The Solar Chromosphere and the General Structure of a Stellar Atmosphere	84

<i>J. B. Zirker</i>	
The Corona	112

<i>George L. Withbroe</i>	
The Chemical Composition of the Photosphere and the Corona	127

	PART III	
	GASEOUS NEBULAE	149
<i>S. J. Czyzak and T. K. Krueger</i>	Optical Line Spectrum	151
<i>Lawrence H. Aller</i>	Chemical Composition of Typical Planetary Nebulae	161
<i>Leo Goldberg</i>	Radio Recombination Lines	169
<i>William Liller</i>	Internal Motions and Kinematics of Planetary Nebulae	182
<i>Donald H. Menzel</i>	Filamentary Structure of Planetary Nebulae	190

PREFACE

The papers in these proceedings were presented at a symposium in honor of Donald H. Menzel on the occasion of his 70th birthday at the Harvard College Observatory, Cambridge, Massachusetts, 8 and 9 April 1971. The symposium was supported in part by the National Science Foundation. The formal Organizing Committee was composed of Leo Goldberg, Lawrence Aller, David Layzer, and Richard Thomas. Robert O. Doyle of Harvard College Observatory did a great deal of organizational work and I wish to thank him and the secretarial staff of Harvard College Observatory, particularly Mrs. Nicki Vance.

To Alice Levine, my production editor, goes the entire credit and responsibility for supervising the production of these proceedings. Working with her is always a joy; for her professional competence and sustained good spirits I am deeply grateful. Judy Schlepp has not only prepared the typescript and assisted in the production but also attended to a myriad of details. Many authors will be grateful to her for the persistence with which she checked their references.

I am indebted to the publications office of the National Bureau of Standards, and in particular to W. R. Tilley and Betty L. Oberholtzer, for the publication of this volume.

Katharine B. Gebbie

July 1971
Boulder, Colorado



DONALD H. MENZEL

FOREWORD

Some two hundred friends and admirers of Professor Donald H. Menzel assembled at Harvard last April for a two-day symposium on progress in the interpretation of atomic spectra, in solar physics, and in the theory of gaseous nebulae, in recognition of Menzel's second retirement. He had retired once in 1966 as Director of Harvard College Observatory, a post he had held from 1954, and on this occasion was retiring from his position on the staff of the Smithsonian Astrophysical Observatory. This volume records the papers that were presented on this occasion.

A two-day symposium was necessarily inadequate even to touch on the many other interests that Menzel has followed in his life with competence and gusto and verve. Not covered was his emphasis on the study of solar-terrestrial relationships, in particular the way changing solar conditions manifest themselves in the terrestrial ionosphere, with consequent enormous changes in the conditions of long-distance radio wave propagation. Menzel was one of the first in this country to recognize the great importance of knowing about these effects in detail, and of organizing the observations in a way that would facilitate the making of predictions of radio communication links at all frequencies and over all paths. This subject was his principal occupation during his service as a naval officer during World War II.

At the end of the war he was a leader in the group that set up the Central Radio Propagation Laboratory in the National Bureau of Standards to provide this essential service for civilian and military communications. This happened during the period (1945-51) when I was Director of NBS, and it provided the opportunity for deepening a personal friendship that had begun in pre-war days in the study of atomic spectra. I am happy that this volume can be included in the NBS publications in recognition of Menzel's scientific and administrative contributions to the establishment of CRPL.

Another area of Menzel's interests that deserves mention is the serious effort he devoted to the study of "flying saucers" on which he wrote two books.* Here he devoted a great deal of effort to providing rational explanations, often in terms of little-known or poorly

understood phenomena of atmospheric optics, for many of the reports which the true believers were uncritically accepting in support of their fantasies about the Earth's being visited by spacecraft from other civilizations. This brought about another happy period (1966-69) of collaboration between us, when he served as a consultant on the U. S. Air Force sponsored project, of which I was Director. This project led to the preparation of *Scientific Study of Unidentified Flying Objects*.†

Menzel was born in Florence, Colorado and raised in Leadville, one of the great mining camps of the Rockies; he still has strong roots here. It was he who introduced me to this area in 1949, on a momentous visit that led to the choice of Boulder as the location for the NBS laboratories for the study of radio propagation.

E. U. Condon

July 1971
Boulder, Colorado

*Donald H. Menzel, *Flying Saucers* (Cambridge, Mass.: Harvard University Press), 1953; and Donald H. Menzel and Lyle G. Boyd, *The World of Flying Saucers* (New York: Doubleday), 1963.

†(New York: Bantam, Dutton) 1969.

portrait of professor D. H. M., as a distinguished martian scholar, on his way from the moon.



J.C. Pecker

ATOMIC ENERGY LEVELS AND TRANSITION PROBABILITIES

*Chairman: David Layzer
Harvard College Observatory*

There are many paths to astronomy,
and I probably followed the most
violent one of all.

Donald H. Menzel

EXPERIMENTAL STUDIES OF ATOMIC SPECTRA
AND TRANSITION PROBABILITIES

W. R. S. Garton

*Imperial College of Science
and Technology, London*

Some special sentiments may be expected from a contributor to the Menzel Symposium who happens to be based at Imperial College, London, because of the long relation between that institution and the centre of astrophysical excellence at Harvard College Observatory. This reflection relates to the close community of interest and a good deal of collaboration and correspondence that occurred years ago between two pioneers in the field of astrophysics: E. C. Pickering - Dr. Menzel's predecessor but one (1877-1919) as Director at Harvard College Observatory - and his counterpart in what ultimately became Imperial College, Sir Norman Lockyer. The closely related activities of these two pioneer investigators can be illustrated by quoting the opening words from the celebrated paper of Saha (1921), written about the time he was working in Imperial College with Lockyer's successor, Alfred Fowler: "The present paper embodies an attempt towards a physical explanation of the ordered gradation in the spectra of stars -- a subject in which pioneering work was done by the late Sir Norman Lockyer, but which was worked up with systematic thoroughness at the Harvard College Observatory, under the lead of the late Professor E. C. Pickering and Miss A. J. Cannon." This historical background gives, understandably, an added flavor to the satisfaction within both institutes that the connections have now been powerfully renewed. From about 1960 there have been close collaborative efforts founded on observational work by rocket- and satellite-borne instrumentation and supporting laboratory astrophysics at Harvard, and on research, mainly on vacuum-ultraviolet and soft X-ray spectra, at the Imperial College Laboratory. A recent spectacular success of this cooperation - in this case involving also the Astrophysics Research Unit, Culham, and the Centre for

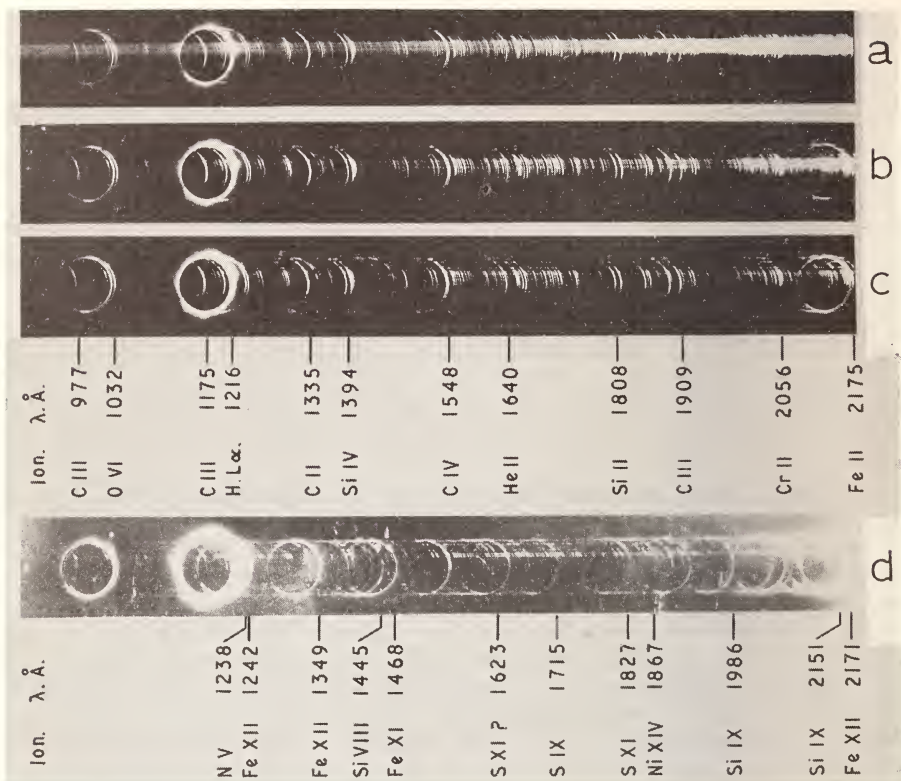


Figure 1. Flash and coronal spectra at the March 7, 1970 solar eclipse: (a) before second contact; (b) and (c) near second contact; (d) at totality.

Research in Experimental Space Science at York University, Toronto - has been the set of spectra of chromosphere and corona in the vacuum ultraviolet, obtained with a rocket-borne spectrograph at Wallops Island during the total eclipse in March 1970 (Speer et al. 1970). A time sequence of fifty stigmatic spectra from before and through totality were registered in the region 850 - 2100 Å; Figure 1 shows sample spectra at several phases of the eclipse. Photometric reduction of the spectra, now completed on the excellent densitometer at Harvard, has produced a wealth of material for interpretation by solar physicists.

The concern of the Menzel Symposium and the present volume is to pay tribute to the significant work done over a period of nearly fifty years, roughly half a century after the pioneering days of Pickering and Lockyer. Menzel's scientific contributions began in

the mid-1920's, when he was among those exploiting the advances in atomic physics of the second and third decades of the twentieth century, which generated the quantum formulation of the structure and mechanics of atoms and molecules. An early comprehensive paper (Menzel 1931), "A Study of the Solar Chromosphere", sets out and applies the theory of spectral line formation and radiative transfer. This contribution inevitably depended on speculative estimates of most of the atomic parameters involved, e.g. f-values of astrophysically important lines of other than H-like ions, line-broadening parameters, and photoionization cross sections of cosmically abundant metals. Because of the decline in laboratory and theoretical work in atomic physics, which began in the early 1930's, Menzel's work on the chromosphere would have had little advantage twenty years later. Such neglect of richly rewarding fields terminated in the 1950's with the emergence of space astrophysics, aeronomy, and plasma physics. The present article sketches some of the results from this period in laboratory astrophysics. This short article deals with a narrow selection of material, much of which is drawn from work done in the author's laboratory or in collaboration with associated institutions, notably the Harvard Observatory, the Argonne National Laboratory, the National Bureau of Standards, and York University, Toronto.

A great deal has been accomplished towards a systematic determination of atomic and molecular f-values and the associated problems of reliable diagnostic methods for the measurement of temperature and particle densities in astrophysical and/or laboratory plasmas. Important and continuing programs were started in the early 1950's by Lochte-Holtgreven (1958) and Maecker (1951, 1955) in Kiel, based on development of several forms of stabilized arc discharge. The many significant experiments in laboratory astrophysics that emerged from this program have been continued in the capable hands of Wiese (1970a,b), at the National Bureau of Standards, on oscillator strengths, and of Griem (1964, 1968), at Maryland, more particularly towards elucidating the mechanisms of spectral line broadening. In the latter field, recent useful contributions have been made by Cooper (1969) at Boulder and by D. D. Burgess (1970, 1971) at Imperial College and Harvard. In spite of strenuous efforts by theorists, a unified explanation of line broadening, valid for both wings and line centers, has yet to be formulated. For many years we have relied on the statistical (micro-field) approach to account for the details of line

wings and on the impact approximation for the line centers. It is hardly surprising that the intermediate region, where neither approach is fully satisfactory and where effects of the correlated motions of the perturbers are most significant, is of the greatest interest to astronomers. Another area, not yet seriously explored, concerns the effects of the cooperation of plasma waves, separated by the plasma frequency or an harmonic or two (Baranger and Mozer 1961). These can be responsible for strongly oscillating electric fields and hence for the production of satellites to spectral lines. Burgess and collaborators (unpublished) have recently observed lines in C IV that are probably satellites such as these; these results are illustrated in Figure 2. It is interesting to speculate on the presence of such satellites in the spectra of flares or of the solar transition layer. Mention should also be made of recent (unpublished) experiments by D. D. Burgess in collaboration with Parkinson and Reeves at Harvard; the object is to study spectral line broadening in cosmically important light elements and metal

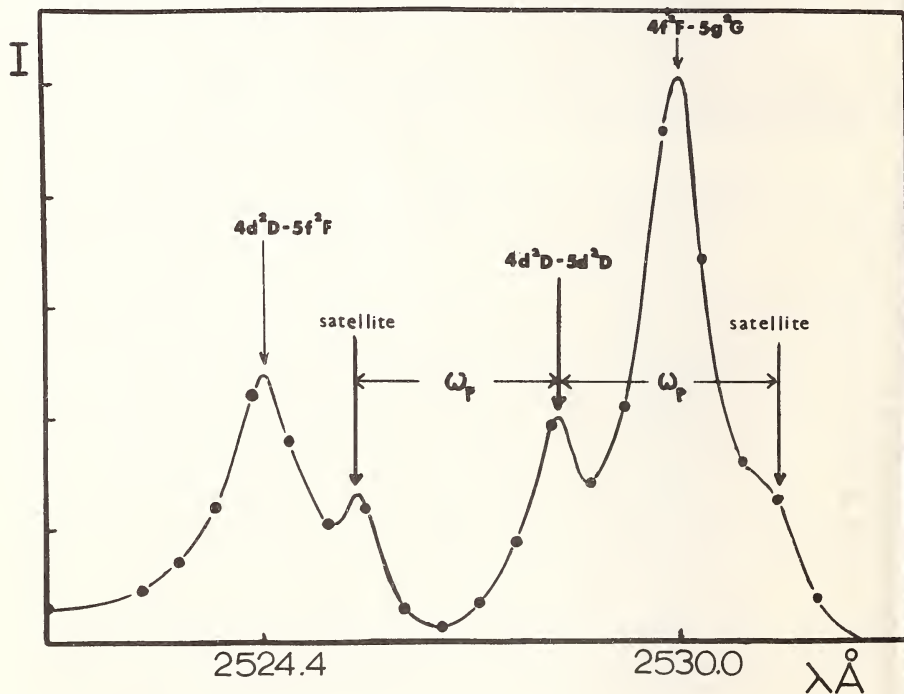


Figure 2. Plasma-wave-induced satellite features in C IV.

atoms in atmospheres of hot but neutral atomic hydrogen. The experiments use a large "piston-compressor" tube, in which hydrogen can be heated adiabatically and dissociated - but only slightly ionized - at pressures and temperatures comparable with those in the upper photosphere; line broadening in the spectra of chosen additives can be investigated. The first successful results (Burgess and Grindley 1970) concerned the broadening of the Na-D line in atmospheres of neutral helium, and current experiments aim at substituting hydrogen for helium.

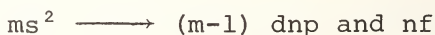
Work on the determination of atomic f-values of astrophysically important transitions is currently in progress by Huber, Parkinson, and Reeves at Harvard. They have applied both equivalent width techniques and measurements of anomalous dispersion ("hook method") to plasmas produced in shock tubes. Until the start of the Harvard experiments, use of the "hook method" was confined almost entirely to the group under Penkin (1964) in Leningrad. This valuable Russian work, which has been in progress for many years, has been restricted chiefly to measurements of f-values of transitions involving the ground state or low excitation states of an atom. The Harvard work has included a wider wavelength range towards the ultraviolet and has extended the technique, by means of shock tubes, to transitions between fairly highly excited states and to ionic species. Examples of some important results are to be found in Huber and Tobey (1968) and Grasdalen et al. (1969) on Fe I and II, Cr I and II, and in Garton et al. (1964) on an autoionizing doublet of Al I near 1930 Å. The special significance of this Al I doublet for solar physics has been emphasized by Goldberg (1966) and by Withbroe (1966).

The Harvard laboratory program has determined molecular f-values - for example, the vibrational transition probabilities of the CO fourth positive system - by measurement of equivalent widths (Rich 1968). At Imperial College, application of the hook method (Anketell and Pery-Thorne 1967; Pery-Thorne and Banfield 1970) has yielded improved f-values for ultraviolet bands of the important radicals OH and NO. At York University, Toronto, a variety of emission and absorption techniques have been applied (e.g. Nicholls 1969; Drake et al. 1967) including the hook method, for many molecules of astrophysical and/or aeronomical significance.

Space allows only passing mention of the large and important programs to measure lifetimes of excited states by means of the relatively new "beam-foil"

method, which is proving prolific in yielding f-values for many transitions in spectra of medium and very high stages of ionization (see Bashkin 1968).

Only during the last twenty years has much progress been made towards the experimental determination and theoretical calculation of photoionization cross sections (Marr 1967; Samson 1966). These are important in many fields of astrophysics, including stellar atmospheres, interstellar material, and the field covered by Menzel and his collaborators in their magnificent compilation "Physical Processes in Gaseous Nebulae". The unhappy position of the astronomer for many years in this respect is illustrated by the photoionization cross section of Ca I: early quantal calculations yielded a cross section at threshold that proved fifty times too high when the first experimental determination was reported by Ditchburn and Hudson (1960). The error lay in the dramatic effects of the autoionization of doubly-excited states on photoionization continua. Though this process was first recognized by Shenstone (1931) and Majorana (1931) and was extensively illustrated by the work of Beutler in the 1930's (see Boyce 1941), the recognition of its astrophysical relevance came rather later; see, for instance Goldberg (1966). Laboratory work of the last ten years has shown that double-electron and/or inner-shell excitation in all of the alkaline-earth and alkali first spectra produce drastic effects on the shapes of the corresponding ionization continua somewhere in the ultraviolet. Thus the Schumann region and short-wavelength part of the quartz-ultraviolet contain important extensions of the spectra Ca I, Sr I and Ba I (Garton and Codling 1965, 1968; Garton and Tomkins 1969). These spectra arise by transitions of the type



and yield a confused series of autoionization resonances, which converge on the metastable 2D levels of the corresponding ions. In addition to the work of Ditchburn and Hudson (1960) on Ca I, measurements of the strongly fluctuating photoionization continua of Sr I and Ba I have been reported by Hudson et al. (1969, 1970).

The universal importance of the autoionization process on all but H-like atomic spectra is nicely illustrated by the fine work of Madden, Codling, and Ederer who, using the NBS 180 MeV electron-synchrotron

as a background light source for absorption spectroscopy, have reported on new absorption spectra of all the inert gases in the short-wavelength part of the vacuum ultraviolet. For example, in He I, in the region around 200 Å, several Rydberg series of double-electron transitions were found superposed upon the photoionization continua shortwards of the first limit at 504 Å (Madden and Codling 1965; Madden 1966). The peculiar line-profiles often exhibited by a transition involving an autoionizing upper state were first seen by Beutler (1935) and shortly afterwards explained by Fano. Much later, Fano (1961) developed this theoretical approach into a quantitative parameterization, which has subsequently been further developed (Fano and Cooper 1965; Comes and Sälzer 1966; Shore 1967) and has proved of great use to the experimenter faced with interpreting atomic and molecular absorption spectra. The type of line profile concerned is shown in Figure 3, which represents photometric measurements of an absorption line of Tl I ($6s^2 6p^2 P_{1/2}^0 - 6s 6p^2 P_{3/2}$); the line is very reasonably characterized by the Fano parameters r (the resonance half-width) and q (the "line-profile index"). The example of Figure 3 concerns an isolated autoionization resonance. A few years ago at Harvard, a more ambitious attempt was made (Garton et al. 1968), which involved the unfolding of a whole group of overlapping and mutually interfering autoionization resonances; the results are displayed in Figure 4, where the full line represents the theoretical unfolding of the course of the photoionization cross section, and the plotted points are observational. A similar analysis for the Ca I structures has been performed by Newsom and Shore (1968).

In addition to the likely relevance of autoionization processes in several astrophysical situations (Goldberg 1966) and related problems concerning the inverse process of "dielectronic recombination" (A. Burgess 1966), there exists the interesting, though little explored, possibility of "forced autoionization". Evidence was given by Garton et al. (1962), that a doubly-excited atomic energy level, which normally lies below the first ionization potential, can be stimulated into autoionization through the effects of microfields of charged particles present in a plasma. The evidence came from a comparison of the absorption spectra of Ca I obtained respectively with a furnace and a shock tube. The interpretation provided in that paper is not entirely certain although the occurrence of the forced autoionization process has been established without doubt by beautiful experiments of Feldman and Novick

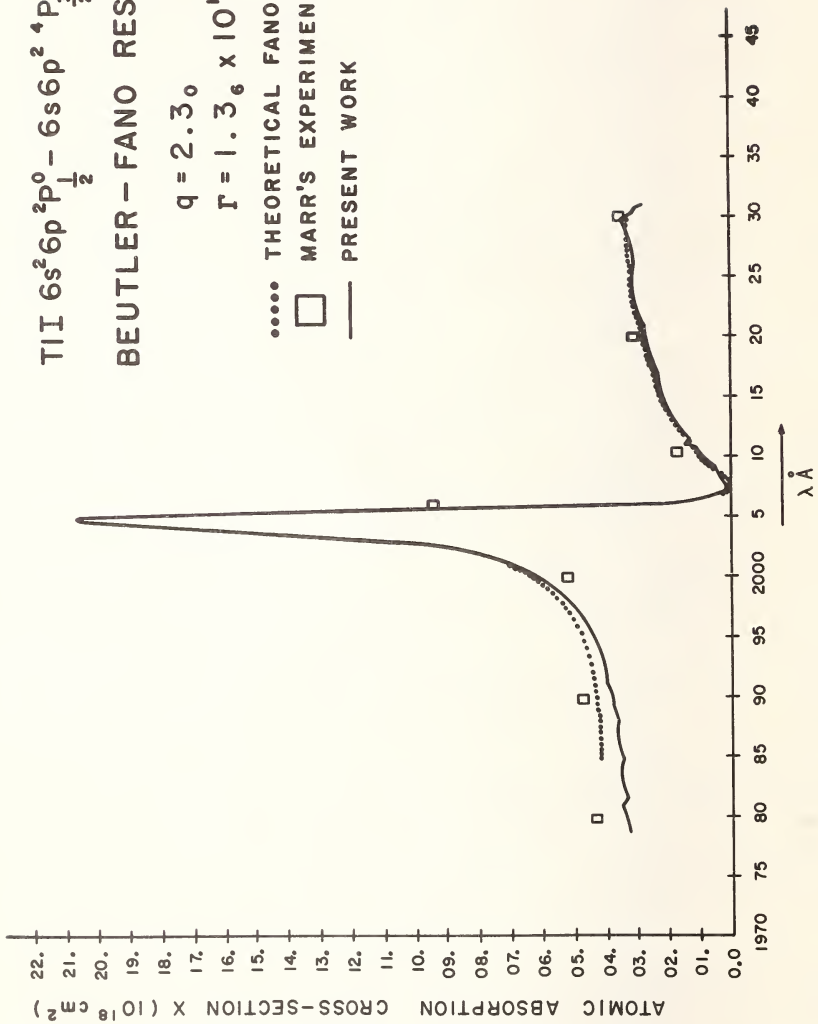
TII $6s^2 6p^2 p^0 - 6s 6p^2 \ ^4P_{3/2}$

BEUTLER - FANO RESONANCE λ 2005 Å

$q = 2.30$

$\Gamma = 1.36 \times 10^{12} \text{ sec}^{-1}$

- THEORETICAL FANO PROFILE
- MARR'S EXPERIMENTAL POINTS
- PRESENT WORK



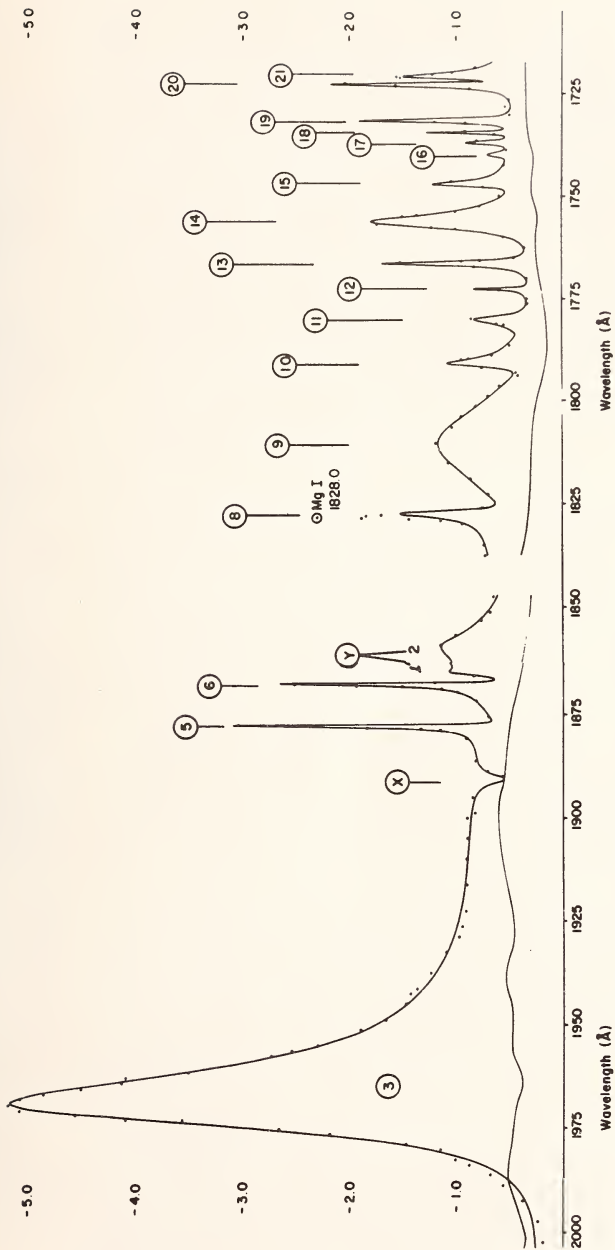


Figure 4. Relative photoabsorption cross section in Sr I continua and superposed autoionization resonances.

(1967), in which beams of doubly-excited alkali atoms, metastable towards both radiation and autoionization processes, were observed to autoionize in the presence of a small electric field. This problem of forced autoionization is closely connected with the still thorny problems of the microfield depression of ionization potentials and the termination of the partition function of a hot gas, both of great significance to the astronomer.

Although the Schumann and near ultraviolet spectra of the alkaline earths exhibit moderately complicated effects of configuration mixing between the doubly-excited series lines themselves and with the underlying continua, the spectra of these elements and those of the alkalis show much greater complexity at even shorter wavelengths, due to excitation of the first underlying p-shells. Connerade (1970a,b) and Mansfield (see Garton et al. 1969, Connerade et al. 1971) have studied the absorption spectra of elements Na through Cs in the range 200-900 Å. Pioneer experiments by Beutler in the 1930's indicated some structures in Rb and Cs due to excitation of the $4p^6$ and $5p^6$ subshells respectively, but work at the Imperial College in the last few years has proved that these studies certainly needed revision. The complicated nature of the absorption spectra of this group of elements is illustrated in Figure 5. The prime reason for the complexity in the spectra of K I, Rb I and Cs I is the severe configuration mixing now known to occur amongst the low levels of the corresponding ions; thus, in Rb II the levels of $4p^5 5s$ and $4p^5 4d$ have overlapping structures. Consequently, whereas Beutler imagined, reasonably enough, that the spectra were arising from transitions of the type



and thus would be expected to converge on the four limits of $(m-1) p^5 ms$, the configuration mixing increases to twelve the number of available limits on which the Rydberg absorption series of the neutral atom converge.

The p-shell absorption spectra of the alkaline earths, Mg I through Ba I, have been photographed by Newsom in the range 100-700 Å and exhibit features of increasing complexity with rising Z . Two of the spectra (Mg I and Ba I) are reproduced in Figure 6. The only completed analysis to date refers to Mg (Newsom

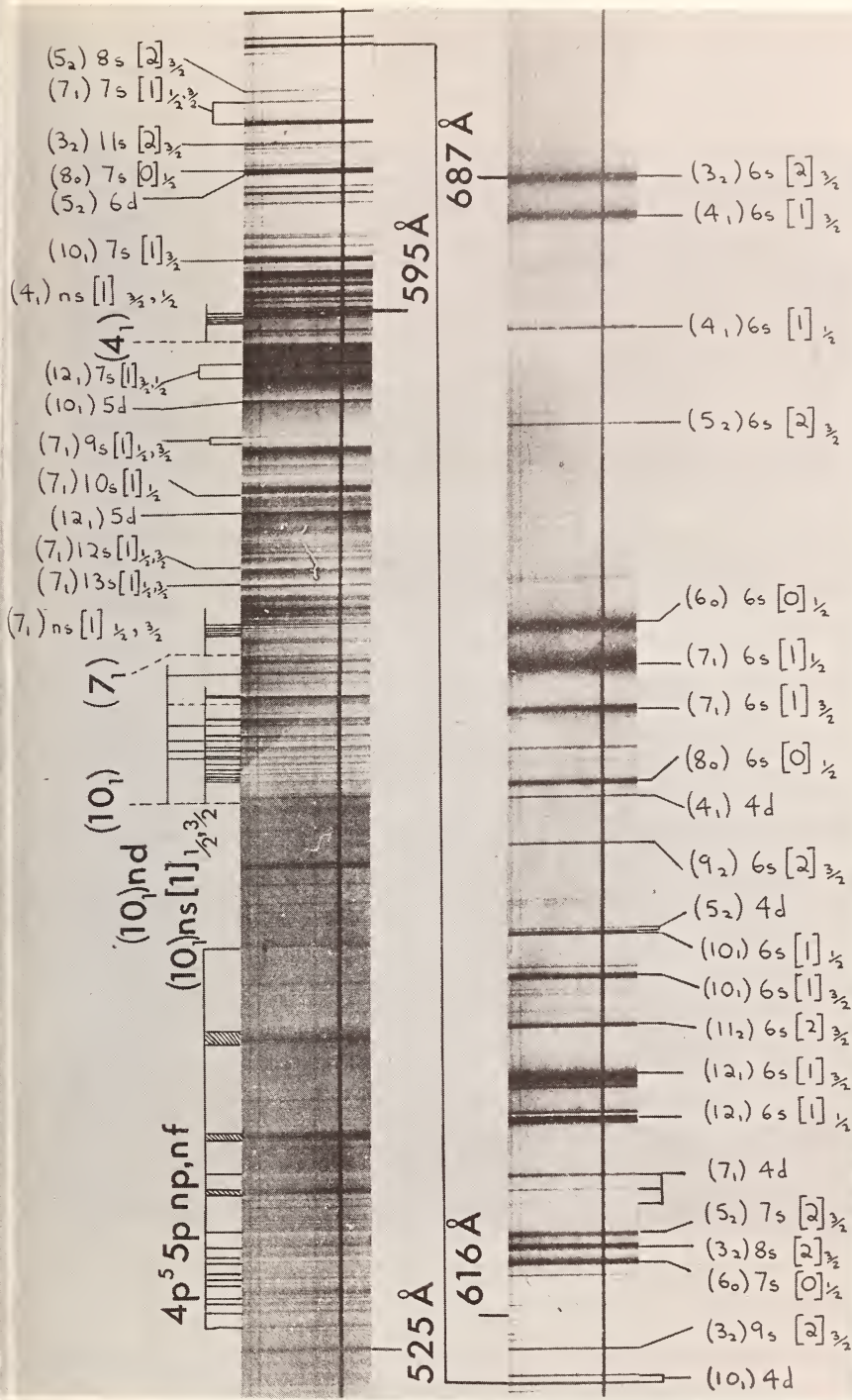


Figure 5. Rb I absorption spectrum due to 4p-shell excitation.

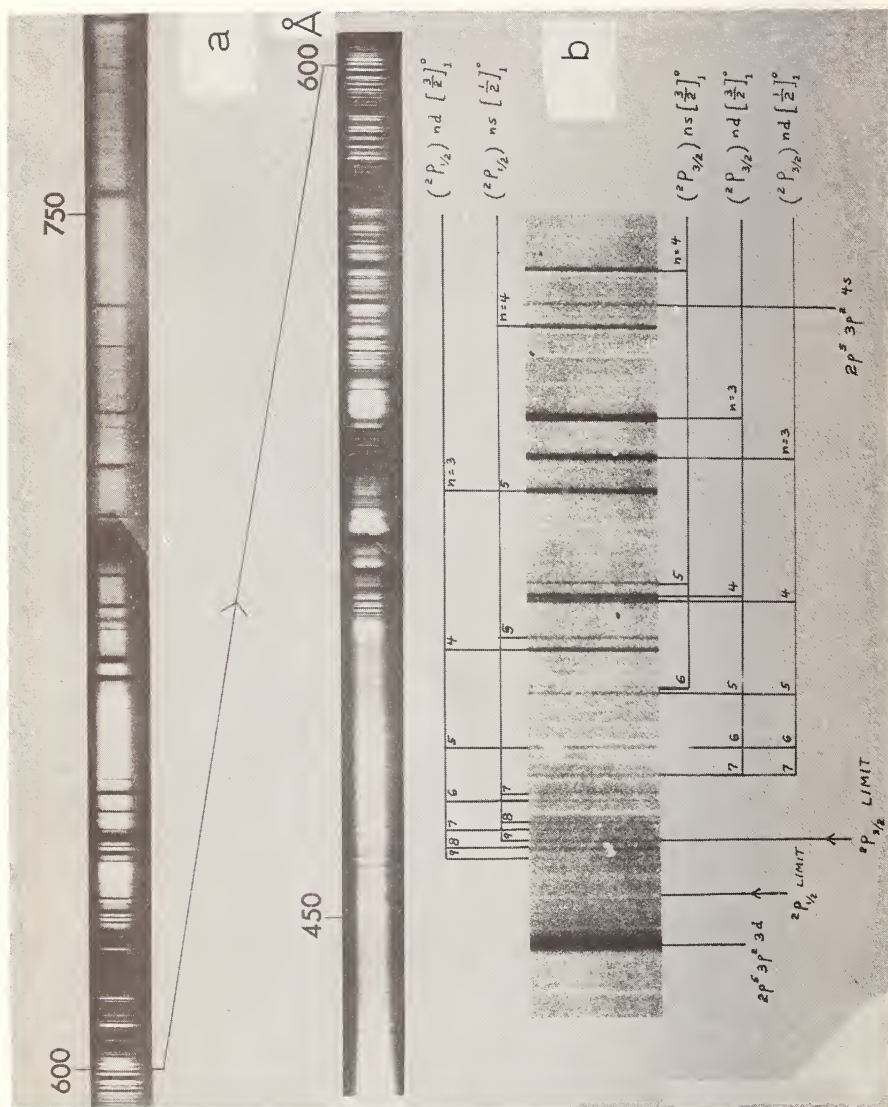


Figure 6. Absorption spectra due to excitation of the

1971) which, though showing the simplest structure of this group of spectra, also contains some surprising features; for instance, the strongest transition of the Mg I spectrum of Figure 6a occurs to the short-wavelength side of both the $2p^5 3s^2$ limits and is tentatively classified, on energetic grounds, as arising from a three-electron transition to the upper state $2p^5 3p^2 3d$.

Much interpretive work remains to be done on all these inner-shell spectra of the alkalis and alkaline earths. It will be obvious from some of the spectra shown in the plates accompanying this article that the "raw data" expected of the experimenter must now include photometric records of the violently fluctuating ionization continua; information restricted to photographic records and analyses of transitions and Rydberg series becomes increasingly inadequate for purposes of theoretical interpretation. The absorption spectrum of Be I, which has been photographed and analyzed by Mehlman-Balloffet and Esteva (1969), is particularly interesting, and the need for photometric data is emphasized, because, rather unusually, theoretical calculation of autoionization resonances and half-widths has been made ahead of the experiment by Altick (1968). The Be I absorption spectrum produces a particular experimental challenge on account of the extreme chemical reactivity of the metal and vapor, and it may be expected that a technique originated by Nelson and Kuebler (1962) and previously mentioned by Garton (1966) under the name "flash pyrolysis" may be useful. This experimental technique has recently been used with great success at Argonne and Harvard by Tondello (1971) in obtaining the absorption spectrum of S I; the spectrum observed contains long absorption series in the range 900-1300 Å, including important autoionization structures. This new spectrum of S I is of obvious astrophysical importance, and, as in the case of Be I, the experiment has the added attraction that possibilities of comparison with theoretical predictions (Conneely et al. 1970) already exist.

Another area of experiment for which the "flash pyrolysis" technique appears promising is in the observation of the absorption spectra of ions. To date, to the author's knowledge, the only observation of an extensive absorption spectrum of this sort is that of La II. This was obtained a few years ago at Harvard, by use of improved shock-tube techniques (Parkinson, Reeves and Grasdalen, unpublished). By careful manipulation of the shock conditions, a spectrum was obtained almost entirely of La II, with La I present only very

weakly. Unfortunately the region between 900 and 1200 Å, in which strong autoionization structure is anticipated, was only poorly obtained because of the use of lithium fluoride optics. The case of La II has a particular interest because the La^+ and La^{++} ions have very different electronic structures from the iso-electronic species Ba and Ba^+ respectively.

Through cooperative work between Argonne, Harvard, and Imperial College (unpublished), some striking new spectra have also been obtained on the absorption spectra of the IIIb elements, Sc and Y. Not surprisingly, the spectra of these elements, which immediately follow the alkaline earths in the periodic table, show greatly increased complexity, as a result of the addition of a d electron in each case. Some features of the new spectra, each of which contains many hundreds of new lines and several hundred identifiable new levels, some falling in a number of series, are shown in Figure 7. The identification of series in these spectra for the first time has enabled reliable values of ionization potentials to be obtained; thus, in Y I the previously listed value of the first ionization potential (Moore 1952) proved to be 2500 cm^{-1} in error. In addition to the need for photometric work on these spectra, analysis of the multitude of lines longward of the first limit requires examination of Zeeman effects. These two spectra are so crowded towards their first ionization potentials that progress was only possible through the use of the fine National Bureau of Standards 10-meter vacuum spectrograph, made available to the Argonne, Harvard and Imperial College workers for a week early in 1970.

REFERENCES

- Altick, P.L. 1968, *Phys. Rev.*, 169, 21.
Anketell, J. and Pery-Thorne, A. 1967, *Proc. Roy. Soc.*, A301, 343.
Baranger, M. and Mozer, B. 1961, *Phys. Rev.*, 123, 25.
Bashkin, S. 1968, *Beam Foil Spectroscopy*, 1, 3 (London: Gordon & Breach).
Beutler, H. 1935, *Z. f. Physik*, 93, 177.
Boyce, J.C. 1941, *Rev. Mod. Phys.*, 13, 1.
Burgess, A. 1966 in *Autoionization*, ed. A. Temkin (Baltimore: Mono Book Corp.), p. 25.

RYDBERG SERIES OF AUTOIONIZATION RESONANCES IN Y⁺ ABSORPTION SPECTRUM
(40 FOOT SPECTROGRAPH)

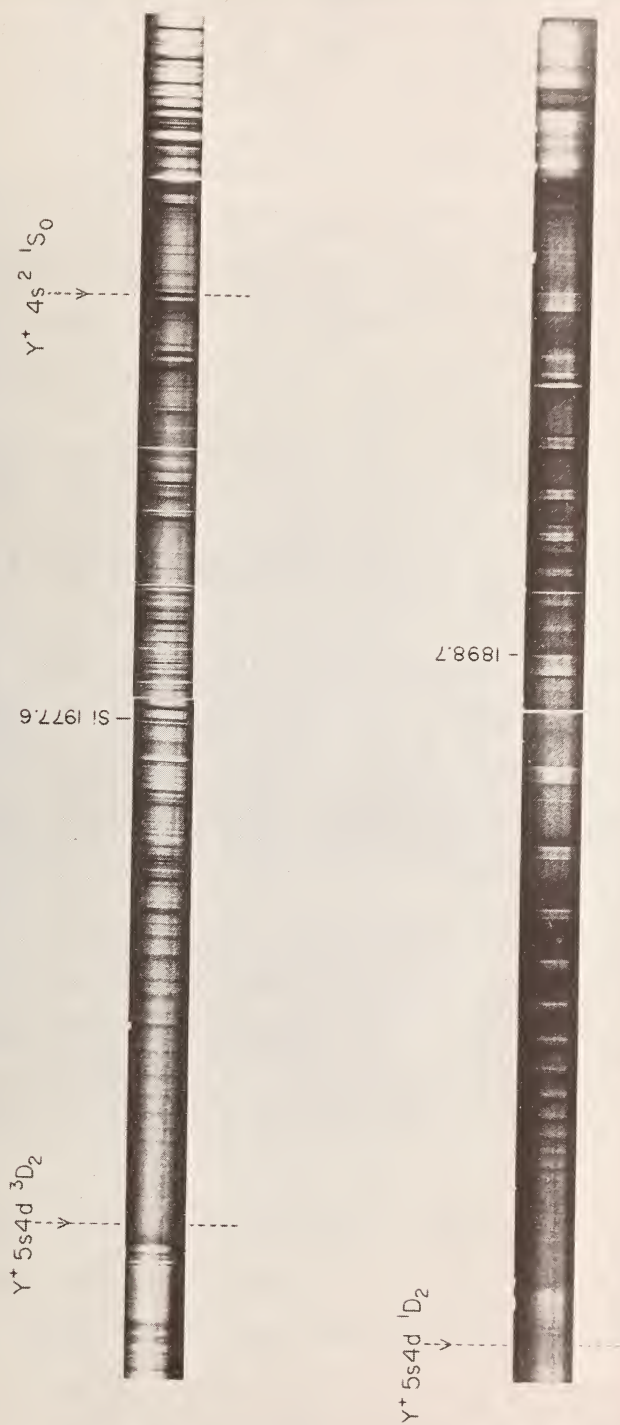


Figure 7.

- Burgess, D.D. and Grindley, J.E. 1970, *Ap. J.*, 160, 343.
- Burgess, D.D. 1970, *J. Phys. B*, 3, L67, L70.
- Burgess, D.D. 1971, *J. Phys. B*, 4, L7.
- Comes, F.J. and Sälzer, H.G. 1966, *Phys. Rev.*, 152, 29.
- Conneely, M.J., Smith, K. and Lipsky, L. 1970, *J. Phys. B*, 3, 493.
- Connerade, J.P. 1970a, *Ap. J.*, 159, 685.
- Connerade, J.P. 1970b, *Ap. J.*, 159, 695.
- Connerade, J.P., Garton, W.R.S., and Mansfield, M.W.D. 1971, *Ap. J.*, 165, 203.
- Cooper, J. 1969, *Lectures in Theoretical Physics XI-C* (New York: Gordon & Breach).
- Ditchburn, R.W. and Hudson, R.D. 1960, *Proc. Roy. Soc.*, A256, 53.
- Drake, G.W.F., Tyte, D.C. and Nicholls, R.W. 1967, *J. Q.S.R.T.*, 7, 639.
- Fano, U. 1961, *Phys. Rev.*, 137, A1364.
- Fano, U. and Cooper, J.W. 1965, *Phys. Rev.*, 137, A1364.
- Feldman P. and Novick, R. 1967, *Phys. Rev.*, 160, 143.
- Garton, W.R.S., Parkinson, W.H. and Reeves, E.M. 1962, *Proc. Roy. Soc.*, 80, 860.
- Garton, W.R.S., Parkinson, W.H. and Reeves, E.M. 1964, *Ap. J.*, 140, 1269.
- Garton, W.R.S. and Codling, K. 1965, *Proc. Roy. Soc.*, 86, 1067.
- Garton, W.R.S. and Codling, K. 1968, *J. Phys. B*, 1, 106.
- Garton, W.R.S. 1966, *Advances in Atomic and Molecular Physics*, Vol. 2 (New York: Academic Press), p. 121.
- Garton, W.R.S., Grasdalen, G.L., Parkinson, W.H. and Reeves, E.M. 1968, *J. Phys. B*, 1, 114.
- Garton, W.R.S., Connerade, J.P., Mansfield, M.W.D. and Wheaton, J.E.G. 1969, *Appl. Opt.*, 8, 919.
- Garton, W.R.S. and Tomkins, F.S. 1969, *Ap. J.*, 158, 1219.
- Goldberg, L. 1966, in *Autoionization*, ed. A. Temkin (Baltimore: Mono Book Corp.), p. 1.
- Grasdalen, G.L., Huber, M. and Parkinson, W.H. 1969, *Ap. J.*, 156, 1153.
- Griem, H.R. 1964, *Plasma Spectroscopy* (New York: McGraw-Hill).
- Griem, H.R. 1968, *Proceedings of the International Conference on Optical and Atomic Line Shape*, Warsaw (Warsaw: Pantswowe Wydawnictwo Nankowe), p. 331.
- Huber, M. and Tobey, F.L. 1968, *Ap. J.*, 152, 609.
- Hudson, R.D., Carter, V.L. and Young, P.A. 1969, *Phys. Rev.*, 180, 77.
- Hudson, R.D., Carter, V.L. and Young, P.A. 1970, *Phys. Rev.*, A2, 643.
- Lochte-Holtgreven, W. 1958, *Rep. Prog. Phys.*, 21, 312.

- Madden, R.P. and Codling, K. 1965, *Ap. J.*, 141, 364.
- Madden, R.P. 1966, in *Autoionization*, ed. A. Temkin (Baltimore: Mono Book Corp.), p. 129.
- Maecker, J. 1951, *Z. f. Physik*, 129, 108.
- Maecker, J. 1955, *Z. f. Physik*, 141, 198.
- Majorana, Q. 1931, *N. Cim.* (ser 8), 8, 107.
- Marr, G.V. 1967, *Photoionization in Gases* (New York: Academic Press).
- Mehlman-Balloffet, G. and Esteva, J.M. 1969, *Ap. J.*, 157, 945.
- Menzel, D.H. 1931, *Pub. Lick Obs.*, 17, 1.
- Moore, C.E. 1952, *Atomic Energy Levels*, Vol. 2, National Bureau of Standards Circ. No. 467 (Washington, D.C.: U.S. Government Printing Office).
- Nelson, L.S. and Kuebler, N.A. 1962, *J. Chem. Phys.*, 37, 47.
- Newsom, G.H. and Shore, B.W. 1968, *J. Phys. B*, 1, 742.
- Newsom, G.H. 1971, *Ap. J.* (in press).
- Nicholls, R.W. 1969, *Can. J. Chem.*, 47, 1847.
- Penkin, N.P. 1964, *J.Q.S.R.T.*, 4, 41.
- Pery-Thorne, A. and Banfield, F.P. 1970, *J. Phys. B*, 3, 1011.
- Rich, J.C. 1968, *Ap. J.*, 153, 327.
- Saha, M.N. 1921, *Proc. Roy. Soc.*, A99, 135.
- Samson, J.A.R. 1966, *Advances in Atomic and Molecular Physics*, Vol. 2, ed. D.R. Bates (New York: Academic Press), p. 178.
- Shenstone, A.G. 1931, *Phys. Rev.*, 38, 873.
- Shore, B.W. 1967, *Rev. Mod. Phys.*, 39, 439.
- Speer, R.J., Garton, W.R.S., Goldberg, L., Parkinson, W.H., Reeves, E.M., Morgan, F.J., Nicholls, R.W., Jones, T.J.L., Paxton, H.J.B. and Wilson, R. 1970, *Nature*, 226, 249.
- Tondello, G. 1971, *Ap. J.* (in press).
- Wiese, W.L. 1970a, *Bibliography on Atomic Transition Probabilities*, National Bureau of Standards Special Pub. No. 320 (Washington, D.C.: U.S. Government Printing Office).
- Wiese, W.L. 1970b, *Nuclear Instrum. and Methods*, 90, 25.
- Withbroe, G.L. 1966, *Ap. J.*, 146, 294.

TOWARDS AN ELEMENTARY THEORY OF THE
PERIODIC TABLE

David Layzer

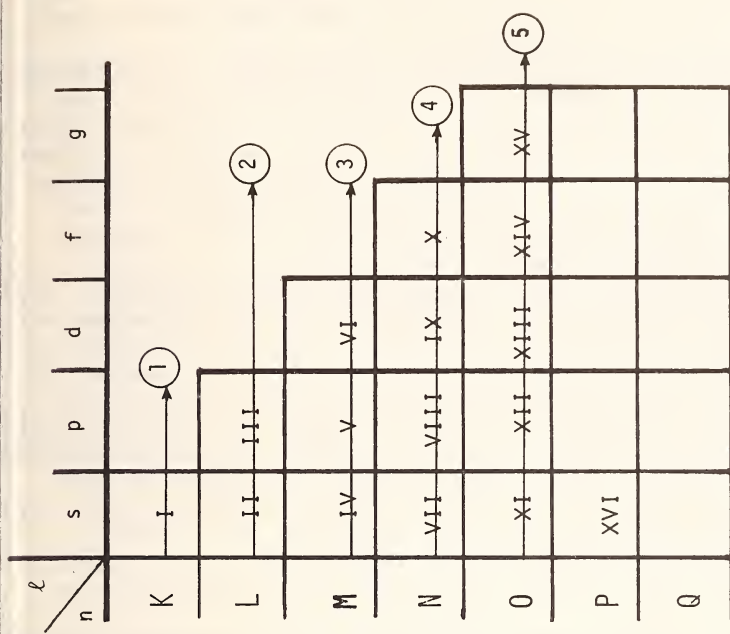
Harvard College Observatory

The motivation of my talk has been well expressed, in another context, by Wigner and Seitz (1955):

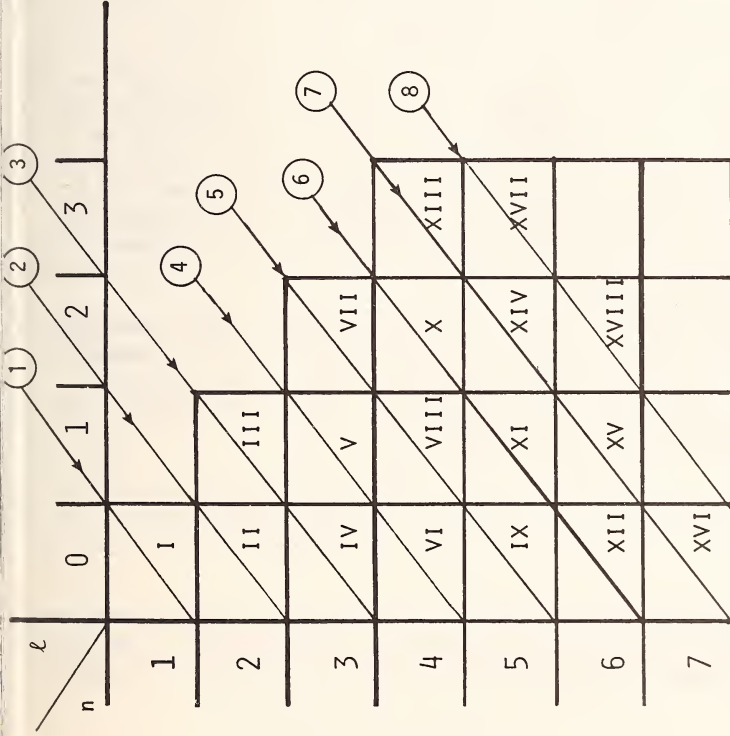
If one had a great calculating machine, one might apply it to the problem of solving the Schroedinger equation for each metal and obtain thereby the interesting physical quantities, such as the cohesive energy, the lattice constant, and similar parameters. It is not clear, however, that a great deal would be gained by this. Presumably the results would agree with the experimentally determined quantities and nothing vastly new would be learned from the calculation. It would be preferable instead to have a vivid picture of the behavior of the wavefunctions, a simple description of the essence of the factors which determine cohesion and an understanding of the origins of variation in properties from metal to metal.

The purpose of this talk is to outline an explanation of the kind favored by Wigner and Seitz for the well-known regularities that characterize the periodic table of chemical elements.

These are illustrated in Figure 1, which shows two idealized versions of the periodic table. In each figure a box represents a subshell consisting of orbitals with given values of n and ℓ . For highly ionized atoms the order in which successive subshells are added is that shown on the right. Each shell, labeled by a fixed value of n , is completed before a shell with the next higher value of n is begun, and subshells, characterized by fixed values of n and ℓ , are added in order



$Z \rightarrow \infty$



$Z = N$

Figure 1. Two idealized forms of the periodic table.

of increasing ℓ . In short, the order of adding subshells is (n, ℓ) -lexicographic.

For neutral atoms, on the other hand, a different rule applies. As was first pointed out by Bohr, the order in which subshells are added is determined first by the value of $n + \ell$ and then by the value of ℓ ; that is, it is $(n + \ell, \ell)$ -lexicographic. This rule is illustrated in the diagram on the left in Figure 1. Subshells are added along the diagonals in the diagram, from upper right to lower left.

Both diagrams are, of course, idealizations. Especially among the heavier elements, the building-up process does not take place in such a regular fashion. Most of the departures from the simple order shown in Figure 1 reflect the dependence of energy levels on quantum numbers other than those characterizing the subshells. For example, it may be energetically favorable to add an orbital out of the order indicated in the appropriate diagram if the resulting spectroscopic term has high multiplicity (a high value of S). Such effects are reasonably well understood, at the qualitative level, and I shall not discuss them further in this talk.

What is the theoretical basis for the regularities illustrated in Figure 1? I remember asking Donald Menzel this question during my first meeting with him. I knew nothing of atomic physics at the time - I had not even heard of the Bohr atom. But instead of sending me off to read a book, Donald sat down with me and covered the whole subject, from Bohr's theory of the hydrogen atom to intermediate coupling in complex atoms in a single afternoon. One of the questions I remember asking concerned the regularities illustrated in Figure 1. Donald's reply, that no adequate answer had yet been given, convinced me that atomic physics was still a live subject, in which more remained to be done than routine calculations.

Let me begin with the regularities that pertain to the sequence of highly ionized atoms ($Z \gg N$), because these are the easier to explain. The energy levels E of an isolated atom can be expressed as functions of nuclear charge Z in the form

$$E = E_0 Z^2 + E_1 Z + E_2 + E_{\text{rel}} + O(Z^{-1}) . \quad (1)$$

In practice the term $O(Z^{-1})$ is usually negligibly small when the degree of ionization ($Z - N$) exceeds 3 or 4. The remaining terms in this formula can all be calcu-

lated. Let me remind you briefly of the nature of these calculations.

(1) E_0 . The coefficient of Z^2 is given, in atomic units, by the hydrogenic formula

$$E_0 = -\sum \frac{1}{2n^2} , \quad (2)$$

the summation extending over all occupied orbitals.

(2) E_1 . This coefficient can be evaluated with arbitrary precision by elementary calculations involving only hydrogenic wavefunctions. It was first calculated for atoms in the first row of the periodic table by Layzer (1959), and these calculations were later extended to more complex atoms by Godfredsen (1963, 1966). The coefficient has the following structure:

$$E_1 = \sum q_{\alpha\beta} [\alpha, \beta] + \Delta E_1 , \quad (3)$$

where $\alpha \equiv n\ell$, $\beta \equiv n'\ell'$, and the summation extends over all $N(N-1)/2$ pairs of electrons. The quantity $[\alpha, \beta]$ is a two-electron interaction energy. As the notation indicates, it depends only on the two orbitals in question and not on the electron configuration or spectroscopic term. The quantity ΔE_1 is responsible for the first-order splitting of a configuration into spectroscopic terms. Its value for a particular spectroscopic term depends in general not only on the interaction of electrons within a given configuration but also on interactions connecting different configurations characterized by the same set of principal quantum numbers (and the same parity). [The interconfigurational contribution to ΔE_1 is responsible for the well-known systematic deviations between predictions based upon the central-field approximation and experiment (Layzer 1959)].

(3) E_2 . The evaluation of this coefficient presents a substantially more difficult mathematical problem than the preceding one, but in principle E_2 can also be evaluated with arbitrary accuracy. The basic theoretical considerations are set forth by Layzer, Horak, Lewis, and Thompson (1964), where it is shown that E_2 can be split up into two terms,

$$E_2 = E_2' + E_2'' . \quad (4)$$

The one-electron part E_2' can be evaluated by means of a finite calculation - most conveniently, using double perturbation theory (Dalgarno and Stewart 1958; Layzer et al. 1964). The evaluation of the two-electron part E_2'' can be reduced to a series of two-electron problems from the solutions of which the value of E_2'' for any N-electron atom can be evaluated in a systematic way.

(4) E_{rel} . This term represents the relativistic contribution to the energy of a many-electron atom. Dirac's relativistic theory of the hydrogen atom and Breit's relativistic theory of two-electron atoms form the theoretical basis for evaluating this term. The Z-dependent many-electron theory was given by Layzer and Bachall (1962) and applied by them to configurations consisting of s electrons. Holly Doyle (1968, 1969) carried out complete calculations of E_{rel} for atoms in the first row of the periodic table. Though extremely intricate, these calculations are exact, and they are based entirely on Dirac one-electron wavefunctions. Snyder (1969, 1970, 1971) has developed a simple but surprisingly accurate approximation method for extending these results to heavier atoms.

From this summary it is clear that all regularities pertaining to highly ionized atoms are *quantitatively* predictable through calculations using hydrogenic wavefunctions. In particular, the rule illustrated by the right-hand diagram in Figure 1 reflects the properties of the coefficients E_0 and E_1 . The ordering of subshells within a shell according to increasing values of ℓ follows from the explicit calculations of E_1 referred to above. By appealing to formula (3), which shows how E_1 is built up from two-electron interactions, one can push the explanation back a step. The average value of E_1 for a given configuration is determined mainly by the sum of two-electron contributions $[\alpha, \beta]$ and depends very little on the term ΔE_1 . Thus one can base an explanation of the regularity on the properties of standard interaction integrals involving hydrogenic wavefunctions.

Turning now to the neutral atoms, we must consider the term $O(Z^{-1}) \equiv E'$. If this term were negligible for neutral atoms, as it is for highly ionized atoms, the periodic table would have the same structure in the two cases. (This statement is based on calculations of E_1 and estimates of E_2 derived from experimental data on term energies in isoelectronic sequences.) Thus the behavior of E' is instrumental in causing the transition from (n, ℓ) -lexicographic ordering $Z \gg N$ to $(n+\ell, \ell)$ -lexicographic ordering as $Z \rightarrow N$.

For a given value of N and sufficiently high val-

es of Z , the term E' has a convergent expansion in powers of Z^{-1} , the leading term in the expansion being proportional to Z^{-1} . By subtracting the theoretically known quadratic and linear terms in Z from experimentally determined term energies in an isoelectronic sequence, we can examine the behavior of E' for $Z \approx N$. (For this purpose we can neglect the relativistic contribution E_{rel} .) One finds that in general it is not possible to represent E' accurately in the vicinity of $Z = N$ by the two leading terms in its Taylor expansion. The data suggest, in fact, that the series expansion breaks down at a value of Z somewhat greater than N in general. That is, E' is not in general analytic in the neighborhood of $Z = N$. Thus the simple Z -expansion theory does not afford an adequate theoretical basis for discussing the transition between the two idealized forms of the periodic table.

Nevertheless, we can gain considerable insight into this problem by very simple theoretical means. I have mentioned that E_1 and E_{rel} can be evaluated by calculations that involve only hydrogenic wavefunctions. In principle one can also evaluate E_2 directly from second-order perturbation theory, using hydrogenic wavefunctions, though in practice other methods are usually preferable (see Layzer et al. 1964). To evaluate E' we go one step further and introduce *screened* hydrogenic wavefunctions $P_{n\ell}^H(Z-s_{n\ell}, r)$, where the screening parameter $s_{n\ell}$ is a function of Z . We regard the screening parameters as variational parameters, to be determined in the usual way from the variation principle. The resulting theory is purely algebraic. It is also physically transparent, in the sense that the mathematical results can be readily translated into physical language.

Before discussing some of the results of variational screening calculations, I must call your attention to one technical point. Screened hydrogenic wavefunctions belonging to the same value of ℓ but different values of n are not orthogonal unless they are also characterized by the same screening parameter. It is this circumstance that has discouraged people from making calculations for complex atoms on such wavefunctions, since the standard formulae for matrix elements connecting many-electron states depend on the assumption that radial wavefunctions belonging to the same value of ℓ but different values of n are mutually orthogonal. If one does not make this assumption, the formulae become exceedingly complicated. We can, however, use nonorthogonal radial functions in the standard formulae and treat the effects of nonorthogonality

as corrections. Fortunately, these corrections often turn out to be small. Moreover, it is not prohibitively difficult to estimate them in a first approximation (see below). A discussion of their physical significance is given by Layzer (1959).

Neglecting the effects of nonorthogonality, one obtains the following formula for the energy levels in terms of the screening parameters:

$$E = \sum_m c_m^2 \left\{ \sum_{\alpha} - \frac{q_{\alpha} (Z - s_{\alpha})^2}{2n_{\alpha}^2} \right\}. \quad (5)$$

Here m denotes a configuration and the sum over m runs over all configurations belonging to a given complex (set of configurations characterized by a given set of principal quantum numbers and a given parity); q_{α} denotes the number of electrons occupying orbitals of the type α in the configuration m . The screening parameter s_{α} depends on the configuration m as well as on the type of orbital. Finally, the screening parameters that figure in this formula are solutions of the variational problem.

Formula (5) is identical, except for the sum over m , with Moseley's well-known semi-empirical formula for X-ray term energies. (The sum over configurations in complex is a necessary feature of the formula. It ensures that the linear term, as well as the quadratic term, in the Z -expansion of E is given correctly.) Each electron contributes "hydrogenically" to the term energy according to its screened nuclear charge. Now, we know, from much more refined calculations that the electric field seen by an electron in a complex atom differs substantially from a screened Coulomb field, and that accurate variational wavefunctions - for example, Hartree-Fock wavefunctions - depart markedly from the hydrogenic form. One might therefore expect formula (5) to provide a rather crude approximation to observed term energies in many-electron atoms.

Some representative comparisons between theory and experiments are shown in Figures 2 to 5. Figure 2 shows, in addition, the effects of the correction for nonorthogonality of the radial wavefunctions for a case where this correction is exceptionally large.

One sees from these comparisons (in which the known quadratic and linear contributions to the energy have been subtracted) that most of the discrepancy between the observed and calculated energies comes from

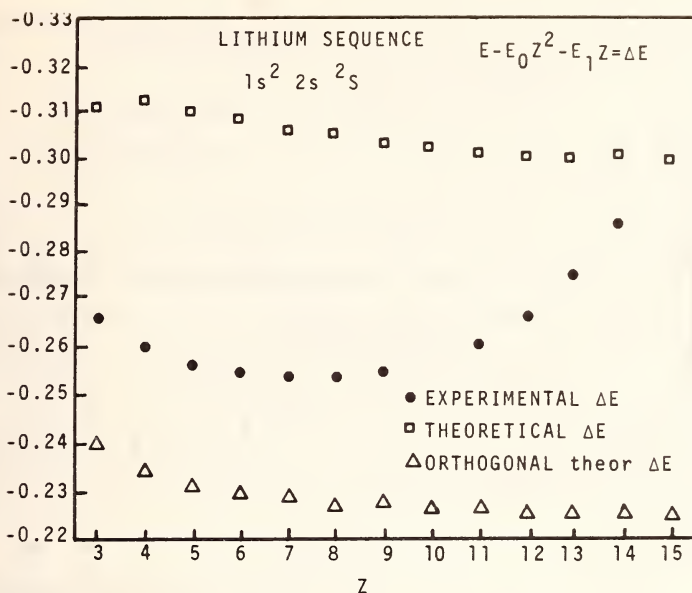


Figure 2. Illustrating the effects of nonorthogonality on variational screening calculations of the energy. These effects have been included in the calculations indicated by triangles and omitted in those indicated by squares. (From David Layzer, 1967, *International Journal of Quantum Chemistry*, Symposium No. 1, p. 45.)

the constant term E_2 and, at large values of Z , from the relativistic contribution. The nonanalytic variation of E' for $Z \approx N$, which is our main concern in the present discussion, is predicted with surprising accuracy by the variational screening theory - even in an atom as heavy as titanium.

It appears, therefore, that the nonanalytic behavior of E' results in large measure from the one-electron contribution to E' , and indeed from the part of that contribution associated with the screening of the nuclear Coulomb field.

To illustrate the connection between nonanalyticity and screening, consider the well-known phenomenon illustrated by the variational screening calculations shown in Figure 6. Plotted are the variational screening parameters s_{3d} and s_{4s} in the configurations $-3p^5 3d$ and $-3p^5 4s$, respectively, as functions of Z along the argon isoelectronic sequence. For values of $Z < 20.4$, the 3d electron is screened almost completely by the other electrons (the variational calculations can be

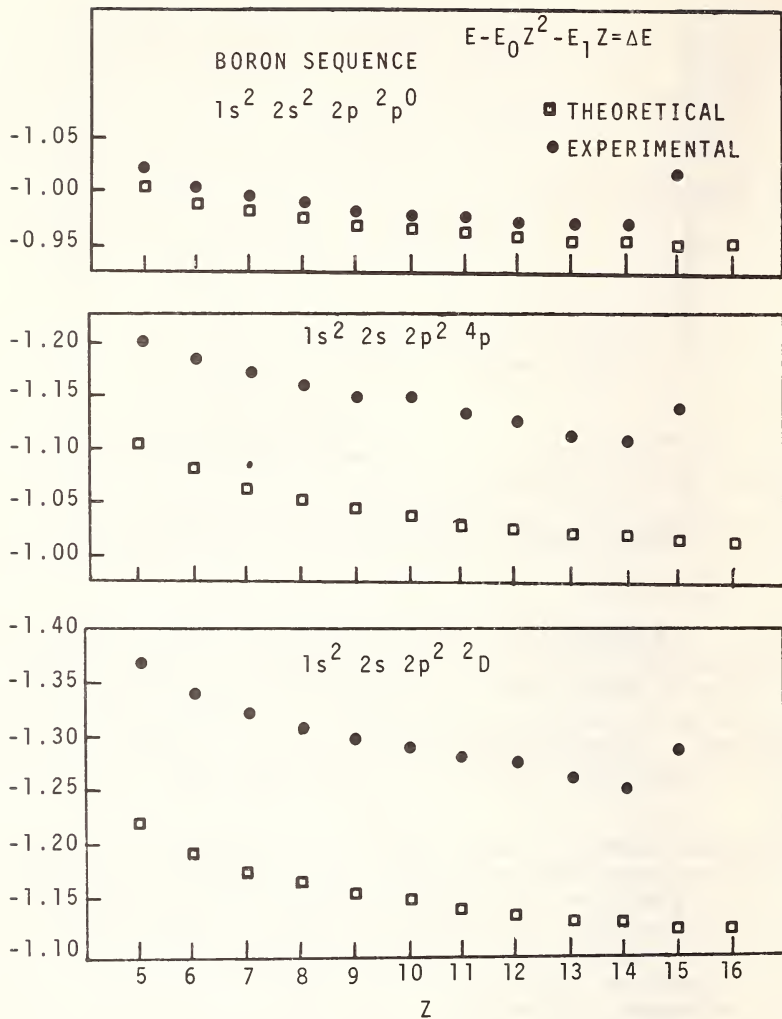


Figure 3. Predicted and observed ionization energies in the boron isoelectronic sequence. The predicted energies are given by the variational screening approximation with no allowance for the effects of nonorthogonality between radial wave functions belonging to the same value of l . Energy contributions proportional to Z^2 and Z have been subtracted from both theoretical and experimental energies. The increasing differences between the experimental and theoretical points at large values of Z reflect relativistic contributions to the energy.

(Figures 3, 4, and 5 are from David Layzer, 1967, *International Journal of Quantum Chemistry*, Symposium No. 1, p. 45.)

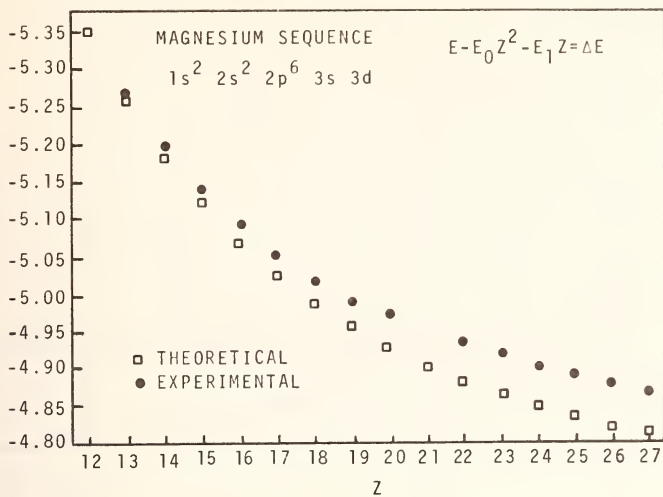


Figure 4.

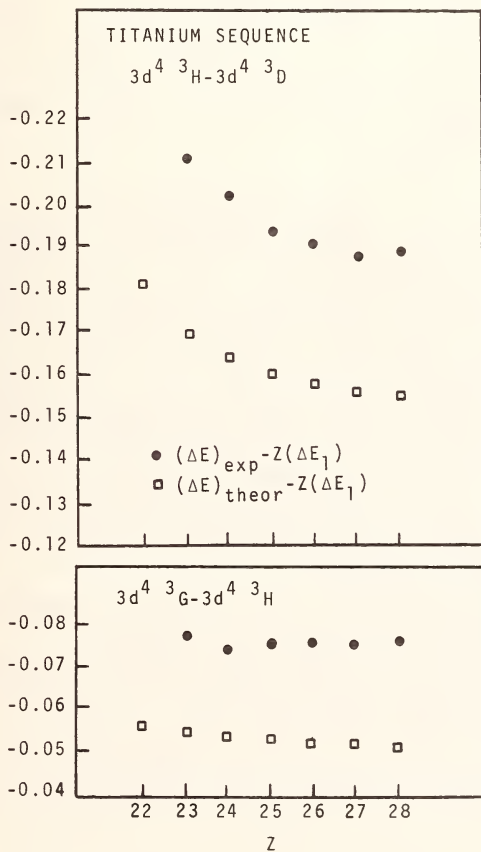


Figure 5.

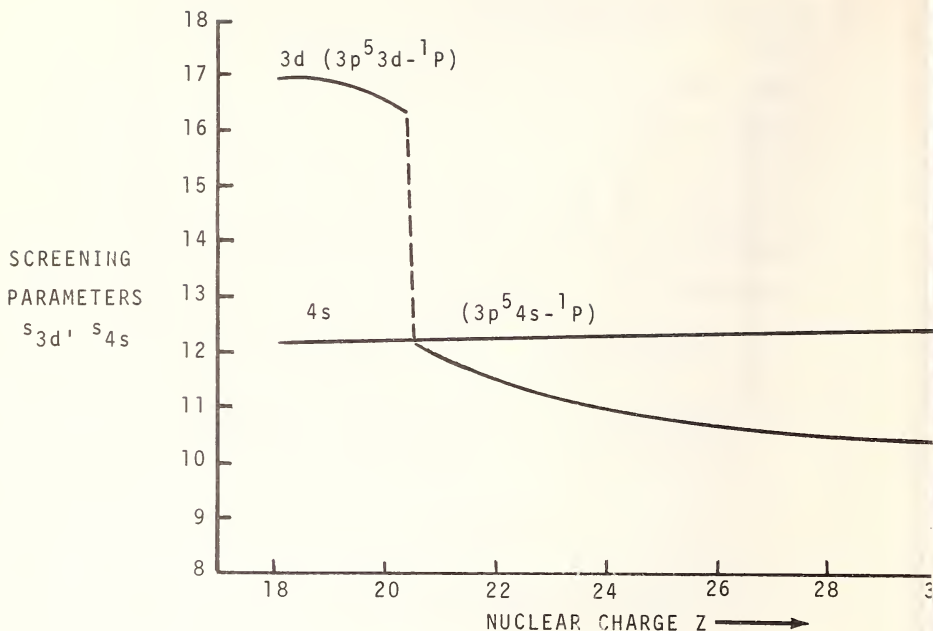


Figure 6. Screening parameters: argon isoelectronic sequence ($N = 18$).

carried out for arbitrary nonintegral values of Z). Around $Z = 20.4$, s_{3d} changes abruptly, increasing by about 33% in an interval $\Delta Z \approx 0.2$. Thereafter s_{3d} remains practically constant. Figure 7 shows how the contribution to s_{3d} from various subshells varies with Z along the isoelectronic sequence, and Figure 8 illustrates the variation with Z of mean nuclear distance of the 3d and 4s electrons. In the configuration $-3p^5 4s$, on the other hand, the screening parameter for the 4s electron varies smoothly over the entire range of Z ; see Figure 6. From formula (5) we see at once that for values of $Z < 20.4$, a 4s electron is more tightly bound than a 3d electron, while for $Z \geq 21$ the 3d electron is the more tightly bound.

Similar results for the calcium isoelectronic sequence are shown in Figures 9 and 10.

The nonanalytic character of the variational 3d screening parameter results from the form of the variational equations for the s_α :

$$s_\alpha = F_\alpha(x_\beta), \quad x_\beta = \frac{Z - s_\beta}{Z - s_\alpha}, \quad (6)$$

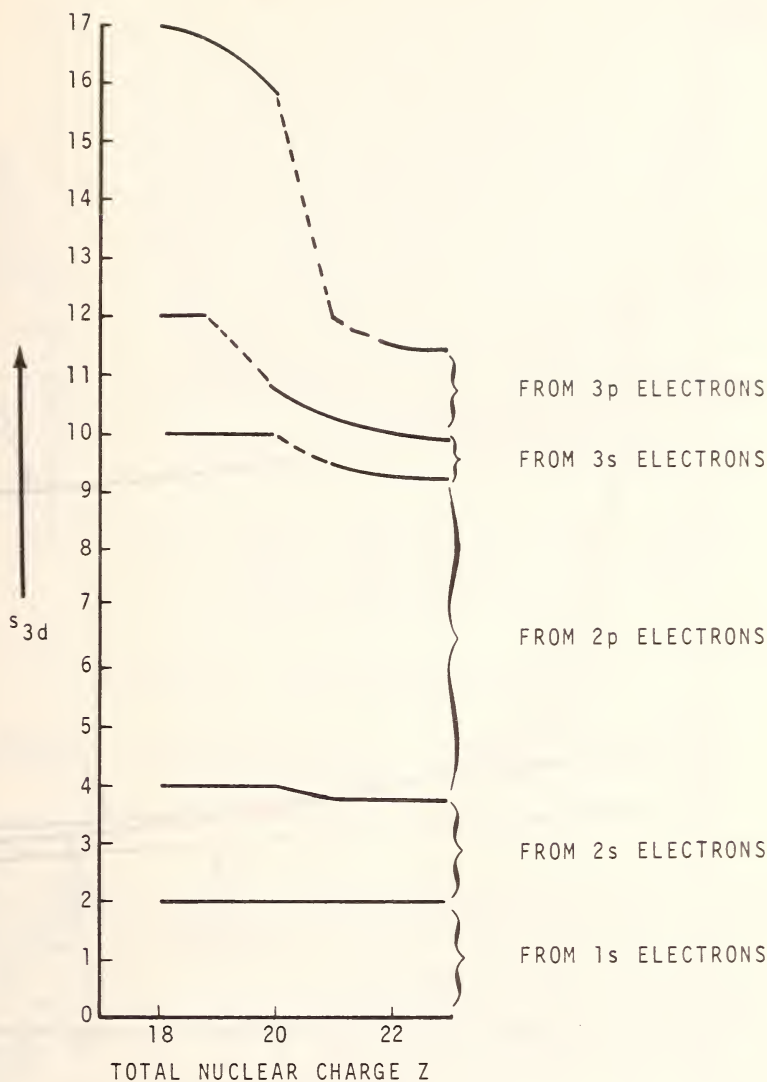


Figure 7. Composition of 3d screening parameters.

where s_{α} is a homogeneous rational function of all the x_{β} . Thus it is clear that the expansion of s_{α} in powers of Z^{-1} has a finite radius of convergence. The quasi-discontinuous variation of the 3d screening parameter reflects the quasi-discontinuous character of screening itself: near $Z = 20.4$, a small change in the radial distance of the peak of the 3d wavefunction can

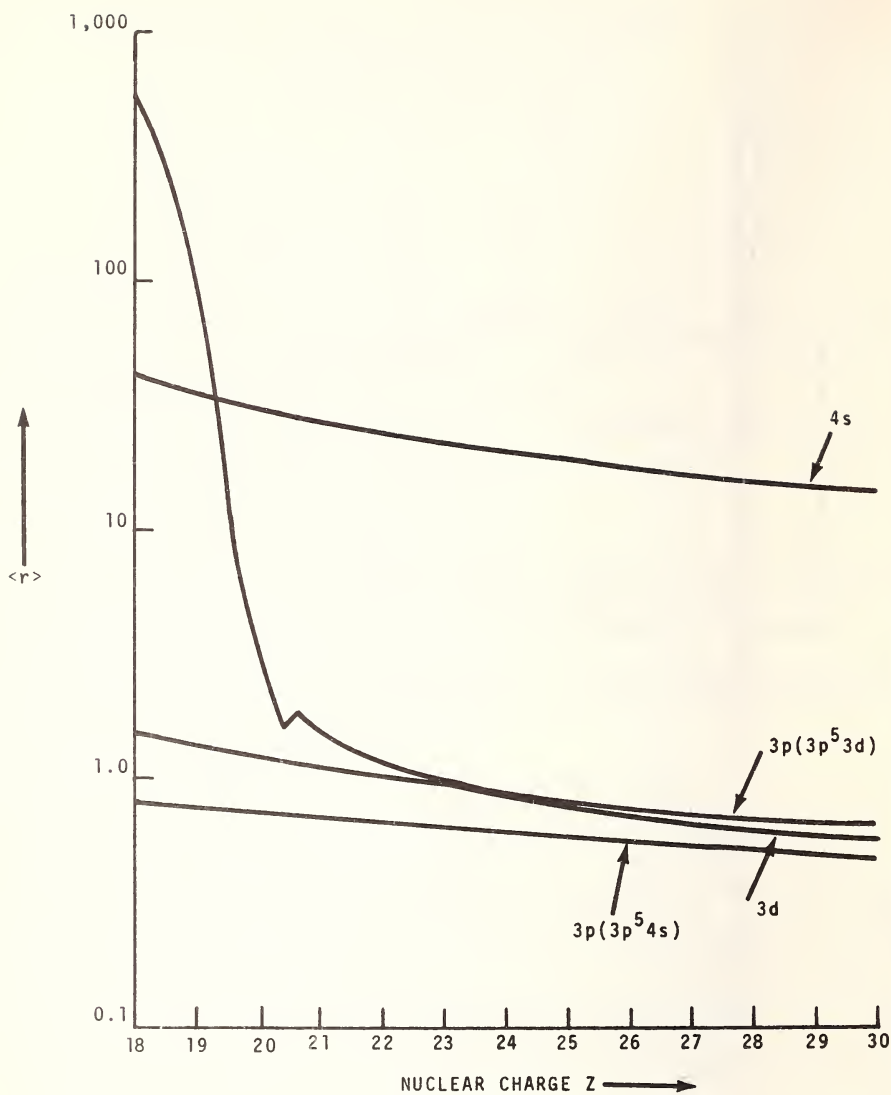
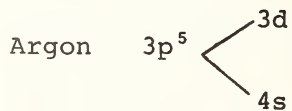


Figure 8. Expectation value of r .



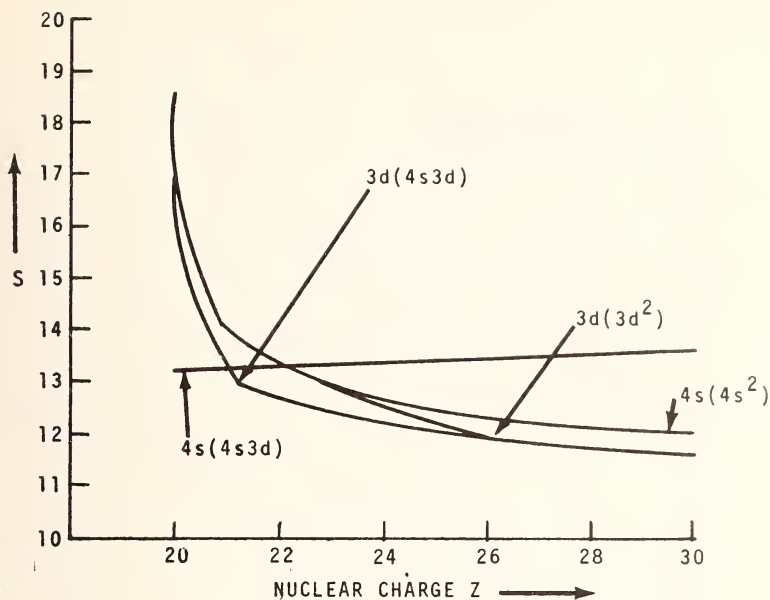
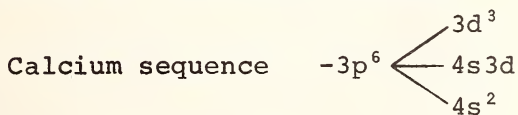


Figure 9. Screening parameters:



cause a large change in the screening of the 3d electron. This situation is illustrated in Figure 11, a simplified schematic plot of s_{3d} and F_{3d} [see formula (6)] as functions of $(Z - s_{3d})$ for various values of Z . Note the abrupt change in F_{3d} between its two asymptotic values, corresponding to the passage of the 3d electron through the 3p subshell, and the corresponding abrupt change in the variational value of s_{3d} , determined by the intersection of the curves F_{3d} and s_{3d} .

These considerations suggest that very simply theoretical methods may suffice to explain the regularities illustrated in Figure 1.

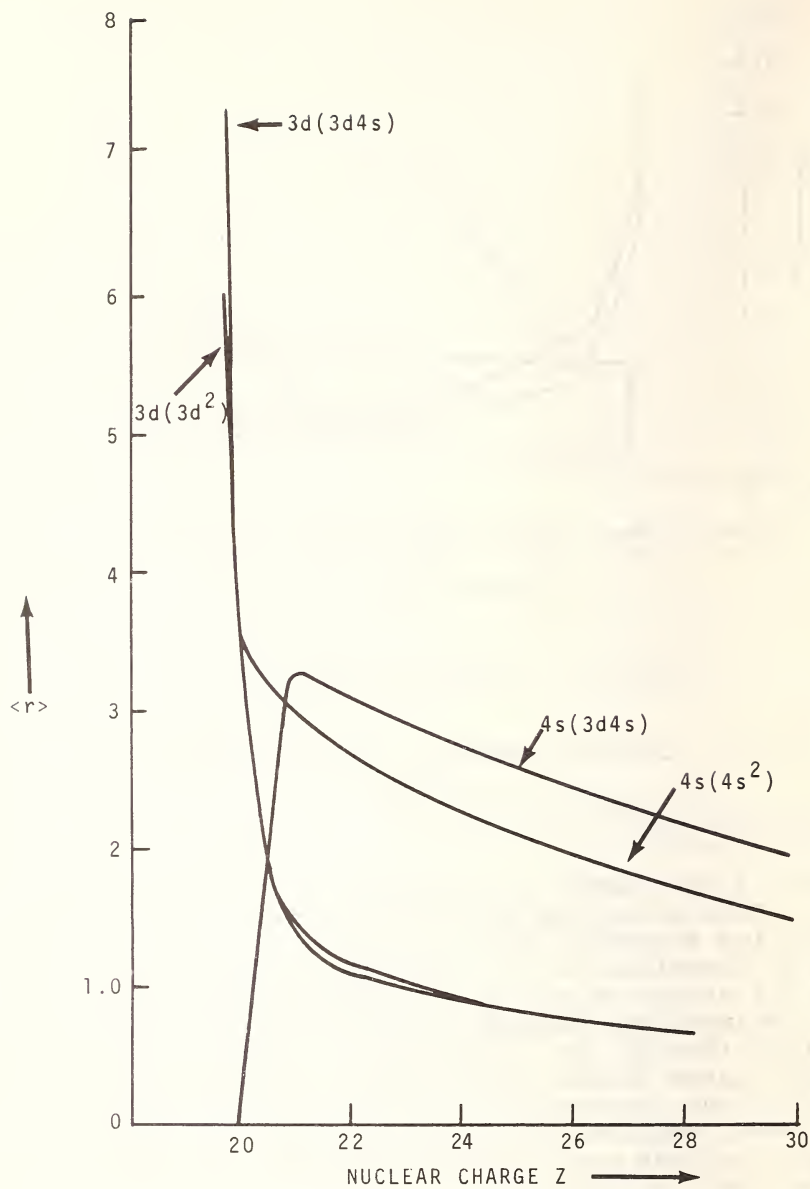


Figure 10. Expectation value of r .
 Calcium sequences $-3p^6 3d^2$, $-3p^6 3d4s$, $-3p^6 4s^2$

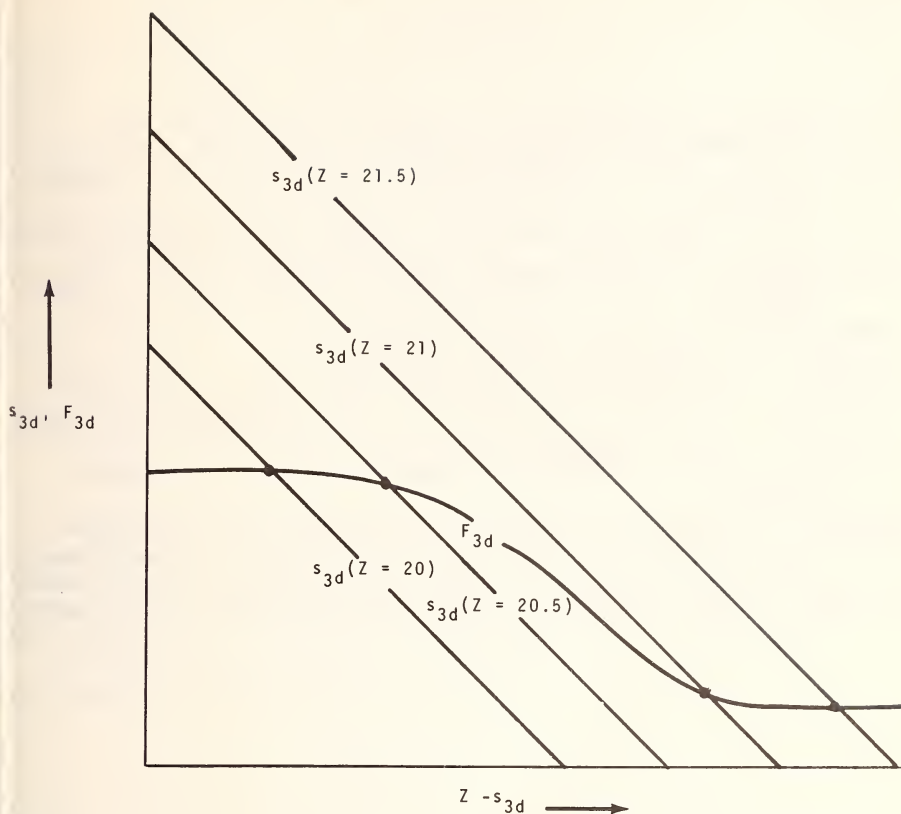


Figure 11. Illustrating the nonanalytic character of s_{3d} , determined as the intersection of s_{3d} and F_{3d} as functions of $Z - s_{3d}$.

ACKNOWLEDGMENT

The calculations on which Figures 6 through 10 are based were carried out by Mrs. Judith Drake and Dr. Margaret Lewis to whom I am indebted for permission to quote the results in advance of publication. Most of the work reported here has been supported by grants from the National Science Foundation.

REFERENCES

- Dalgarno, A. and Stewart, A. 1958, *Proc. Roy. Soc. (London) Ser. A*, 247, 245.
- Doyle, H.T. 1968, Thesis, Harvard University, (unpublished).
- Doyle, H.T. 1969, *Advances in Atomic and Molecular Physics*, 5, 337-413.
- Godfredsen, E. 1963, Thesis, Harvard University (unpublished).
- Godfredsen, E. 1966, *Ap. J.*, 145, 308.
- Layzer, D. 1959, *Ann. Phys.*, 8, 271.
- Layzer, D. and Bachall, J. 1962, *Ann. Phys.*, 17, 177.
- Layzer, D., Horak, Z., Lewis, M. and Thompson, D. 1964, *Ann. Phys.*, 29, 101.
- Snyder, R. 1969, Thesis, Harvard University (unpublished).
- Snyder, R. 1970, *J. Phys. Soc. London B* (2) 3, 177.
- Snyder, R. 1971, *Highlights of Astronomy* (ed. de Jager), (Dordrecht-Holland: Reidel Publishing Corp.), 338.
- Wigner, E. and Seitz, F. 1955, *Advances in Solid State Physics*, I.

MANY-BODY CALCULATIONS OF ENERGIES AND
TRANSITION PROBABILITIES

Hugh P. Kelly
University of Virginia

I. INTRODUCTION AND REVIEW

This paper is concerned with the applications of the many-body perturbation theory of Brueckner¹ and Goldstone² to problems in atomic structure. Our methods for applying many-body perturbation theory to atoms have been discussed elsewhere^{3,4,5}.

In the applications to an N-electron system we start with the simplified problem

$$H_0 \phi_0 = E_0 \phi_0 , \quad (1)$$

where

$$H_0 = \sum_{i=1}^N H_{0i} , \quad (2)$$

and

$$H_{0i} = - \frac{\nabla_i^2}{2} - \frac{Z}{r_i} + V(r_i) . \quad (3)$$

The effective single-particle potential to be used is arbitrary and could, for example, be chosen as the Hartree-Fock potential V_{HF} . The unperturbed solution is a determinant or linear combination of determinants of single particle states ϕ_n which satisfy

$$H_{0i} \phi_n(\mathbf{r}_i) = \epsilon_n \phi_n(\mathbf{r}_i) . \quad (4)$$

Our exact non-relativistic wave function satisfies

$$H\Psi = E\Psi , \quad (5)$$

where

$$H = H_0 + H' , \quad (6)$$

with

$$H' = \sum_{i < j=1}^N r_{ij}^{-1} - \sum_{i=1}^N V(r_i) . \quad (7)$$

Atomic units are used throughout this paper unless specified otherwise. According to the theory of Brueckner and Goldstone (BG),

$$\Psi = \sum_{\Sigma} \left(\frac{1}{E_0 - H_0} H' \right)^n \Phi_0 , \quad (8)$$

where Σ indicates that only "linked terms" are to be included.

Also,

$$E = E_0 + \langle \Phi_0 | H' | \Psi \rangle . \quad (9)$$

We note from Equation (8) that Ψ is not normalized to unity, but rather $\langle \Phi_0 | \Psi \rangle = 1$.

In order to carry out the perturbation calculations of Equations (8) and (9), we use the complete set of single particle states ϕ_n from Equation (4). We include only a limited number of orbital angular momentum states (usually $l \leq 4$). We explicitly calculate bound states up to $n=10$ to 15 and then sum over perturbation contributions from higher n values by the n^{-3} rule⁴. We obtain perturbation contributions from continuum states by numerical integration.

We have used these methods to calculate correlation energies for the ground state multiplets of beryllium^{3,4}, carbon⁶, oxygen⁷, and iron⁸. For Be, C and O, the correlation energies are in excellent agreement with experiment. As yet, there are no experimental results for Fe. These methods may also be used to calculate energies of excited states, although very little work has as yet been done on them.

These methods have also been used to calculate polarizabilities, shielding factors, and hyperfine constants⁹. In these cases we must add an additional term $V_{ex}(r_i)$ to Equation (7). The dipole polarizability, for example, is proportional to the sum of all energy terms that are second order in ΣV_{ex} and contain any number of interactions with the correlation term $(\Sigma r_{ij}^{-1} - \Sigma V)$. These methods have also been used for electron-atom scattering^{10,11}.

In this paper our major emphasis is on the calculation of transition probabilities and, in particular, on transitions from bound to continuum states. Much of the important initial work in this area was carried out by Professors Menzel and Pekeris¹². The importance of photoionization (bound-free transitions) in astrophysics has also been stressed by Professor Menzel in his book *Stellar Interiors*¹³. In Section II we present some oscillator strengths for bound-bound transitions in Be including correlations. We also present preliminary results for an oscillator strength in Fe. In Section III we present results for the photoionization cross section of Fe in the ground state.

II. OSCILLATOR STRENGTHS

Oscillator strengths for the transitions $(2s)^2 \ ^1S \rightarrow 2s np \ ^1P$ have been calculated⁴ with electron correlations in the ground state included by use of Equation (8). Our excited np states were calculated in the presence of a "frozen core" $(1s)^2(2s)$ with the $1s$ and $2s$ being Hartree-Fock orbitals for the ground state. Results are given in Table 1 and are discussed in more detail in reference 4. Results for f_{ni} are expected to be close to Hartree-Fock results. The large reduction in the oscillator strength for $n=2$ is due to strong configuration mixing in the ground state between the $(2s)^2 \ ^1S$ and $(2p)^2 \ ^1S$ configurations.

We have very recently begun to calculate the oscillator strength for the FeI spectral line 3719.9 Å arising from the transition $(3d)^6 4s(a^6D) 4p(z^5F^o) \rightarrow (3d)^6 (4s)^2(a^5D_4)$. The experimental value¹⁴ for this oscillator strength is 0.0421. Our calculations used the single-particle states for Fe calculated previously¹⁵. The $4s$ and $3d$ orbitals are Hartree-Fock solutions for the $(3d)^6(4s)^2 \ ^5D$ ground state. The excited np states ($n \geq 4$) were calculated with a "frozen core" $(3d)^6(4s)$. Our result without correlations is

TABLE I
 OSCILLATOR STRENGTHS FOR TRANSITIONS
 $(2s)^2 \ ^1S \rightarrow 2snp \ ^1P$ in Be

n	f_{ni}^*	$f_{ni}(\text{corr})$
2	2.0293	1.2540
3	0.00541	0.01676
4	0.00530	0.01013
5	0.00318	0.00549
6	0.00194	0.00321
7	0.00125	0.00202
8	0.00084	0.00135
∞		
Σ	0.00295	0.00467
n=9		

*Correlations not included. Excited np states calculated in field of frozen core $(1s)^2(2s)$.

†Correlations in the ground state included.

0.3962, which is almost a factor of ten from the experimental value. Including the lowest-order correlation corrections among 4s and 3d electrons, we obtain 0.171. We estimated the normalization corrections⁴ as causing a further reduction to 0.085. We are at present calculating the normalization corrections explicitly and investigating higher-order terms in the perturbation expansion. The very great effects of correlations on this oscillator strength are striking. In the ground state, the mixing of $(4s)^2$ with $(4p)^2$ causes a significant reduction. However, there is also considerable mixing of 4s3d with 4pkf. In the excited state there is also configuration mixing, for example, of 3d4p with 4skf and of 4s4p with 4skp. It is clear that considerable additional calculations are required and that our present results are very preliminary.

III. PHOTOIONIZATION CROSS SECTION FOR Fe

This calculation was stimulated by its relevance for astrophysics¹⁶ and by the fact that there does not seem to be any measurement of $\sigma(\omega)$ for Fe¹⁷. In these calculations we use the relation¹⁸

$$\sigma(\omega) = \frac{4\pi}{c} \omega \text{Im}\alpha(\omega) \quad , \quad (10)$$

where $\alpha(\omega)$ is the frequency-dependent polarizability^{19,20}.

In calculating the perturbation theory diagrams²⁰ for $\alpha(\omega)$, we treat energy denominators according to the principal value prescription $P-i\pi\delta$, where P represents a principal value integration. Then $\text{Im } \alpha(\omega)$ consists of all diagrams in which we have an odd number of contributions from $-i\pi\delta$. The lowest order diagram contributing to $\alpha(\omega)$ is shown in Figure 1(a). The horizontal line represents use of $-i\pi\delta$. This notation has also been used by Wendin who has discussed calculation of resonances in $\sigma(\omega)$ by many-body theory²¹. In Figure 1, a heavy dot represents matrix elements of z . (In calculating $\alpha(\omega)$ we take the perturbing electric field in the \hat{z} direction and average over M_L .) Dashed lines without a dot represent Coulomb correlations. In the first order of perturbation theory, there are diagrams shown in Figure 1(b) and 1(c). These diagrams also occur inverted and there are corresponding exchange diagrams. When there is no horizontal line, denominators are treated by principal value integration.

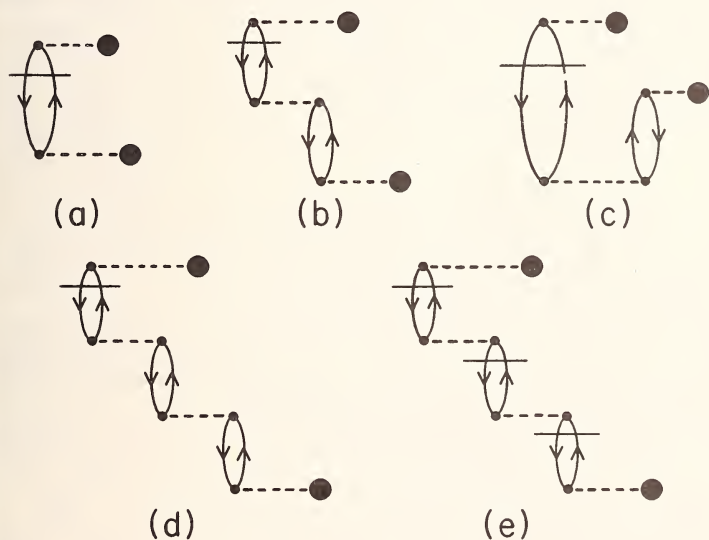


Figure 1. Diagrams contributing to the photoionization cross section or $\text{Im } \alpha(\omega)$. The horizontal line indicates that the denominator should be treated according to $P-i\pi\delta$. The large solid dot indicates a matrix element of z . The dashed line without the large dot represents a Coulomb interaction.

In calculating $\sigma(\omega)$ for the $(3d)^6(4s)^2\ ^5D$ ground state of Fe, we have used our complete set of single particle states from our calculation¹⁵ of the hyperfermion contact interaction in Fe. We carried out the calculations with $M_S = +2$ and averaged over M_L . Our cross section of course is independent of M_S . There are higher-order diagrams²⁰ which shift the single-particle energies $\epsilon(n)$ to give correct ionization energies $\epsilon'(n)$. We calculated the shifted energies of $\epsilon(4s^+)$ and $\epsilon(4s^-)$ agreed well with the experimental ionization energy²². We used spectroscopic data²² to determine $\epsilon(3d^-)$, and we obtained an average $\epsilon(3d^+)$ by calculating the difference from $\epsilon(3d^-)$. Our shifted energies for $\epsilon(4s^-)$ and $\epsilon(4s^+)$ are -0.2903 a.u. and -0.3104 a.u. respectively. For $\epsilon(3d^-)$ and $\epsilon(3d^+)$ we obtained -0.3965 a.u. and -0.5811 a.u. respectively. The difference between $\epsilon(4s^-)$ and $\epsilon(4s^+)$ is due to the fact that (for $M_S = +2$) the $4s^+$ electron has exchange interactions with the five $3d^+$ electrons whereas the $4s^-$ electron has an exchange interaction with the single $3d^-$ electron.

Results for $\sigma(\omega)$ are shown in Figure 2. The dashed line represents the Hartree-Fock result obtained

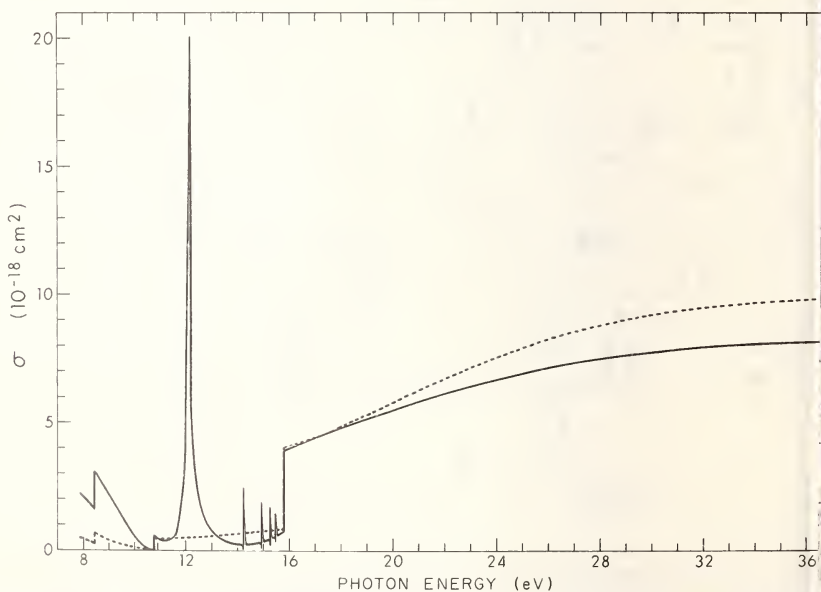


Figure 2. Total photoionization cross section of Fe
 ----- lowest order results.
 _____ including correlations for contributions from
 $(4s)^2$ and $(3d)^6$ subshells.

rom the diagram of Figure 1(a). The solid line is the result including correlations. We included diagrams like Figure 1(b) and 1(c), their inverses, and also the corresponding exchange diagrams. We also included some higher-order diagrams like Figure 1(b) and 1(c) in which the part of the diagram above the horizontal line is identical to that below. Diagrams like Figure 1(d) were approximately included. Diagrams like Figure 1(e) were also included. The maximum contribution from Figure 1(e) came near threshold and reduced $\sigma(\omega)$ by approximately eight percent. Our results in Figure 2 have only included correlations among 4s and 3d electrons and correlations of 3d electrons with 3p electrons. The 3d-3p correlations were found to be small, and it was estimated that the omitted correlations affect $\sigma(\omega)$ very little.

The large increase over the Hartree-Fock result is due mostly to the diagram of Figure 1(b) when the bottom matrix element is $\langle 4p|z|4s \rangle$. This matrix element is so much larger than $\langle kp|z|4s \rangle$ that it more than compensates for the reduction due to the Coulomb matrix element. This diagram corresponds to configuration mixing in the many-particle final state between 4s kp and 4p 4s. We expect that this effect will be found in all atoms with an outer $(ns)^2$ subshell with $n \geq 2$. In such atoms, Hartree-Fock results may be expected to differ significantly from experiment. In diagrams like Figure 1(d), when all but the top excited states are p^\pm and the hole lines are $4s^\pm$, we may sum the diagrams geometrically⁴.

In Figure 2 we note the strong resonance at 2.13 eV and lesser resonances from 14.26 eV to 15.81 V. The resonance at 12.13 eV is due to $3d^+ \rightarrow 4p^+$ excitations which are degenerate in energy with $s^\pm \rightarrow kp^\pm$ and $3d^- \rightarrow kf^-$, kp^- excitations. These resonances occur in diagrams like Figure 2(b) in which the bottom excitation is $3d^+ \rightarrow np^+$. It is to be emphasized that we have not made an accurate determination of the height and shape of the resonances, which would involve including many higher-order diagrams. There are also arrow resonances (not shown in Figure 2) from $d^+ \rightarrow nf^+$ excitations and from $4s^+ \rightarrow np^+$ for high n . Many other resonances also occur in higher-order diagrams. We expect that the most important of these involve $(4s)^2 \rightarrow mpns$ or $(4s)^2 \rightarrow mpnd$ excitations. We plan to investigate these effects in future work. The present calculations merely indicate the presence of resonances.

At higher energies than shown in Figure 2, there are contributions to $\sigma(\omega)$ from the inner subshells, and

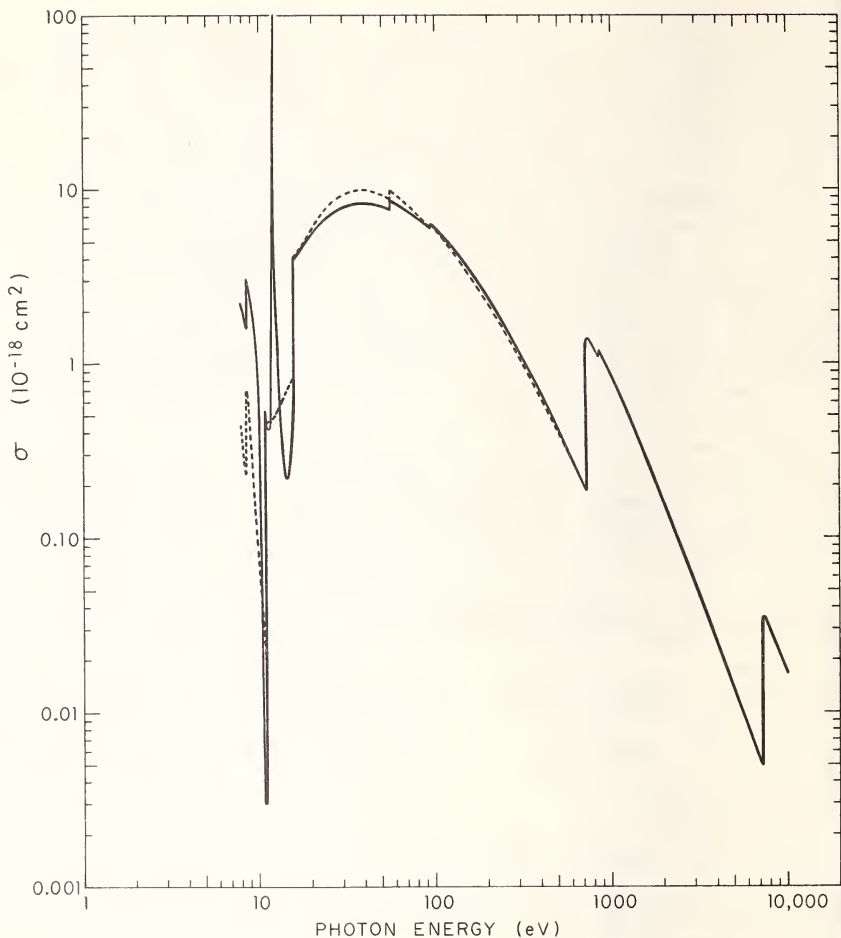


Figure 3. Total photoionization cross section of Fe to 10 keV.

----- lowest order result.

———— including correlations in contributions from $(4s)^2$ and $(3d)^6$ subshells.

these are shown in Figure 3. Only the $3d \rightarrow 4p$ resonance is shown in Figure 3. Correlations were not included in the contributions from the $(3p)^6$ subshell and inner subshells. A more complete account of this work will be published elsewhere²³.

At present we are calculating contributions $\sigma(\omega)$ in which two or more electrons are ejected and also processes in which one electron is ejected and the atom is left in an excited state. The lowest order diagram

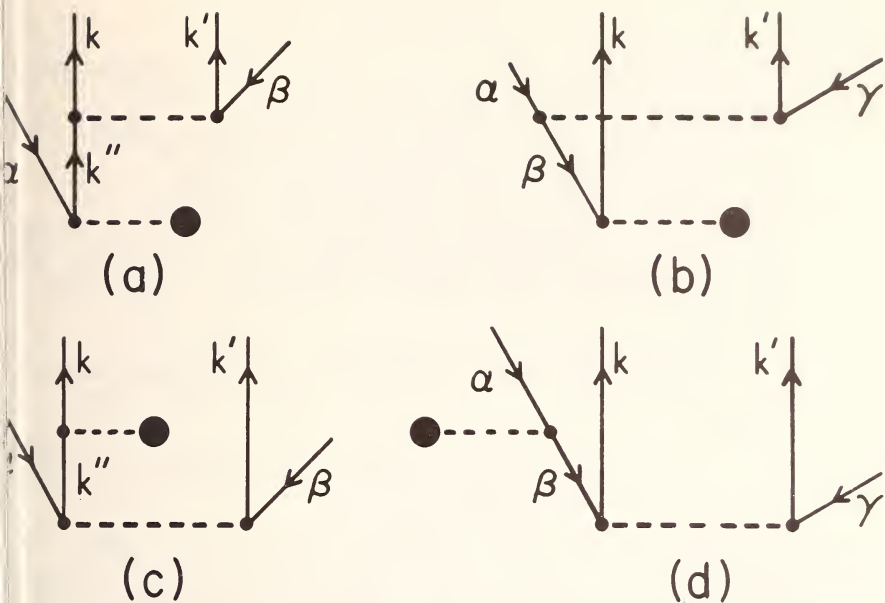


Figure 4. Lowest order diagrams contributing to double photoionization when both k and k' are continuum states. When either k or k' is a bound excited state and the other is a continuum state, these are the lowest order diagrams contributing to photoionization accompanied by excitation to a bound state. The cross section is proportional to the square of the sum of diagrams (a) to (d).

Contributing to such processes are shown in Figure 4. For example, in the diagram of Figure 4(a) α and β could be the $4s^+$ and $4s^-$ states, k could be either a continuum $\ell=0$ or $\ell=2$ state, and $k'=4p$. In this process the photoabsorption has resulted in a $4s^+$ electron being ejected and there is also a $4s^- \rightarrow 4p^-$ excitation. So, k' could represent the continuum state and k the bound state. Contributions to the same excitations also occur in the diagrams of Figures 4(b), (c), and (d). All processes such as these should be included in the total photoabsorption cross section.

ACKNOWLEDGMENT

This research has been supported by the Aerospace Research Laboratories, Office of Aerospace Research, United States Air Force, Contract No. F33615-69-C-1048.

REFERENCES

1. K.A. Brueckner, *Phys. Rev.*, 97, 1353 (1955); *The Many-Body Problem* (Wiley, New York, 1959).
2. J. Goldstone, *Proc. Roy. Soc. (London)*, A239, 267 (1957).
3. H.P. Kelly, *Phys. Rev.*, 131, 684 (1963).
4. H.P. Kelly, *Phys. Rev.*, 136, B896 (1964).
5. H.P. Kelly, *Advances in Chemical Physics*, Vol XIV (Interscience Publishers, New York, 1969), p. 12
6. J.H. Miller and H.P. Kelly, *Phys. Rev.*, A3, 578, (1971).
7. H.P. Kelly, *Phys. Rev.*, 144, 39 (1966).
8. H. Kelly and A. Ron, *Phys. Rev.* to be published.
9. H.P. Kelly, *Int. J. of Quant. Chem. IIIS*, 349 (1970).
10. R.T. Pu and E.S. Chang, *Phys. Rev.*, 151, 31 (1966)
11. H.P. Kelly, *Phys. Rev.*, 160, 44 (1967); 166, 1 (1968); 171, 54 (1968).
12. D.H. Menzēl and C.L. Pekeris, *M.N.R.A.S.*, 96, 77 (1935).
13. D.H. Menzel, P.L. Bhatnager, and H.K. Sen, *Stellar Interiors* (Chapman and Hall, London, 1963).
14. R. Wagner and E.W. Otten, *Z. Physik*, 220, 349 (1969).
15. H. Kelly and A. Ron, *Phys. Rev.*, A2, 1261 (1970).
16. O. Gingerich, private communication.
17. G.V. Marr, *Photoionization Processes in Gases* (Academic Press, Inc., New York, 1967).
18. U. Fano and J.W. Cooper, *Revs. Mod. Phys.*, 40, 44 (1968).
19. A. Dalgarno, in *Perturbation Theory and Its Applications in Quantum Mechanics*, ed. C.H. Wilco (J. Wiley & Sons, Inc., New York, 1966), p. 145.
20. H.P. Kelly, *Phys. Rev.*, 182, 84 (1969).
21. G. Wendin, *J. Phys.*, B3, 455 (1970); 3, 466 (1970).
22. C.E. Moore, *Atomic Energy Levels*, National Bureau of Standards Circular No. 467 (U.S. Government Printing Office, Washington, D.C., 1949).
23. H. Kelly and A. Ron, *Phys. Rev.* to be published.

RADIOACTIVE TRANSITIONS IN THE HELIUM
ISOELECTRONIC SEQUENCE

Alexander Dalgarno
Harvard College Observatory

1. INTRODUCTION

In collaboration with Bruce Shore, Donald Menzel wrote a basic text, *The Principles of Atomic Spectra* (Shore and Menzel 1968). In this paper I describe the application of those principles to the quantitative study of radiative transitions in two-electron helium-like atomic systems.

2. QUANTUM THEORY OF RADIATION

The absorption and emission of a single photon in a radiative transition between two stationary states of an atomic system described respectively by wave functions ψ_i and ψ_f can be obtained from the matrix element $\langle \psi_i | H | \psi_f \rangle$ of the interaction H between the radiation field and the atom. The interaction H can be expressed in terms of the vector potential \underline{A} of the radiation field, which can be expanded as a sum over multipoles $A_{LM}^{(\lambda)}$ of magnetic and electric type. The multipole fields have well-defined parities $(-1)^{L+\lambda+1}$ where $\lambda = 0$ designates a magnetic and $\lambda = 1$ an electric multipole. The transition matrix element vanishes unless the parity selection rule is satisfied. If π_i is the parity of the initial atomic state and π_f the parity of the final atomic state, the parity requirement is

$$\pi_i = \pi_f (-1)^{L+1+\lambda} . \quad (1)$$

The allowed values of the photon angular momentum L are further restricted by the angular momentum selection rules

$$|J_i - J_f| \leq L \leq J_i + J_f \quad (2)$$

but

$$J_i = 0 \nrightarrow J_f = 0$$

where J_i and J_f are the total angular momenta, spin and orbital, of respectively the initial and final states.

Apart from vector spherical harmonics, $A_{LM}^{(\lambda)}$ contains the spherical Bessel function $g_L(\hbar\omega r/c)$ where $\hbar\omega$ is the photon energy and r is the distance of the electron from the atomic nucleus. For small values of the argument, g_L can be expanded as the power series

$$g_L(x) = \frac{4\pi(ix)^L}{(2L+1)!!} \left\{ 1 - \frac{x^2}{2(2L+3)} + \dots \right\} \quad (3)$$

If the wavelength of the photon is large compared to the dimensions of the atom, the major contribution to the transition matrix element comes from the region where $\omega r/c \ll 1$, and in most cases only the first term of (3) need be retained. The assumption that the wavelength is large compared to the atomic dimensions implies that the electron velocities are small compared to the velocity of light so that the Dirac wave functions ψ_i and ψ_f can be replaced by non-relativistic Pauli wave functions. The probability of a spontaneous transition $W_{LM}^{(\lambda)}$ can then be related to the electric and magnetic multipoles

$$Q_{LM}^{(1)} = e \left(\frac{1}{2L+1} \right)^{1/2} \sum_{i=1}^N r_i^L Y_{LM}^* (r_i/r_i) \quad (4)$$

$$Q_{LM}^{(0)} = \left(\frac{1}{2L+1} \right)^{1/2} \sum_{i=1}^N \nabla_i r_i^L Y_{LM}(r_i/r_i) \left\{ \frac{e}{m(2L+1)} \underline{l}_i + \underline{\mu}_i \right\} \quad (5)$$

where $\underline{l}_i = r_i \times p_i$ is the orbital angular momentum of the i th electron of the N -electron atom and $\underline{\mu}_i$ is the spin angular momentum $eg_i/2m$. The explicit formulae are

$$Q_{LM}^{(1)} = \frac{2(L+1)}{L(2L+1)[2L-1]!!} \omega^{2L+1} \left| \langle f | Q_{LM}^{(1)} | i \rangle \right|^2 \quad (6)$$

$$Q_{LM}^{(0)} = \frac{2(L+1)}{L(2L+1)[(2L-1)!!]^2} \omega^{2L+1} \left| \langle f | Q_{LM}^{(0)} | i \rangle \right|^2 \quad (7)$$

3. RADIATIVE DECAY OF HELIUM

The energy level diagram for the low-lying states of helium is reproduced in Figure 1. For ions heavier than C V, the ordering changes and the 2^3P levels lie below the 2^1S level.

Consider first the decay of the 2^1P_1 level. It has $J_i = 1$ and is of odd parity. Below it there lie two states of even parity with $J_i = 0$. The selection rules are satisfied by an electric dipole E1 transition and the $2^1P_1 - 1^1S_0$ and $2^1P_1 - 2^1S_0$ are typical examples of strong allowed transitions. Reliable values are readily obtained from accurate variationally determined two-electron non-relativistic wave functions and Table 1 contains a list of transition probabilities for various nuclear charges Z .

The $2^1P_1 - 1^1S_0$ transition probability increases as Z^4 for large Z but because the 2^1P_1 and 2^1S_0 states are asymptotically degenerate, the $2^1P_1 - 2^1S_0$ non-relativistic probability increases only as Z .

The 2^3P levels are more interesting. They have total angular momentum $J_i = 2, 1$ and 0 and are of odd parity. They can all decay by an electric dipole E1 transition to the 2^3S_1 state. No change of multiplicity is involved and the decay occurs through a typical allowed transition. The corresponding transition probabilities are included in Table 1. As for the

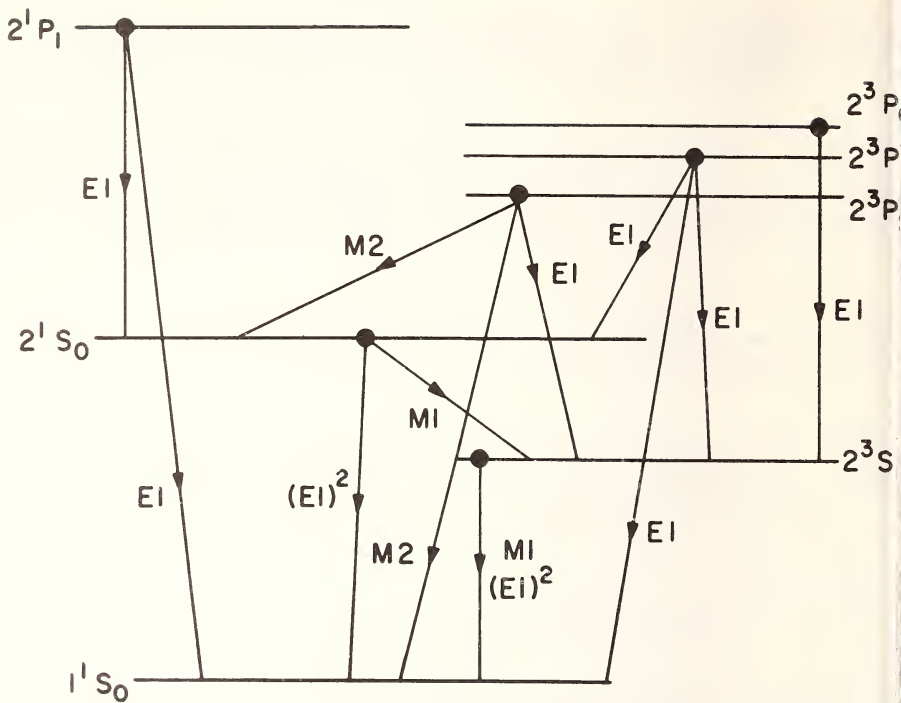


Figure 1. Energy level diagram for neutral helium showing the ordering of the levels.

$2^1P_1 - 2^1S_0$ transitions, the probabilities increase as Z for large Z .*

The 2^3P_0 level can decay by no other single photo mechanism because $J_i = 0 \rightarrow J_f = 0$ transitions are strictly forbidden. The selection rules allow the 2^3P level to decay by an electric dipole $E1$ transition to the ground 1^1S_0 level. A change of spin multiplicity is required which is effected theoretically by the mixing of 1P_1 and 3P_1 states through the Breit interaction V_B . Thus the triplet wave function can be written to first order in V_B as

$$|2^3P_1\rangle = |2^3P_1\rangle_0 + \sum_{\tilde{n}} \frac{\langle 2^3P_1 | V_B | n^1P_1 \rangle \langle n^1P_1 |}{E_n - E(2^3P_1)} \quad (8)$$

*The limiting Z dependence is modified by relativistic effects on the transition frequencies.

TABLE 1

RADIATIVE TRANSITION PROBABILITIES A FOR THE
 2^1P_1 STATES OF THE HELIUM SEQUENCE IN SEC^{-1}

Z	System	$2^1P_1 - 1^2S_0^*$	$2^1P_1 - 2^1S_0^*$
2	He I	1.80 (9) [†]	1.97 (6)
3	Li II	2.56 (10)	5.14 (6)
4	Be III	1.22 (11)	8.73 (6)
5	B IV	3.72 (11)	1.25 (7)
6	C V	8.87 (11)	1.65 (7)
7	N VI	1.81 (12)	2.05 (7)
8	O VII	3.31 (12)	2.46 (7)
9	F VIII	5.58 (12)	2.87 (7)
10	Ne IX	8.87 (12)	3.29 (7)
11	Na X	1.34 (13)	3.70 (7)
12	Mg XI	1.96 (13)	4.12 (7)
13	Al XII	2.76 (13)	4.54 (7)
14	Si XIII	3.78 (13)	4.96 (7)
15	P XIV	5.07 (13)	5.38 (7)
16	S XV	6.66 (13)	5.80 (7)
17	Cl XVI	8.59 (13)	6.22 (7)
18	Ar XVII	1.09 (14)	6.64 (7)

From G.W.F. Drake (unpublished).

1.80 (9) $\equiv 1.80 \times 10^9$

where

$$\left\{ H_0 - E(2^3P_1) \right\} |2^3P_1\rangle_0 = 0 \quad (9)$$

and

$$\left\{ H_0 - E_n \right\} |n^1P_1\rangle_0 = 0, \quad (10)$$

H_0 being the non-relativistic electrostatic two-electron Hamiltonian. The transition matrix element reduces to

$$\langle \psi_i | H | \psi_f \rangle = \sum_{\tilde{n}} \frac{\langle 2^3P_1 | V_B | n^1P_1 \rangle \langle n^1P_1 | Q_{10}^{(0)} | 1^1S_0 \rangle}{E_n - E(2^3P_1)}. \quad (11)$$

The singlet-triplet mixing increases rapidly with increasing Z , and the $2^3P_1 - 1^1S_0$ transition probability increases initially as $Z^{1.0}$ (though ultimately as Z^4) and the spin-forbidden $2^3P_1 - 1^1S_0$ E1 decay mode must eventually dominate the allowed $2^3P_1 - 2^3S_0$ E1 decay mode.

The infinite summation (11), which includes an integration over the continuum, can be evaluated to arbitrary precision by a variational approximation to the two-electron Greens function; the results (Drake and Dalgarno 1969) are given in Table 2. For ions heavier than C V, the forbidden transition is more probable than the allowed.

Values for N VI and O VII have been measured by beam foil techniques. The measured probabilities of $(1.7 \pm 0.3) \times 10^8 \text{sec}^{-1}$ for N VI (Sellin, Donnelly, and Fan 1968) and $(5.8 \pm 0.5) \times 10^8 \text{sec}^{-1}$ for O VII (Sellin, Brown, Smith, and Donnelly 1970) are in harmony with the theoretical predictions.

TABLE 2
RADIATIVE DECAY TRANSITION PROBABILITIES OF THE
 2^3P STATES OF THE HELIUM ISOELECTRONIC SEQUENCE
IN SEC^{-1}

Z	System	$2^3P_{0,1,2} - 2^3S_1^*$	$2^3P_1 - 1^1S_0$	$2^3P_2 - 1^1S_0$
2	He I	1.02 (7)	1.80 (2)	3.27 (-1)
3	Li II	2.28 (7)	1.81 (4)	3.50 (1)
4	Be III	3.44 (7)	4.01 (5)	6.17 (2)
5	B IV	4.57 (7)	4.23 (6)	5.01 (3)
6	C V	5.72 (7)	2.84 (7)	2.62 (4)
7	N VI	6.89 (7)	1.40 (8)	1.03 (5)
8	O VII	8.13 (7)	5.53 (8)	3.34 (5)
9	F VIII	9.44 (7)	1.85 (9)	9.23 (5)
10	Ne IX	1.09 (8)	5.43 (9)	2.27 (6)
11	Na X	1.24 (8)		5.10 (6)
12	Mg XI	1.41 (8)		1.06 (7)
13	Al XII	1.60 (8)		2.09 (7)
14	Si XIII	1.81 (8)		3.88 (7)
15	P XIV	2.06 (8)		6.91 (7)
16	S XV	2.34 (8)		1.18 (8)
17	Cl XVI	2.67 (8)		1.96 (8)
18	A XVII	3.05 (8)		3.14 (8)

*These are weighted means of the individual $2^3P_J - 2^3S_1$ transitions.

The 2^3P_2 level cannot reach the 1^1S_0 level by an E1 transition but the selection rules are satisfied by a magnetic quadrupole M2 transition. The calculation of the magnetic quadrupole transition probabilities is straightforward. The values in Table 2 are taken from the work of Drake (1969, 1971). Because of the ω^{2L+1} factor in (15), the M2 probabilities increase rapidly as Z^8 along the isoelectronic sequence, and the magnetic quadrupole $2^3P_2 - 1^1S_0$ decay is more probable than the electric dipole $2^3P_2 - 2^3S_1$ for ions more massive than Cl XIV.

The M2 decay mode may have been detected experimentally. Marrus and Schmieder (1970a), using the Berkeley heavy-ion linear accelerator, have measured a lifetime of (1.7 ± 0.3) nanosec for the 2^3P_2 level of Ar XVII. The predicted $2^3P_2 - 2^3S_1$ E1 probability is $3.55 \times 10^8 \text{sec}^{-1}$ and the predicted $2^3P_2 - 1^1S_0$ M2 probability is $3.14 \times 10^8 \text{sec}^{-1}$, giving a 2^3P_2 lifetime of 1.5 nanosec. Without the M2 decay mode, the lifetime would be 2.8 nanosec.

The 2^1S_0 and 2^3S_1 states of helium are metastable, and there is no accessible state to which either can decay by an electric dipole transition. Because $0 \rightarrow 0$ is strictly forbidden, the 2^1S_0 state cannot decay to the 1^1S_0 state by any single photon process, and Breit and Teller (1940) long ago pointed out that it would decay by a two-photon (E1)² process



giving rise to a continuum emission. The process occurs through a second order interaction with the radiation field and its quantitative description involves the evaluation of infinite summations of the kind

$$\tilde{M} = \sum_{\tilde{n}} \frac{\langle 2^1S_0 | Q_{10}^{(1)} | n^1P_1 \rangle \langle n^1P_1 | Q_{10}^{(1)} | 1^1S_0 \rangle}{E(2^1S_0) - E_n + \nu} .$$

These can be evaluated variationally (Victor and Dalgarno 1967; Drake, Victor and Dalgarno 1969).

The spectrum is symmetric about the central frequency where it reaches its maximum probability. The

TABLE 3
 RADIATIVE TRANSITION PROBABILITIES A FOR THE
 2^1S_0 AND 2^3S_1 STATES OF THE HELIUM SEQUENCE
 IN SEC^{-1}

Z	$2^1S_0 - 1^1S_0$	$2^3S_1 - 1^1S_0$	
		(E1) ²	M1
2	5.13 (1)	4.02 (-9)	1.27 (-
3	1.95 (3)	1.50 (-6)	2.04 (-
4	1.81 (4)	6.36 (-5)	5.62 (-
5	9.26 (4)	1.01 (-3)	6.70
6	3.31 (5)	8.93 (-3)	4.86 (1
7	9.43 (5)	5.44 (-2)	2.53 (2
8	2.31 (6)	2.54 (-1)	1.04 (3
9	5.05 (6)	9.73 (-1)	3.61 (3
10	1.00 (7)	3.20	1.09 (4
11	1.85 (7)		2.94 (4
12	3.22 (7)		7.24 (4
13	5.34 (7)		1.66 (5
14	8.47 (7)		3.56 (5
15	1.31 (8)		7.25 (5
16	1.96 (8)		1.41 (6
17	2.83 (8)		2.62 (6
18	4.04 (8)		4.71 (6

two-photon decay rates are given in Table 3. They increase as Z^6 and the radiative two-photon emission is the main decay mode for the 2^1S_0 states of the heavier ions in the solar corona. However, the two-photon processes do not contribute significantly to the soft x-ray spectrum of the solar corona (Dalgarno and Drake 1969).

The two-photon emission spectrum of Ne IX has probably been observed in a high temperature laboratory plasma (Elton, Palumbo, and Griem 1968), and two measurements of the lifetime of the 2^1S_0 state of neutral helium have been reported. Pearl (1970) has measured a lifetime of (38 ± 8) millisecc; and Van Dyck, Johnson and Shugart (1970) a lifetime of (20 ± 2) millisecc. The theoretical lifetime from two-photon decay is 19.5 millisecc (Drake, Victor and Dalgarno 1969).

The selection rules also allow the decay of the 2^1S_0 state to the 2^3S_1 state by a single-photon magnetic dipole M1 transition. This magnetic dipole decay

ode is more important in connection with the 2^3S_1 state which can decay to the 1^1S_0 state with the emission of a magnetic dipole photon. Because of the change in spin multiplicity and because the initial and final state parities are even, the single-photon transition probability is very small. An estimate of the singlet-triplet mixing induced by the Breit interaction led to negligible probabilities (Breit and Teller 1940), and it was generally believed that the 2^3S_1 state decayed by the two-photon $(E1)^2$ process.

Two developments altered this view. It had been supposed that apart from the singlet-triplet P state mixing that was required for the $2^3S_1 (E1)^2$ decay, the 2^3S_1 decay process was similar to the 2^1S_0 decay, and the expected transition probability for the $2^3S_1 - 1^1S_0 (E1)^2$ decay mode was of the order of 10^{-5} sec^{-1} . However the fact that the triplet state has angular momentum of unity causes the transition probability to vanish at the central frequency (Drake and Dalgarno 1968, Bely 1968) where the 2^1S_0 probability is greatest. The predicted transition probabilities (Drake, Victor and Dalgarno 1969, Bely and Faucher 1969) are listed in table 3. The neutral helium value is $4 \times 10^{-9} \text{ sec}^{-1}$.

The second development was the identification by Gabriel and Jordan (1969) of lines in the spectrum of the solar corona as $2^3S_1 - 1^1S_0$ transitions of the helium-like ions C V to Si XIII. Confirmation that the 2^3S_1 states decay by line emission was provided by beam foil measurements on Si XIII, S XV and Ar XVII (Marrus and Schmieder 1970b). The identifications by Gabriel and Jordan and the measurements of Marrus and Schmieder provided observational support for the revised two-photon decay rates and they also established that the main decay mode is the emission of a single magnetic dipole photon; the selection rules permit no other possibility. The correct interpretation was soon put forward by Griem (1969, 1970) who pointed out that a relativistic mechanism discussed by Breit and Teller (1940) for the metastable $2^2S_{1/2}$ state of hydrogen, but shown by them to be negligible compared to the two-photon $(E1)^2$ decay, also operated in the case of the 2^3S_1 state of helium. Using a hydrogenic model, Griem showed that this relativistic magnetic dipole mechanism is more efficient than the two-photon emission in causing the decay of the 2^3S_1 levels.

The original development by Breit and Teller (1940) used Dirac wave functions. In order to proceed to more reliable quantitative predictions for two-electron systems, it seems necessary to express the matrix element in terms of Pauli wave functions. The

contribution from the leading term in the fine structure constant α vanishes and higher order terms must be retained in the theory. The generalization has been carried out by Drake (1971) and by Feinberg and Sucher (1971), who showed that it is also necessary to keep the second term of (3), a point made previously for the $2^2S_{1/2} - 1^2S_{1/2}$ transition of atomic hydrogen by Zhukovskii, Kolesnikova, Sokolov and Kherrman (1970).

Table 3 gives the transition probabilities calculated by Drake (1971). They increase with Z as Z^{10} . His value of $1.27 \times 10^{-4} \text{sec}^{-1}$ for neutral helium is in harmony with, but more precise than, that of Feinberg and Sucher (1971). It modifies in an important way the theory of helium line emission in planetary nebulae. Drake's values for heavier ions are consistent with the interpretation of solar coronal observations (Gabriel and Jordan 1970; Freeman, Gabriel, Jones and Jordan 1971).

Schmieder and Marrus (1970) have recently succeeded in measuring the lifetime of the 2^3S_1 state of the Ar XVII. They obtain a value of (172 ± 30) nanosec compared to the predicted value of 212 nanosec. It seems clear that Schmieder and Marrus have observed the operation of the Breit-Teller relativistic mechanism. Whether or not the quantitative discrepancy between theory and experiment is significant is unclear.

It is interesting to note the rapidity with which the astrophysical observation of line emissions led to fundamental theoretical and experimental studies of the interaction of matter and radiation.

ACKNOWLEDGMENT

This work has been supported partly by the National Aeronautics and Space Administration and partly by the National Science Foundation.

REFERENCES

- ely, O. 1968, *J. Phys. B. (Atom. Mol. Phys.)*, 1, 718.
- ely, O. and Faucher, P. 1969, *Astron. Astrophys.*, 1, 37.
- reit, G. and Teller, E. 1940, *Astrophys. J.*, 91, 215.
- algarno, A. and Drake, G.W.F. 1969, *Mén. Roy. Soc. Liège*, 17, 69.
- rake, G.W.F. 1969, *Astrophys. J.*, 158, 1199.
- rake, G.W.F. 1971, *Astrophys. J.*, 163, 439.
- rake, G.W.F. 1971, *Phys. Rev.*
- rake, G.W.F. and Dalgarno, A. 1968, *Astrophys. J. Letters*, 152, 121.
- rake, G.W.F. and Dalgarno, A. 1969, *Astrophys. J.*, 157, 459.
- rake, G.W.F., Victor, G.A., and Dalgarno, A. 1969, *Phys. Rev.*, 180, 25.
- lton, R.C., Palumbo, L.J., and Griem, H.R. 1968, *Phys. Rev. Letters*, 20, 783.
- einberg, G. and Sucher, J. 1971, *Phys. Rev. Letters*, 26, 681.
- reeman, F.F., Gabriel, A.H., Jones, B.B., and Jordan, C. 1971, *Proc. Roy. Soc. A.*
- gabriel, A.H. and Jordan, C. 1969, *Mon. Not. Roy. Astron. Soc.*, 145, 241; *Nature*, 221, 947.
- gabriel, A.H. and Jordan, C. 1970, *Phys. Letters*, 32A, 166.
- riem, H.R. 1969, *Astrophys. J. Letters*, 156, 103.
- riem, H.R. 1970, *Astrophys. J. Letters*, 161, 155.
- arrus, R. and Schmieder, R.W. 1970a, *Phys. Rev. Letters*, 25, 1689.
- arrus, R. and Schmieder, R.W. 1970b, *Phys. Letters*, 32A, 431.
- earl, A.S. 1970, *Phys. Rev. Letters*, 24, 703.
- ellin, I.A., Brown, M. Smith, W.W., and Donnally, B. 1970, *Phys. Rev.*, A2, 1189.
- ellin, I.A., Donnally, B., and Fan, C.Y. 1968, *Phys. Rev. Letters*, 21, 717.
- schmieder, R.W. and Marrus, R. 1970, *Phys. Rev. Letters*, 25, 1245.
- hore, B.W. and Menzel, D.H. 1968, *Principles of Atomic Spectra* (Wiley: New York).
- an Dyck, R.S., Johnson, C.E., and Shugart, H.A. 1970, *Phys. Rev. Letters*, 25, 1403.
- ictor, G.A. and Dalgarno, A. 1967, *Phys. Rev. Letters*, 18, 1105.
- ukovskii, V.Ch., Kolesnikova, M.M., Sokolov, A.A., and Kherrman, L. 1970, *Opt. Spectrosc.*, 28, 337.

SOLAR ASTRONOMY

*Chairman: Donald H. Menzel
Harvard College Observatory*

Once you've seen one of Menzel's
invisible prominences, you've seen
them all.

Harlow Shapley



SOLAR INSTRUMENTATION

(PART I)

John W. Evans

Sacramento Peak Observatory

Solar astronomy, like other areas of experimental or observational physical science, is increasingly dependent on refined optical, mechanical, electronic, and software equipment. All of it is expensive, a fact which, unfortunately, narrows the range of experiment with new devices, which might or might not work. The optical, radio, and space observations of the Sun are three distinct technologies, each of which provides essential information obtainable in no other way. A meaningful discussion of all of them is beyond the capacity of this short survey. I shall, therefore, take relief from necessity and consider only the field with which I have some acquaintance, the instruments for old-fashioned optical observations of the Sun.

Our optical solar studies naturally depend exclusively on the information brought to us by sunlight. The best we can hope to do is to obtain a complete quantitative description of this light, on the basis of which we try to deduce some of the physical characteristics of the Sun. I have entertained myself while enduring committee meetings and the like by reflecting on what constitutes a complete description. It does not seem to be too complicated in principle. If we can determine the four Stokes parameters, or their equivalent, as functions of wavelength, time, and position on the Sun in each $\Delta\lambda$ Δt Δx Δy resolution element of the smallest size compatible with the photon flux received, then I think we know nearly all there is to know about the light delivered by a given aperture. This is the ultimate observational goal. It is a pretty big order, and there is little danger of our filling it very soon. The current efforts to improve our observations can be described, rather academically, as steps to reduce the magnitude of the resolution element and expand the observable intervals of λ , t , x , and y for one or more of the Stokes parameters.

Dr. Dunn, who follows me here, will talk about the explicit down-to-earth problems he has encountered in the wringing out of a rather complex system of a modern telescope and its attendant accessories, problems he brought on himself by designing the system originally.

The modern urge is to observe the smallest possible details of the solar atmosphere; that urge is justified empirically by the fact that every advance in angular resolving power has led to important new research results. This is a recognition that the inhomogeneities of the photosphere, chromosphere, and corona are much more than small perturbations on a mean background. It is evident that many of the significant physical processes of the Sun are small scale phenomena. Some of them must surely be too small ever to be observed directly from one astronomical unit, but we can hope to include the most important features if we can study surface elements with characteristic dimensions approximately equal to the density scale height. This means something like 150km, or 0.2 arc seconds for features in the photosphere. It is reassuring to note that at higher levels of the solar atmosphere, where scale heights are larger, the smallest observed features also tend to be larger.

At any rate, my point is that much of the effort in the development of solar optical instruments is aimed at improved angular resolution in direct photographs, magnetograms, and high dispersion spectrograms. The primary instrument is, of course, the telescope, and I think it is important to recognize its limitations. We are accustomed to rough and ready estimates of resolving power in terms of the smallest distinguishable objects in a photograph or spatially resolved spectrogram. This is certainly a useful estimate for distinguishing between good and bad performance, which is usually limited by seeing rather than the telescope. But if we want to be able to take advantage of nearly perfect seeing when it comes, we do have to be sure the telescope can do the job. Here something more than the size of the smallest observable features is needed as a measure of performance.

One very useful figure of merit is the two-dimensional modulation transfer function. Giovanelli (*Atti del Convegno Sulle Macchie Solari*, Rome Observatory, 1964) has calculated this function for the mythical perfect telescope undisturbed by atmospheric seeing effects. His results are a little dismaying to those of us accustomed to thinking in terms of a resolution limit without thought for contamination of a resolved element by light diffracted from the surrounding area.

the ultimate resolution where the image contrast of sinusoidal elements first vanishes is for elements separated by angle $\delta = 0.61\lambda/A$, the familiar Rayleigh limit. Unumbral filaments separated by 1.1δ , for instance, could be just barely separated by a slight intensity dip. This is useful resolution for seeing the configuration of solar features, but the problem of restoring their true photometric character in the presence of inevitable observational noise is at best very difficult, and probably impossible. The smallest surface elements that are even moderately clean, with no more than 20% contamination from the surrounding field, have diameter of about 6δ . In terms of practical hardware, a 5-inch telescope has a resolving power of 1 arc second, but to do meaningful photometry on elements of this size we need a diffraction limited system with an aperture of about 30 inches, and seeing to match. (The resemblance to the aperture of the Sacramento Peak solar telescope is not entirely accidental.) The point I want to make here is that photometrically useful resolution and the kind of resolution we usually talk about differ by a factor of 5 or 6. This factor is probably not too far off whether the limit is set by diffraction at the telescope or by reasonably good seeing. The required photometric resolution dictates a minimum telescope size, and it is pretty big.

I do not intend to discuss the several forms a solar telescope can take. I think it has been demonstrated that if the optical quality is really good, and the seeing is good, the particular optical configuration is not crucially important. It is important, however, to avoid air convection inside the telescope and from nearby external structures like domes near the optical paths. Several recent examples of solar telescopes show careful attention to such details, with evacuated optical systems and open air mounts equipped with surface cooling devices and hot air scavengers. I am sure these measures pay.

There is no need for me to emphasize the fundamental importance of spectrographs, or to discuss the various forms they may take. The performance of any well-constructed spectrograph of conventional type can be equated with the performance of its grating. Very fine gratings have been happening in the improvement of gratings during the past few years. Dr. George Harrison at MIT began about 20 years ago to see what could be done in the control of a ruling engine with interferometers in place of the classical screw. I have watched as a most interested spectator as he patiently overcame one obstacle after another. He realized at the outset that

there were many problems beyond that of simply moving the grating blank on its ways a predetermined distance for each stroke of the diamond. Compared with the accuracy of spacing required, the flexures of the machine are enormous, and must be corrected somehow. He summarized the difficulties back around 1950 with the remark that the problems of ruling a good grating are analogous to those in the painting of a miniature portrait with a floor mop on the end of a six-foot rubber handle. Dr. Harrison has succeeded brilliantly in adapting two commercially available instrument-making machines to interferometer control, and using them to rule gratings up to 16 inches wide. They very nearly achieve their theoretical resolution, with ghosts of less than 10^{-4} at blaze angles of 63° , and blaze efficiency of more than 50%. He told me the other day that his next effort will be the ultimate grating he has been working toward -- a 16 by 24-inch ruling.

Parallel with Harrison's ruling development, several commercial firms have worked out methods for making replicas of the original rulings. Over the past years, the best of the replicas have fully reproduced the high qualities of the master rulings, except for the blaze efficiency, which is invariably better in a first generation replica than in the master. The quality of replicas has, however, been spotty. The most usual fault has been a slight deviation from flatness which results in serious astigmatism at large angles of diffraction, although the spectroscopic resolution at the proper focus seems to be little affected. Our experience at Sac Peak with large replicas has been very satisfactory. If one insists on rigid specifications for a replica it is now possible to secure one that is in no way inferior to an original ruling, is appreciably more efficient, and, of course, much less expensive. I am assured that we solar astronomers are fussier about our gratings than anyone else, mainly because of our requirement for spatial resolution along the slit as well as high spectroscopic resolution. However, the insistence on stigmatic replicas for astronomy seems to have had a good effect, and the quality of replication has improved notably over the last couple of years.

If we want the very best grating performance, whether from an original ruling or a replica, we are going to have to get used to working with echelles. These are coarse gratings working at high angles of diffraction in high orders, and they call for carefully designed devices for isolating the relatively short free spectral range. Dr. Harrison tells me that the

optimum grating constant is about 79 grooves/mm when he has to balance the problems of thick aluminum coats, diamond loading, and diamond wear. He can blaze this grating at 63° with extraordinary efficiency. At 5000 Å he is working in about the 45th order with a free spectral range of 110 Å.

Right now ruled gratings are the practically available dispersing elements for the classical style of spectrograph. However, promising experiments are under way to produce gratings by a photographic etching process. I do not know very much about this. The lines originate in interference fringes between two plane wavefronts, and the grating constant is controlled by varying the angle between these wavefronts. The fringes are photographed and processed to produce a wash-off relief of successive ridges. When the surface is aluminized we have a grating. I believe there are several difficult problems of flatness and blazing that have not yet been completely solved, particularly for large grating spaces of more than a micron or so. However, this process looks promising and may eventually lead to less expensive gratings.

Gratings are the basic elements in classical types of spectrographs -- nice direct devices that do the job very well in ways that are easy to understand. Now we are hearing about other instruments for observing and measuring spectra, and among them may be some that solar astronomers should investigate. The Fourier spectrograph is certainly the most interesting at present, since it has been spectacularly successful in defining the infrared spectrum beyond the sensitivity range of photography and photomultipliers. I have had no experimental experience with a Fourier spectrograph, so my remarks here are only those of an interested spectator. Although there are possible alternatives, the practical Fourier spectrograph is built around a Michelson interferometer in which the path difference in the two arms varies, either at a steady rate or in steps. When light in a defined spectral band (anything from a few angstroms to some thousands of angstroms wide) is fed in, the resulting curve of transmitted intensity as a function of path difference is the Fourier transform of the spectrum of the incident light. The Fourier spectrograph has advantages over its classical analog, the photoelectric scanning spectrometer. First, the product of angular area of the source and area of aperture can be very much larger than for a normal spectrometer, and the throughput is correspondingly greater. Second, the whole spectrum is measured simultaneously. If detector noise is independent of light intensity, the

whole measurement can be performed in the same observing time as that required for one spectral resolution element in a spectrometer of the same throughput. Thus the speed of the system is greater than that of an equivalent spectrometer by a factor equal to the number of resolution elements in the spectrum, which can be enormous. This is known as the multiplex advantage. Third, in any practical setup the significant signal frequencies that define the spectrum are much higher than those frequencies introduced by scintillation or scattered light. Hence these effects, which can be very troublesome in a spectrometer, are easily and elegantly eliminated from the Fourier spectrogram.

With this rosy picture before us, one may wonder why we are still fussing around with gratings. The multiplex advantage of the Fourier spectrograph is fully realized when the ratio of detector to photon noise is large, since a spectrometer must average the detector noise out for each spectral element separately. This is the situation for infrared detectors, which is the reason for the vastly superior infrared performance of the Fourier spectrograph. The picture is not so clear in the visible spectrum, however, where we have a relatively small ratio of detector to photon noise. As the ratio approaches zero, the speed of the spectrometer approaches that of the Fourier spectrograph. With the detectors presently available for the visible spectrum, it turns out that the Fourier spectrograph has little advantage in measuring a short section of the spectrum from a 1 arc second² area, but if the range exceeds 10 angstroms or so, it begins to realize a fraction of the multiplex advantage, which increases steadily with the wavelength range. Hence for making a spectrum atlas, the Fourier spectrograph has a large speed advantage.

The throughput advantage of the Fourier spectrograph is somewhat diluted by the solar astronomer's penchant for studying very small elements of the solar surface. He can make this up completely, however, with a multiple channel system that observes many small elements of area simultaneously, provided he can deal with the overwhelming data rate entailed. Since the same option is available with the spectrometer, and with the same data rate, there is no real throughput advantage in the Fourier spectrograph unless one is content with the average spectrum for a large area of the solar disk.

Finally, I suspect that the Fourier spectrograph's insensitivity to relatively low frequency fluctuations in light intensity and scattered light is quite a genuine advantage. This alone is a strong reason for con-

Considering the Fourier spectrograph for measuring the visible solar spectrum. The technical difficulties in achieving the resolving power and accuracy of a modern scanning spectrometer are enormous, however. The problems are not too different from those of ruling a grating each time one observes the spectrum. In spite of the fearsome difficulties, Brault at Kitt Peak is undertaking the first attempt at a high resolution visible light Fourier spectrograph, while the cheering section of less courageous souls looks on with interest.

A more recent addition to the solar astronomer's tool kit is the magnetograph. Everyone agrees that solar magnetic fields are fundamentally important, and a number of our theoretical friends express some impatience with the not too smart observers who cannot provide charts of the magnetic vectors at all levels in the solar atmosphere with 10-second time resolution. The Zeeman effect is right there, isn't it? Why don't you get busy and measure it? Well, there are problems, some of them very fundamental such as the finite flux of photons.

No one doubts the importance of determining the magnetic vector, but I think it should be realized that we cannot measure it. What we can measure is the profile of the Stokes parameters across a Zeeman sensitive line. The magnetic vector must be deduced from the resulting data, a process beset with some real uncertainties at present. So as far as instruments go, we need a Stokes polarigraph capable of defining the parameters at enough points in the line profile to define the Stokes profiles with sufficient accuracy for the purpose. Furthermore, a quick calculation shows that the limited photon flux from the solar surface will not allow us the luxury of point measurement, if we require a two-dimensional array of, say, 10^4 magnetic vectors in squares of one arc second and a useful time resolution. We are going to have to measure many such surface elements simultaneously. One can easily enough dream up a digital video scheme with rapidly tunable filters that would do the job. Components with desired qualities presently exist. I am afraid the fulfillment of this dream is still years away because the quantitative requirements are considerably beyond the present capabilities, particularly in video systems. But I predict that these requirements will ultimately be met, and it will at least be possible to construct the dream Stokes polarigraph that simultaneously measures the Stokes profiles of a line in 10^4 one arc second squares with a time resolution of less than 10 seconds. By then, we may not want to because someone

has thought of an easier way.

Meanwhile, let's face the immediate prospects of what we can do right now. The interpretation of the circular polarization in the wings of Zeeman sensitive lines in terms of the sightline field component is fairly straightforward. Most investigators at present are directing their efforts in this direction with variants of the Babcock magnetograph or the Leighton spectroheliomagnetograph.

There are several recent developments of interest. Two of them are efforts to perform the image subtraction required by the Leighton spectroheliomagnetograph method by means of video camera tubes. Leighton himself has assembled an analog system, and Janssens at Aerospace Corporation Observatory has made a digital system. Both have been in preliminary operation with encouraging results, but I believe it is fair to say that the pictures of the magnetic field obtained are not yet as good as those made by photographic subtraction.

I think the most promising advance is due to Livingston at Kitt Peak. He has made a multiple channel magnetograph of the Babcock type, which simultaneously measures the sightline components of the field and mass velocity at 40 points along the slit of the spectrograph. The beautiful pictures of the field he has shown us have spatial resolution comparable with that of the photographic spectroheliomagnetograms, and the accuracy of the photoelectric method. This strong arm approach has been so successful in Livingston's hands that we are building a similar instrument in which the channels can be distributed in a variety of ways between many points along the slit in different spectral lines or at several wavelengths in a single line profile.

Perhaps the best prospect for determining Stokes profiles from which to calculate the full magnetic vectors over an extended field is Alan Title's "spectra-spectroheliograph". This is a stepping spectroheliograph with an exit slit wide enough to transmit a band sufficiently wide to include a whole line profile, which is recorded on a stepping film. This is, of course, an extension of Delandras' Spectro Enregistreur for determining velocity distributions. I believe that Title has used it so far to study the distribution of sightline magnetic components and velocities with very fine spatial resolution better than one arc second. This instrument could clearly be adapted to the measurement of all the Stokes parameters to photographic accuracy, which is certainly sufficient to give a rea-

onable signal to noise ratio in the strong fields of active centers.

The last instrumental item I will mention is the narrow band filter. For years the birefringent filters have been unchallenged here, but new types are making their appearance now. These are all variations of the Fabry Perot interferometer and have fairly stringent angular field limitations. Title has shown that the filtering action of a single Fabry Perot filter is not quite as good as that of a birefringent filter of the same bandwidth, but two Fabry Perot filters in series are better. Practical experiments by Harry Ramsey and Title with two types of solid Fabry Perot filters with pass bands of 1 \AA or less give beautiful pictures of H α detail. There are still some deficiencies in uniformity over the field, but I think these will be eliminated. These filters are now commercially available on a notably shorter time scale than the birefringent filters, which should be an attraction. Unfortunately, they are still quite expensive.

John Ramsay of CSIRO in Sydney has produced a beautiful filter consisting of three conventional Fabry Perot interferometers in series. Each interferometer is held in adjustment and tuned by an ingenious servo system, which is capable of modulating the wavelength of the transmission band over a long spectral range. Any passband from 0.01 \AA up is possible, but the free spectral range of the filter is only about 100 times the bandwidth. Blocking the unwanted transmission bands becomes a serious problem for passbands less than 0.1 \AA wide.

I think the only new development in birefringent filters is the production of achromatic $\lambda/2$ and $\lambda/4$ plates by Zeiss. This removes the only obstacle to full tunability over a very wide spectral range. Zeiss is presently making a filter for Sac Peak that will be tunable over the range from about 4200 to 7000 \AA . The bandwidth is roughly proportional to λ^2 , and is $\frac{1}{2} \text{ \AA}$ at $\lambda = 4200 \text{ \AA}$.

Telescopes, spectrographs, magnetographs, and narrow band filters, with some of their derivatives like spectroheliographs, are the primary optical tools of solar astronomy. We have seen important improvements in all of them over the past 10 or 15 years that have resulted in an enormous improvement in solar observational data. I see no reason to expect the developments of these tools to stop now. But I think we have a great need for a new detector that will have the high quantum efficiency and signal to noise ratio of the best photoelectric surfaces, and record simultaneously

the intensity distribution over an extended field. We could reduce the effects of poor seeing very appreciably with a detector 20 or 30 times as sensitive as a photographic plate. If one is willing to ignore the inconvenience of conducting a campaign comparable to preparation for an eclipse expedition for a set of several photographs, the electronographic camera of the type developed by Lallemand probably comes closest to meeting the need. Other image tubes of various types, and signal generating video tubes find occasional use, but all of them are deficient in photometric accuracy. At present we lack the detector we need, and I hope this will be one of the major developments of the next ten years.

SOLAR INSTRUMENTATION

(PART II)

Richard B. Dunn

Sacramento Peak Observatory

I. INTRODUCTION

Jack Evans has discussed the broad aspects of the state of the art of solar instrumentation in the first part of this joint presentation. In the following I wish to emphasize a few of the facets of the Solar Vacuum Telescope, in particular: (1) the thermal distortion of the window and mirrors; (2) the slit-jaw viewing system on the spectrograph, which represents a typical observing aid presently required by solar astronomers; and (3) recent photographs of the spicules at the limb and on the disk.

II. THERMAL DISTORTIONS

The Vacuum Solar Telescope described by Dunn (1964, 1969) eliminates the turbulence caused by the sun's heat on the optical path of the telescope by evacuating the telescope. The conventional dome is replaced by a "turret" that withstands the elements and is sealed by a vacuum window to form a boundary between the telescope and the atmosphere. In spite of these efforts the image is not perfect due to distortion of the glass vacuum window, which is 34 inches in diameter and 4 inches thick, and to thermal bending of the 4-inch diameter, 8-inch-thick flats made from fused quartz situated in the turret. These and other effects have been described elsewhere (Dunn 1971).

The vacuum window is studied by using the telescope to collimate laser light onto the window. This light is reflected from the two surfaces of the window back into the telescope, which focuses an image of the laser source. A small lens at this focus forms an

image of the window and combines the two reflected beams, one from the outside surface of the window and the other from the inside, to form an interferogram that shows the optical path difference within the window. The window has a slight wedge that causes 76 fringes in the interferograms. These fringes would be straight and evenly spaced if the window were perfect. Shortly after sunlight strikes the window, or if the ambient temperature rises, the fringes show a turned-up edge. By afternoon the edge has distorted by a dozen or so fringes. If a circle could be drawn through one of the central fringes one would have a spherical wavefront, and only the focus would be changed with no loss in image quality. However, Figure 1 (left) shows that this is impossible, and so we have spherical aberration and consequently a "soft" image after several hours exposure to sunlight.

We tried several methods of eliminating the heating of the edge, including shading the cell, insulating the turret, spacing the window away from the metal cell by an epoxy-glass spacer, and insulating the edge of the window. None of these schemes effected any improvement. However, circulating a cooled water-glycol mixture around the edge of the window and cell does appear to solve the problem. Figure 1 (right) shows the state of the fringes after the window was exposed all day to sunlight. The chiller was simply turned on for 5 minutes every 30 minutes, and the liquid was circulated continuously. Ideally the liquid solution should be kept at the temperature of the center of the window. The tolerance on the straightness of the fringes is 1 fringe. This represents a path difference of $1/6$ wave when the window is used in transmission. We plan to add a control system, and perhaps this problem will be solved.

The two turret mirrors have been studied by observing the change in focus of the telescope, which is 14.5 cm after several hours exposure to sunlight. Calculation shows that the mirrors are deformed about 3 waves convex. This would only change the focus of the telescope and not spoil the image if the angle of incidence of the light on the mirrors were 0° . Unfortunately, our mirrors are mounted at 45° and the tolerance for flatness to prevent astigmatism is $1/4$ wave. We must improve the coefficient of expansion by a factor of approximately 10. The present mirrors are fused quartz so the obvious solution is to change to one of the new low expansion materials like "Cer-Vit". Within our operating temperature range (-10° to $+30^\circ\text{C}$), the published curves of coefficient of expansion of Cer-Vit

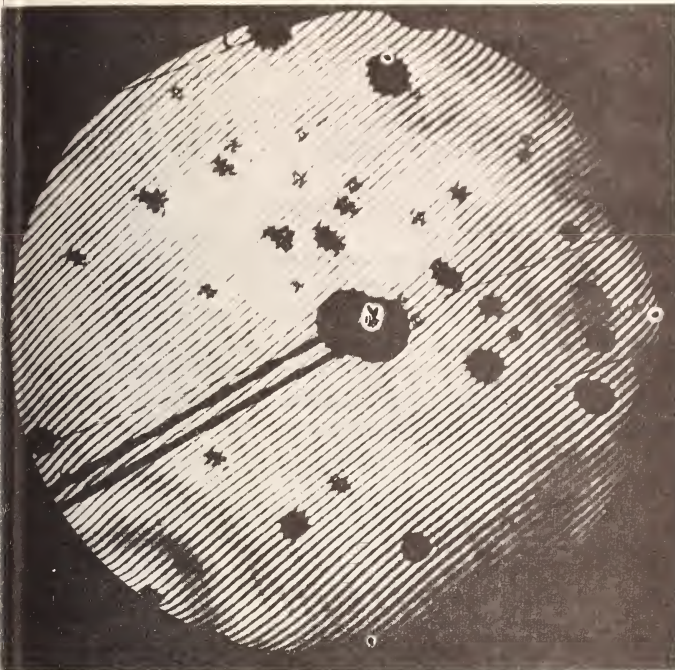


Figure 1. Interferograms of the Vacuum Window: *Left.* Interferogram of the window after approximately four hours exposure to sunlight without cooling. The edge is turned up. The shadow in the center is the mirror and support of the guiding telescope. Sunlight illuminating a piece of black tape near the right edge locally deforms the window. *Right.* Interferogram of the window after approximately four hours exposure with the edge cooled by liquid. Blotches are defects in the coating on the main mirror. (Sacramento Peak Observatory, Air Force Cambridge Research Laboratory)

compared with fused quartz indicate that we would gain the factor of ten required. More recent measurements by Jacobs (1970a), on our new Cer-Vit blanks (see Figure 2), show the published curve is very optimistic and that in fact the entire expansion curve is shifted downwards and to the hot end. This is in agreement with Bradford's (1969) and Jacobs' et al. (1970b) measurements on another sample of Cer-Vit. The slope of the curve is approximately six times greater than advertised, and in the opposite direction. It is actually equal to fused quartz at -10°C ! The coefficient of expansion of the new Cer-Vit mirrors will be enormously improved over fused quartz only near 14°C .

These are two examples of thermal problems in solar telescopes. We expect to obtain greatly improved pictures when we are able to show that the telescope is

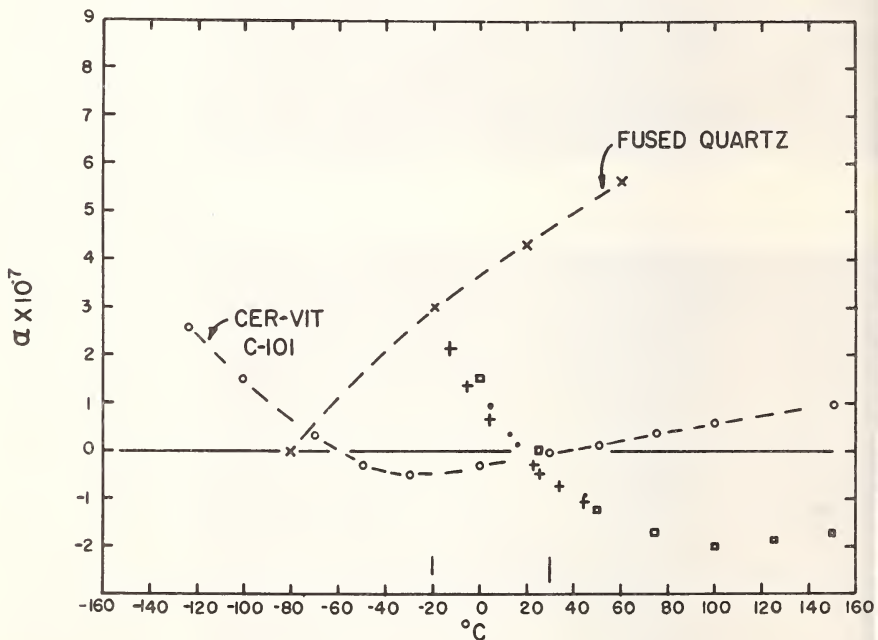


Figure 2. Coefficient of expansion of Cer-Vit and fused quartz. Operating temperature range of the telescope is -10 to $+30^{\circ}\text{C}$. Dashes and circles: Advertised curve for Cer-Vit C-101. Squares: Jacob's measurements on Cer-Vit. Crosses and dots: Jacob's measurements on the center and edge of the Sac Peak Cer-Vit.

eally diffraction limited after the sunlight has shone
n it and through it for many hours.

III. A SLIT-JAW VIEWING SYSTEM

Solar astronomers are often unsatisfied with simply the spectra of an event. We find that they want to see the relationship of their spectra to pictures taken in white light, $H\alpha$, or the K line. We have evolved a unique slit-jaw viewing system that allows simultaneous photographs and viewing of all these wavelengths. In addition it allows the observer to view the white-light image on a TV monitor. The image on the TV is good enough to show the granulation and sunspot details. Thus seeing quality and guiding inaccuracies are clearly visible. The TV image has become indispensable for those observers who want to follow a particular detail or who want to take their pictures only at instants of the very best seeing.

A diagram of the system is shown in Figure 3. Light comes up from the telescope and is reflected by the polished slit jaws down to lens L1. This lens must be large enough to accommodate the field and the expansion of the field at the distance of the lens from the slit jaw. In our case the field is 7.5 cm and the beam expands at $f/72$. A 10 cm diameter lens with a focal length of 87 cm is adequate. This same lens forms an image of the telescope objective in the vicinity of the edge beamsplitter at W_2 . The beamsplitter W_1 consists of an uncoated glass wedge whose front surface reflects 8% of the light to L2 and thence to a white-light camera. Its rear surface reflects 4% of the light to L3 and thence on to a Vidicon TV camera. The remainder of the light is transmitted and strikes the wedge beamsplitter W_2 . Its first surface is coated to reflect 7% of the K light to L4 and to a Halle K-line birefringent filter. The same coating transmits 95% of the $H\alpha$ light to L5 and to a Halle $H\alpha$ birefringent filter. The lens system L6 is flexible and can accommodate magnifications of 1:1 to 1: $\frac{1}{2}$ and also various polarizing optics. L2, L3 and L4 have the same focal length as L1.

The system and its relationship to the spectrograph are shown in Figure 4.

Figure 5 is a picture through the slit-jaw system of a prominence and the chromosphere taken by William Wagner. The slit opening shows as a horizontal gap. Two vertical hairs locate the picture along the slit.

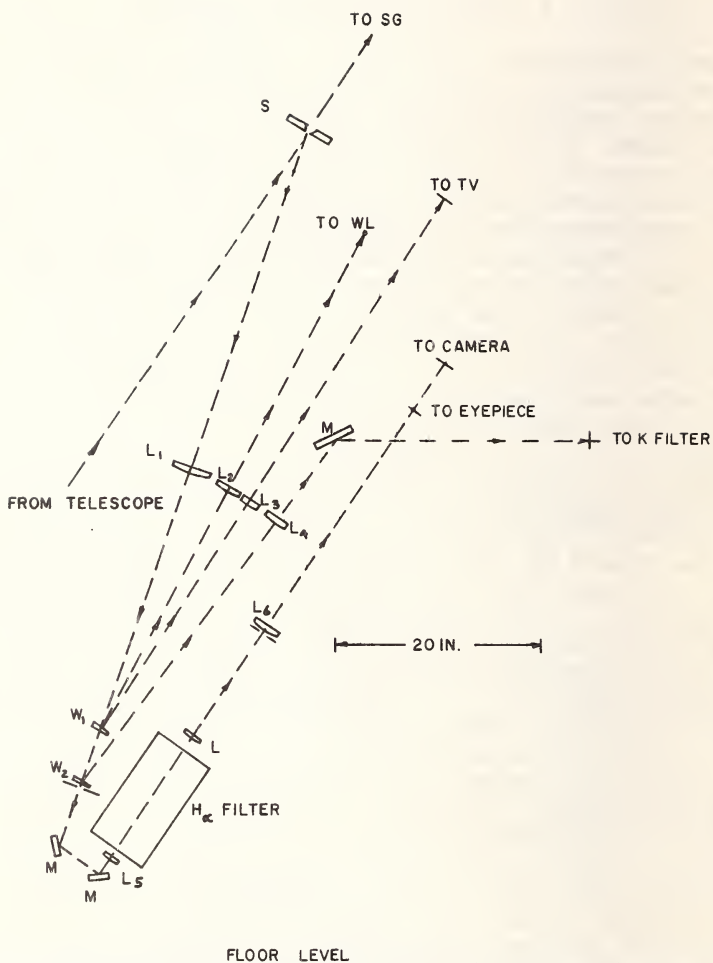


Figure 3. Diagram of the optical system of the slit viewing system.

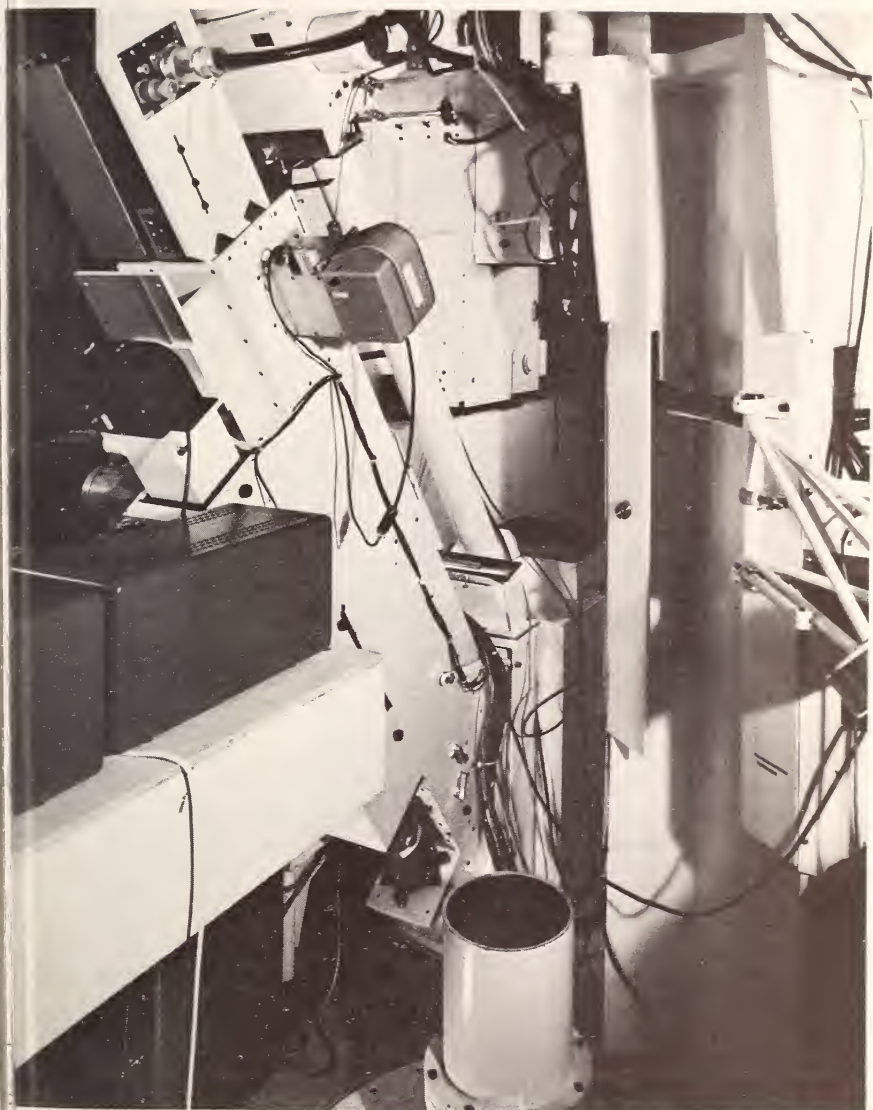


Figure 4. The Slit Viewing System. The TV camera is on the top left. Directly below it is the H α camera. To the right is the white light camera. (Sacramento Peak Observatory, Air Force Cambridge Research Laboratory)



Figure 5. Photograph of prominence taken through the slit viewing system. (Sacramento Peak Observatory, Air Force Cambridge Research Laboratory)

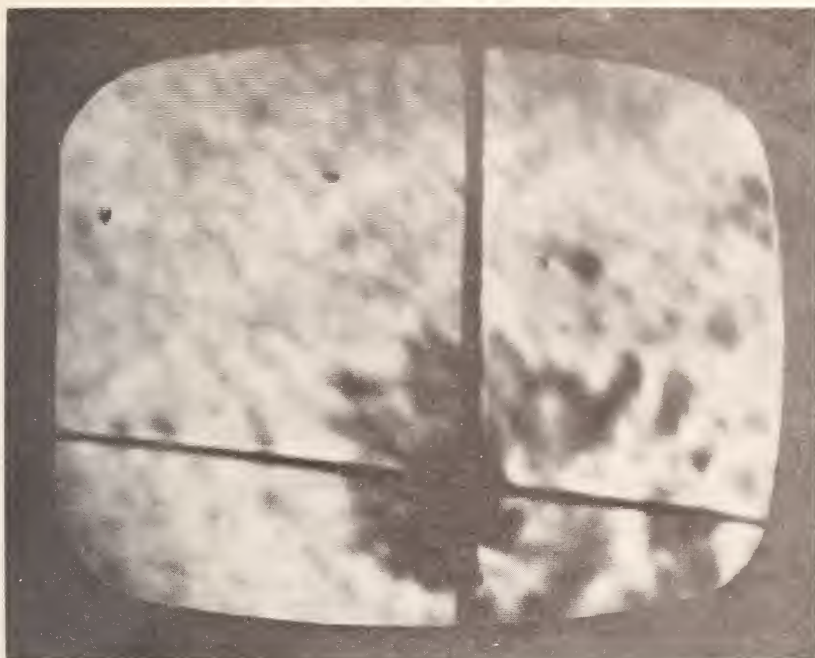


Figure 6. Photograph of television monitor showing granulation and sunspot. (Sacramento Peak Observatory, Air Force Cambridge Research Laboratory)

Scratches on the slit surface are clearly visible to the left of the hairs and show that the surface of the reflecting slit jaw could be greatly improved. Granulation is clearly visible in the picture of the TV monitor in Figure 6.

IV. RECENT PHOTOGRAPHS WITH THE VACUUM TELESCOPE

In spite of the thermal problems described in Section II, we have managed to obtain some fine pictures of the solar granulation and chromosphere in $H\alpha$, especially with the aperture of the telescope reduced from 30 inches to 20 inches to lessen the effects of the solar heating on the window. So far we have not used the new Cer-Vit flats or the window cooling system.

The first scene, Figure 7, is a montage of the chromosphere taken through a $\frac{1}{4}\text{\AA}$ -bandwidth Zeiss filter at different wavelengths near $H\alpha$. Comparison of the plus 1\AA with the minus 1\AA scene shows that spicules are moving rapidly along the line of sight. Since 1\AA near

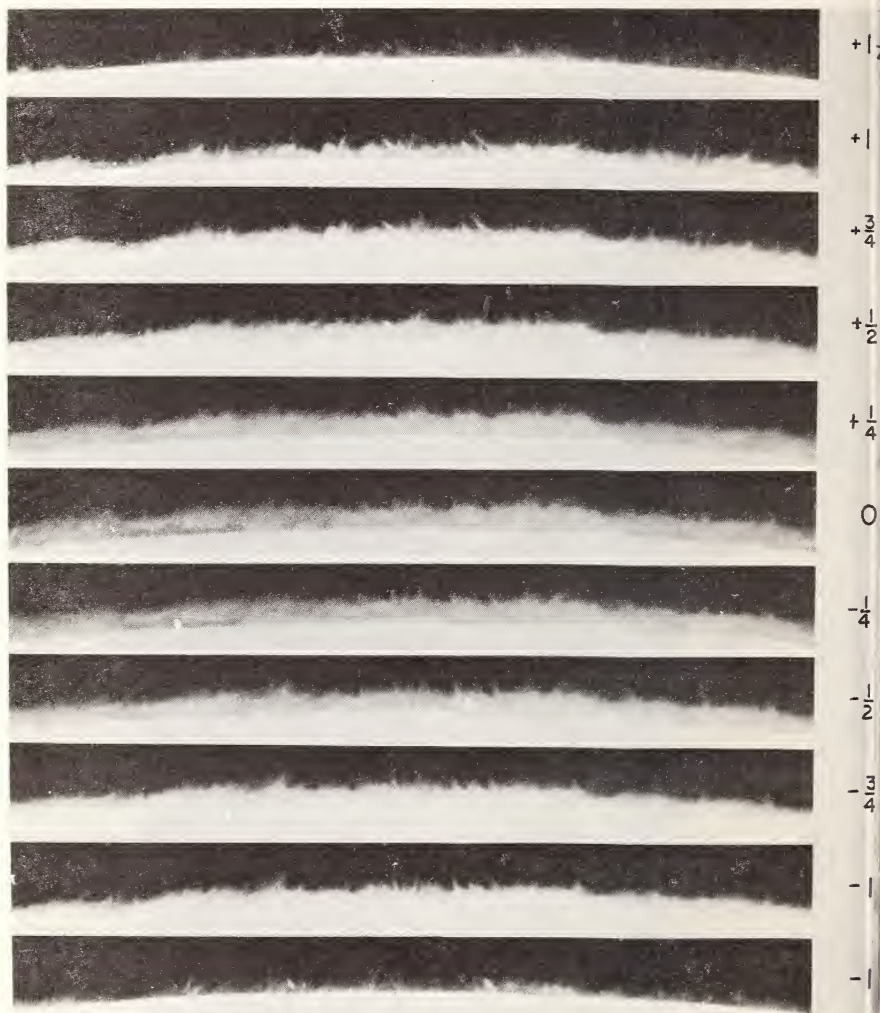


Figure 7. The $H\alpha$ chromosphere at the solar limb take with a $1/4 \text{ \AA}$ bandwidth Zeiss filter tuned through the $H\alpha$ line, Oct. 14, 1970. (Sacramento Peak Observatory Air Force Cambridge Research Laboratory)



Figure 8. The $H\alpha$ chromosphere on the disk with the 4 \AA bandwidth Zeiss filter tuned $+7/8 \text{ \AA}$ off the center of the $H\alpha$ line, Feb. 13, 1971. (Sacramento Peak Observatory, Air Force Cambridge Research Laboratory)

H α corresponds to a radial velocity of 45 km per second, and the measured velocity of spicules in the plane of the sky is about 40 km per second (Lippencott 1957), spicules must be highly inclined. Note the lack of correspondence between the spicules in the plus and minus 1 \AA scenes, which indicates the line profiles are not widened, but are really narrow and displaced by radial velocity. Also note the lack of spicules in the 0 \AA picture. The "gap" near the photosphere is clearly visible in the 1 \AA pictures. Spicules are seen almost detached in the 1 $\frac{1}{2}$ \AA pictures. The "double limb" in the 0 \AA scene is due to continuum light leaking through the filter. This line of demarcation disappears when a 1 \AA interference filter is placed in front of the Zeiss. This montage is a great improvement over the pictures in my thesis (Dunn 1960). Part of this improvement is due to the better telescope resolution, but most is due to the $\frac{1}{2}$ \AA -bandwidth Zeiss filter as compared to the 3.4 \AA -bandwidth filter used in the earlier study. Clearly a 3.4 \AA filter melds all the pictures in the montage together.

Figure 8, taken with the $\frac{1}{2}$ \AA -bandwidth Zeiss filter $7/8 \text{ \AA}$ off the center of H α , shows spicules on the disk. They are seen to form "picket fences" at the edges of supergranule cells. At the base of the spicules one often sees a gap in the spicule and then, in the photosphere, a bright dot very similar to an "Ellerman Bomb" or "moustache" as seen on spectra. Perhaps this picture links Leighton's (1964) picture of the random walk of magnetic fields away from active regions and the motion of Sheeley's magnetic knots (1969) with the H α chromosphere structure and detail. We are anxious trying to obtain movies at various wavelengths of the bright network below the spicules.

These two scenes are typical of many photographs accumulating with this tower telescope.

REFERENCES

- Bradford, James N. 1969, *Ultraprecise Measurement of Thermal Expansion Coefficient*, Technical Report 48, Optical Sciences Center, U. of Arizona.
- unn, R.B. 1960, Thesis, *Photometry of the Solar Chromosphere*, Harvard University.
- unn, R.B. 1964, *Applied Optics*, 3, 1353.
- unn, R.B. 1969, *Sky and Tel.*, 38, 368.
- unn, R.B. 1971, *Optical Performance of the Vacuum Solar Telescope*, presented at the AAS meeting in Huntsville, Alabama, in press.
- acobs, S.F. 1970a, private communication.
- acobs, S.F., Bradford, J.N., and Berthold III, J.W. 1970b, *Applied Optics*, 9, 2477.
- eighton, R.B. 1964, *Astrophys. J.*, 140, 1547.
- ippencott, S.L. 1957, *Smithsonian Contr. Astrophys.*, 2, 15.
- heelley, N.R. 1969, *Solar Phys.*, 9, 347.

THE SOLAR CHROMOSPHERE AND THE GENERAL STRUCTURE
OF A STELLAR ATMOSPHERE

Richard N. Thomas

and

Katharine B. Gebbie

*Joint Institute for Laboratory Astrophysics**

I. INTRODUCTION

The aim of this symposium is to say thanks to Don Menzel for the ideas and people he has launched on the astronomical world. Useful ideas evolve in a successively more realistic sequence. Productive people ensure such evolution. Whether the resulting picture supports or refutes the original ideas is less important than the generation of such a sequence. Evolving ideas and productive people characterize the Menzel school.

As an example, we outline the evolution of the interpretation of the "solar chromosphere anomaly". This interpretation, which began as a purely solar one, now has broad implications as a key to the general structure of a stellar atmosphere. By "solar chromosphere anomaly", we mean certain observed features, first identified in eclipse spectra, that cannot be reconciled with the classical model of the solar atmosphere. We begin by classifying the essential features of these anomalies and then show how Menzel's interpretation in terms of a collision-free atmospheric appendage has evolved into a more general one in terms of an arbitrary atmosphere diagnosed by what we call the "new spectroscopy". By linking the diagnostic methods of the new spectroscopy to some of Menzel's suggestions on the interpretation of symbiotic spectra, we extend the evolution to a general stellar model. By invoking the concept of transfer and population effects, we distin-

*of the National Bureau of Standards and the University of Colorado.

guish those aspects of the solar chromosphere anomaly that are peculiar to the chromosphere as a distinct region from those that are common to the atmosphere as a whole.

The evolution of the interpretation of the solar chromosphere anomaly reflects a more general evolution in the whole approach to stellar atmospheres. It began with the classical approach, and has, for some of us, culminated in an interpretation of the atmosphere as a transition region between the interior of the star and the interstellar medium. Classically, the atmosphere was viewed simply as the surface of the stellar interior and was assumed to be described by the same state parameters as were used to construct the interior model: pressure, density, and temperature. The single aim of the associated diagnostics was to determine the boundary values of these parameters. Model atmospheres were, by assumption, constructed in terms of these parameters and the relations between them that were used for the interior model. Viewed, however, as a transition region extending from the deepest observable layers to some point at which the star ceases to be the dominant influence on the medium, the atmosphere includes chromospheres, coronas, shells, nebulae, circumstellar dust, and any other phenomena controlled primarily by the star. Here the state parameters and the relations between them must be determined, and a diagnostic procedure developed to obtain the distribution of these parameters from all the available observations. Similarly, the construction of models must be attempted without any a priori assumptions either on the state parameters or the relations between them. In practice, because of our lack of experience with such transition regions, the empirical analysis of observations must go hand in hand with the theoretical construction of models.

Initially the classical atmosphere was thought of as a thin homogeneous surface layer throughout which the interior state parameters were constant at their boundary values. The debate over whether such a model was consistent with the observations first arose over the implications of the existence of a line spectrum. Could a line be produced by scattering in an isothermal atmosphere (Schuster-Schwarzchild) or did its presence require a temperature gradient in the observed layers (Milne-Eddington)? The view prevailed that it did require a temperature gradient, and diagnostic methods based on a non-homogeneous model, but one locally in thermodynamic equilibrium, were introduced to interpret the observations.

The essential characteristic of the classical approach was the use of conventional thermodynamic equilibrium parameters to describe the observable atmosphere. The approach was defined by the five assumptions: local thermodynamic equilibrium for the microscopic distribution functions of matter (LTE-R), hydrostatic equilibrium (HE), radiative or quasi-static convective transport of energy (RE or CE), a spherically symmetric atmosphere (SS), and the absence of macroscopic electric and magnetic fields. The essential physics of this approach is developed in Unsöld's book, *Physics of Stellar Atmospheres*, which, properly supplemented by subsequent developments in atomic physics and computing techniques, remains the classic reference in the field today. The approach has been used to investigate the variation, as a function of T_{eff} , g , and abundances, in the boundary values over the Hertzsprung-Russell plane. If the physical basis of the approach were sound, these analyses would provide the essential link between the observations and their interpretation in terms of atmospheric structure and evolution. If, however, the classical assumptions are not valid, the results of these diagnostics provide only a preliminary survey, the meaning of which remains to be assessed. Not only may the derived values of the parameters be unreliable but in particular their physical significance may also be in question. Such ad hoc parameters as turbulence, excitation and ionization temperatures, and mixing lengths have been introduced to reconcile the observations with the classical model, but the self consistency and influence of these parameters on the state of the gas has not been satisfactorily explored.

If, on the other hand, the atmosphere is regarded as the transition region between the stellar interior and the rest of the Universe, all those phenomena associated in any way with the domain of influence of the star must be taken into account. The innovation of Menzel and his early collaborators was that in analyzing stellar spectra and constructing stellar models, they implicitly attached as much weight to the chromospheric anomaly, symbiotic spectra, circumstellar shells, and nebulae as to the Fraunhofer spectrum of the star itself. Their early results gave insight into the kind of microscopic interactions that are important in gaseous matter under atmospheric conditions.

At this point, we should perhaps ask whether we are discussing two different but equally valid approaches to a stellar atmosphere, each of which fulfills the purpose for which it was designed. Can the solar atmosphere, for example, be divided into two ind

pendent regions? The lower region would then produce the observed disk spectrum; its structure would be obtained, and its spectrum analyzed, by the classical approach. The upper region, including all the other phenomena in our more extended definition of an atmosphere, would require more general diagnostic methods and data but would in no way affect either the lower region or the disk spectrum. The significance of the solar chromosphere anomaly lies in the answer it provides to this question.

Until recently, most people would have agreed that such a division of the atmosphere was indeed possible. About a decade ago, however, the results of a long-range program of observation and analysis proved to the contrary, showing conclusively that the chromosphere does seriously affect the disk spectrum (Thomas and Athay 1961). The observational approach was a refinement of that pioneered by Menzel (1931) and developed by his students (Evans, Roberts, and Thomas 1950-51). The diagnostic approach evolved from a viewpoint introduced by Menzel and his associates (Menzel 1931; Cillie and Menzel 1935; Goldberg and Menzel 1948), as extended and refined by his students (Thomas 1948 et seq.; 1950 et seq.). The results of this program showed that (1) as a part of the atmosphere that affects the disk spectrum, we must include a definite region called the "chromosphere", the structure of which is fixed by conditions that violate a number of the assumptions defining the classical model, and (2) there are also parts of the disk spectrum formed in regions below the chromosphere to which the classical diagnostic methods are not applicable.

It is being gradually accepted that neither of these two conclusions is peculiarly solar, but rather that the solar chromosphere anomaly is of great significance for our general picture of a stellar atmosphere. Although the original solar investigations focused on the first conclusion, it is the second that has been more widely accepted in the stellar context. In essence, the second conclusion implies that the assumption of LTE-R should be dropped. It is now becoming fashionable to build models of a classical atmosphere without this assumption; that is, the "New Classical Atmosphere" (Mihalas 1970). That the assumption of LTE-R is untenable was demonstrated by some of us from the Menzel school who, using the solar disk spectrum, showed that LTE-R precluded a self-consistent interpretation first of the chromospheric lines, then of all lines for which the optical thickness at the line center exceeded about one, and then of the chromospheric

continuum. By establishing the theoretical basis for the empirical conclusions, we showed the results to apply to stars as well as to the Sun. We suspect that this conclusion has now become popular mainly because models can in some cases be computed as accurately without LTE-R as with it. The problem remains, however, that again some of us from the Menzel school have shown that the assumptions of hydrostatic equilibrium, radiative (or convective) equilibrium, and spherical symmetry are also invalid in parts of the solar chromosphere, and a great variety of observational work on solar magnetic fields indicates that the remaining assumption of the classical model is also doubtful. Furthermore, we now realize that the whole rocket UV, the far-infrared, and the radio spectrum of the Sun all originate in the chromosphere and corona. Thus "chromospheric effects" on the "normal disk spectrum" can be ignored only if the "normal spectrum" is limited to the visible continuum and weak lines. We doubt that even the strongest proponent of the classical atmosphere would maintain such a position.

We conclude then that in any model of the solar atmosphere, some of the classical assumptions must be dropped in almost all of the atmosphere, and all of the classical assumptions must be dropped in some of the atmosphere. We suggest this may also be true for most stellar atmospheres. Is it perhaps significant that model builders are now apparently willing to construct wholly theoretical model atmospheres for any star *except* the Sun?

In Section II we review the observations and ideas that have led to the rejection of each of the classical assumptions in the solar chromosphere and discuss our replacements for them. In Section III, we suggest how this overall picture of the chromosphere clarifies our general picture of a stellar atmosphere.

II. THE SOLAR CHROMOSPHERE ANOMALY

There are two ways to try to resolve the chromospheric anomaly. The first way is to examine individually the validity of each classical assumption, theoretically and empirically. Unfortunately, we don't know enough about the character of transition regions in astronomical environments to treat the theoretical problem in full generality; and since the assumptions are coupled in their observational consequences, a

wholly empirical approach is ambiguous. A second way to try to resolve the anomaly is to abstract the essential features of all the observed anomalies into a few coherent groups. It is this approach that in practice has proven the more productive. Indeed, the evolution of Menzel's original ideas into our present picture reflects the evolution of the categories into which the anomalies have been grouped and of our understanding of the implications of these categories.

A. *The Observed Anomalies*

1. *Emission Height Gradients.* Anomalously low emission height gradients as observed at eclipse in both lines and continua, and the variation in these gradients with excitation and strength of lines, and among the various lines and continua.

Menzel was the first to obtain extensive eclipse data of sufficient precision to allow a quantitative determination of these well-known qualitative effects. Subsequent HAO-Sac Peak eclipse expeditions increased the accuracy and height resolution to the point where differential values of emission height gradients could be investigated as functions of excitation and line strength. At atmospheric densities predicted by the classical model, these observed emission gradients should not be affected by self-absorption and could therefore be identified with the gradients of the occupation numbers. If these gradients were in turn identified with the total density gradient, it would be lower by factors of up to ten than that predicted by a purely thermal classical model; the same density gradient interpreted on the basis of a "turbulence" arbitrarily introduced into the classical model implies supersonic velocities for the turbulent elements. If, on the other hand, the gradient of the occupation numbers is not identified with the density gradient, the implication is that the excitation and ionization increase for some lines and decrease for others in the same atmospheric region.

2. *Excitation State.* Anomalous relation between emission in lines and continua of the same ion as observed at eclipse, and anomalous intensities and structures of the cores of strong lines as observed on the disk and at the limb.

Eclipse observations in the H⁻, Balmer, and Paschen continua, interpreted simultaneously, give temperatures and densities inconsistent with the classical model. Nor do combined observations of the Balmer lines and continuum give occupation numbers for the

energy states of hydrogen that are consistent with the classical model. Recent observations of the Lyman continuum lead to the same conclusions.

Interpreted on the basis of an unblanketed classical model, disk observations of certain lines (Na I and the hydrogen Balmer lines) imply temperatures of up to about 1300°K below those predicted, while others (Ca II) require that the temperature first decrease, then increase, and then decrease again. The appearance of emission lines on the disk, such as those observed in the rocket UV, has no interpretation on the basis of a classical model.

3. *Ionization State.* The observation of ions that should not exist.

The earliest example, often emphasized by Menzel, is the presence of He I and He II lines. Identification of the coronal lines by Edlèn intensified the problem, and more recently many more such ions have been identified from the rocket UV spectrum in both the corona and chromosphere.

4. *Inhomogeneities.* The presence of inhomogeneities in at least the upper chromosphere.

Menzel's early picture of the upper chromosphere was that of a "burning prairie". Later studies at HAO and Sac Peak defined this phenomenon more specifically in terms of the properties of the spicules. Additional evidence is obtained from the anomalous emission in different lines and continua as observed at the solar limb during eclipse.

B. *The Implications*

This grouping of the observed anomalies suggests the following implications for the structure of the atmosphere and our interpretation of it. (1) Those parts of the atmosphere that contribute to the observed spectrum, including the disk spectrum, extend to greater heights than would be predicted from the solar gravity and effective temperature on the basis of the classical model, which thus represents at most some lower part of the atmosphere. (2) Either the distribution of excitation is quasi-random or this effect is an artifact produced by faulty diagnostics. (3) The energy available for ionization is greater than the classical limit set by the effective temperature. (4) The outer atmosphere is unstable against the production of inhomogeneities. Whether the instability arises in radiative processes or in a differential input of non-radiative energy or momentum or possibly in other sources, remains to be established.

Thus to resolve the chromosphere anomaly, we must identify, describe the operation of, and assess the relative importance of those effects that can cause a real or apparent distribution of absorbing and emitting atoms to differ from that predicted by the classical model. Because the distribution of excited atoms reflects the distribution of both density and excitation, we must specify the factors that fix the density (input of kinetic energy and momentum, and the stability of a homogeneous structure against their differential input) and those that fix the excitation (input of internal energy and its partition). The classical assumptions impose a particular set of relations that fix these distributions in a way that requires no knowledge of the details of the microscopic processes; but in doing so, these assumptions are all coupled in their effect on any empirical test of their validity. Because equipartition is assumed for the kinetic and internal energies, and it is assumed there are no microscopic, non-quasistatic velocity fields, the density and excitation distributions are completely coupled and measured by the distribution of the single parameter, T_e . Thus we seek a more general approach in which there is neither coupling between nor restrictions on the distributions of density and excitation. To approach the problem in full generality is impractical. We do, however, have the observational guide that the anomaly increases outward in the atmosphere, whereas the applicability of the classical model improves with increasing depth. Furthermore, there is nothing in the structure of the classical assumptions that incorporates an effect of the boundary. Since the chromosphere, as part of the transition region, appears to have many of the physical properties associated with a true non-adiabatic boundary, a first logical step toward understanding its structure would be to include boundary effects in such a way that the structure produces the chromospheric anomalies at large heights and approaches the classical model at great depths. We now examine the character of a chromosphere viewed as such a transition region.

C. The Chromosphere as a Transition Region

The presence of a non-adiabatic boundary may affect a system in two ways. First, the exchange of energy at the boundary will, in general, result in an energy flux that causes a gradient in the state parameters. Second, the microscopic rate processes that determine the density and excitation distribution func-

tions will become inhomogeneous and so depart from detailed balance.

We consider first the effect of an energy flux. In an adiabatically bounded system, there is no energy flux; the particle concentrations and the distribution of internal energy levels may vary with position, but the temperature and excitation are uniform, fixed wholly by the total energy of the system. In a stellar atmosphere, however, which is characterized by a non-adiabatic boundary and an energy flux, the excitation at each point depends upon: (1) the amount of energy available to be absorbed, (2) the amount of energy actually absorbed, and (3) the process by which the absorbed energy is apportioned over the various energy states. The amount of available energy is fixed by the transport processes, and the amount of energy absorbed is fixed by the density and relative populations of the energy levels, which also describe how the energy is apportioned. Transport and population processes are, in general, coupled. The classical approach restricts the kind of coupling: LTE-R describes the absorption and partitioning of the available energy; radiative equilibrium, hydrostatic equilibrium, and spherical symmetry specify the available energy by eliminating all but radiative transport processes. A more general approach, from which these assumptions are removed, must make possible the calculation of (1) to (3) in terms of the total energy flux and certain other properties of the star that remain to be determined. According to the classical approach, T_{eff} and g suffice.

We consider next how the presence of the boundary introduces inhomogeneities into microscopic processes causing departures from detailed balance. There are four such effects: (1) Radiative processes reflect the boundary-induced asymmetry in the radiation field and the effects of the resulting discrepancy between color and density of radiation often referred to as dilution effects. (2) Collision rates will decrease with decreasing density; hence there will be an increase in the relative importance of radiation rates. (3) Aerodynamic motions will amplify with decreasing density, ultimately providing a non-radiative energy source with a potential for excitation that is not necessarily related to that of the radiation. (4) These aerodynamic motions, together with any material instabilities associated with radiative effects, may induce geometric inhomogeneities, hence additional boundaries.

To include these boundary effects, we must, in practice, combine two approaches: (1) a synthetic approach, in which theoretical models incorporate these

fects, and (2) an analytical approach, in which a diagnostics is developed to infer empirically the relative importance of the effects. In the latter approach, a major problem has been to avoid imposing diagnostic methods that, while more general than those of the classical model, still pre-condition the derived results. In the following sections, we consider Menzel's original suggestions and then show how they have evolved to our current approach.

The original Menzel approach

At the time the Menzel school began to worry about nonclassical effects, astronomers implicitly assumed that collisions maintained LTE-R in a stellar atmosphere. Any departure from LTE-R would then be expected to occur in low-density regions, where, it was also assumed, the optical depth in all but the Lyman continuum and lines was sufficiently small that the continuum radiation field could be described as the product of a dilution factor and a Planck function characteristic of the central star. In their initial investigations, therefore, Menzel and his early collaborators considered only the first and second effects of the boundary on the microscopic processes in a pure hydrogen atmosphere (Menzel 1937 et seq.; Cillie and Menzel 1935). This limitation appeared to be justified by observation: the excited energy levels in planetary nebulae and in the solar chromosphere appeared to be underpopulated relative to the local value of T_e , in accordance with the theory of recombination in a dilute radiation field.

The electron temperature, T_e , in planetary nebulae is determined by the balance between "dilute" photoionizations in the Lyman continuum - a non-LTE process - and free-free radiative transitions - an LTE process - in radiative equilibrium. Thus the computed value of T_e lay below the radiation (or "color") temperature of the central star, its value in a collision-free region, but well above its LTE value as determined by the energy density of the radiation field. Embarrassingly enough, this approach was not applied to non-nebular atmospheric regions until 1963 when it was reintroduced by Cayrel who applied it to the H^- free-bound continuum of the solar chromosphere. It is interesting for the evolution of the classical model that if the collision-free solution were valid down to $\tau_e \approx 1$, and if there were no LTE processes, the model would closely resemble that of the Schuster-Schwarzchild isothermal atmosphere.

Such an atmosphere would include everything we have defined as the transition region, including the solar chromosphere and planetary nebulae. The presence of lines would not affect this picture as long as they were formed by pure scattering. Thus we see that deviations from such an isothermal atmosphere arise from collisions, from non-scattering processes in line formation, and from deviations from radiative equilibrium.

In both the prediction and interpretation of the Balmer and Paschen spectra, the error of the Menzel approach lay in assuming the solar atmosphere to be optically thin in the Balmer lines. An empirical analysis (Thomas 1950) allowing for a non-zero opacity in these lines showed the energy levels $n \geq 3$ to be over rather than underpopulated. A theoretical analysis (Thomas 1949) showed that the partition of energy among the internal degrees of freedom was controlled by the radiation field in the Balmer lines. Thus the stage was set for the modern non-LTE approach in which the populations of the energy levels and the transfer of radiation are inescapably coupled. Because this approach in terms of a collision-free region with a dilute radiation field suffices for the Balmer, Paschen and higher spectra, it gives information on the partition of energy over the discrete energy levels, but not over the energy levels of the electron continuum. Thus it is relatively insensitive to T_e .

2. *Subsequent evolution*

The most significant empirical extension of Menzel's work was that of the HAO-Sac Peak eclipse expeditions of 1952 and 1962. The aim of these expeditions was first to repeat Menzel's 1932 observations with greater accuracy and height resolution and second to extend his analysis along the directions just summarized. The primary idea was to adopt the above approach to an empirical analysis of the Balmer and Paschen continua and lines, but to treat the Lyman region theoretically (Pottasch and Thomas 1959) in order to obtain the ionization equilibrium for hydrogen. Combined with an analysis of the H^- continuum, this approach gave an accurate interpretation of the energy in the continua, i.e. of T_e .

At this point, one had for hydrogen an empirical measure of the partial distribution of an unspecified total amount of energy. By not forcing the value of this total energy to be that of the radiation field, but rather by comparing the empirical T_e with values

limited by radiative equilibrium, one obtained an empirical measure of the validity of radiative equilibrium. It is interesting that this empirical analysis, incorporating for the first time a correct treatment of coupled line and continuum effects, produced a $T_e(h)$ distribution toward which the various subsequent models seem to be converging (Utrecht Reference Photosphere 1954; Bilderberg Continuum Atmosphere 1968; Revised Bilderberg Continuum Atmosphere 1969; Harvard-Smithsonian Reference Atmosphere 1971). In Figure 1, we reproduce this model (Thomas and Athay 1961) together with other representative models. The outstanding success of this model was that its wholly theoretical prediction of the Lyman continuum of hydrogen came within a factor of two of the observed value. The subsequent models, all of which include some part of the classical assumptions, still failed by several orders of magnitude to predict the Lyman continuum. The current models based explicitly on the Lyman continuum (Boyes and Kalkoven 1970) and one including the effect of spectral lines in the rocket UV (Avrett, Vernazza, and Chipman 1970) predict a $T_e(h)$ distribution very close to that of the 1961 model.

In extending the non-LTE approach to the Lyman region, one had to take into account the third effect, the boundary on the microscopic processes; namely, a possible difference in energy between collisional and radiative processes. In doing so, one had extended the Menzel approach to include all such effects except a geometrical departure from spherical symmetry. And when this effect could be studied from the eclipse observations by comparing the free-bound emissions in hydrogen and He I (Athay and Menzel 1956), and the emission in neutral and ionized metals (House 1961). These comparisons provided evidence for departures from spherical symmetry at heights of about 1500 km and possibly even as low as 750 - 1000 km.

To analyze Balmer and higher lines in the disk spectra, we extended the Menzel approach to opaque but still collision-free atmospheric regions. The evolutionary step was the recognition that it was necessary to solve equations of radiative transfer in order to obtain either the source function or the occupation numbers of the energy levels; that is, it was finally accepted that radiative processes in the line dominated all other terms in the source function. In the transfer equation for the radiation field in the line, the photoionization terms became recognized as source and sink terms rather than as competitive processes in fixing the numerical value of the source function at a

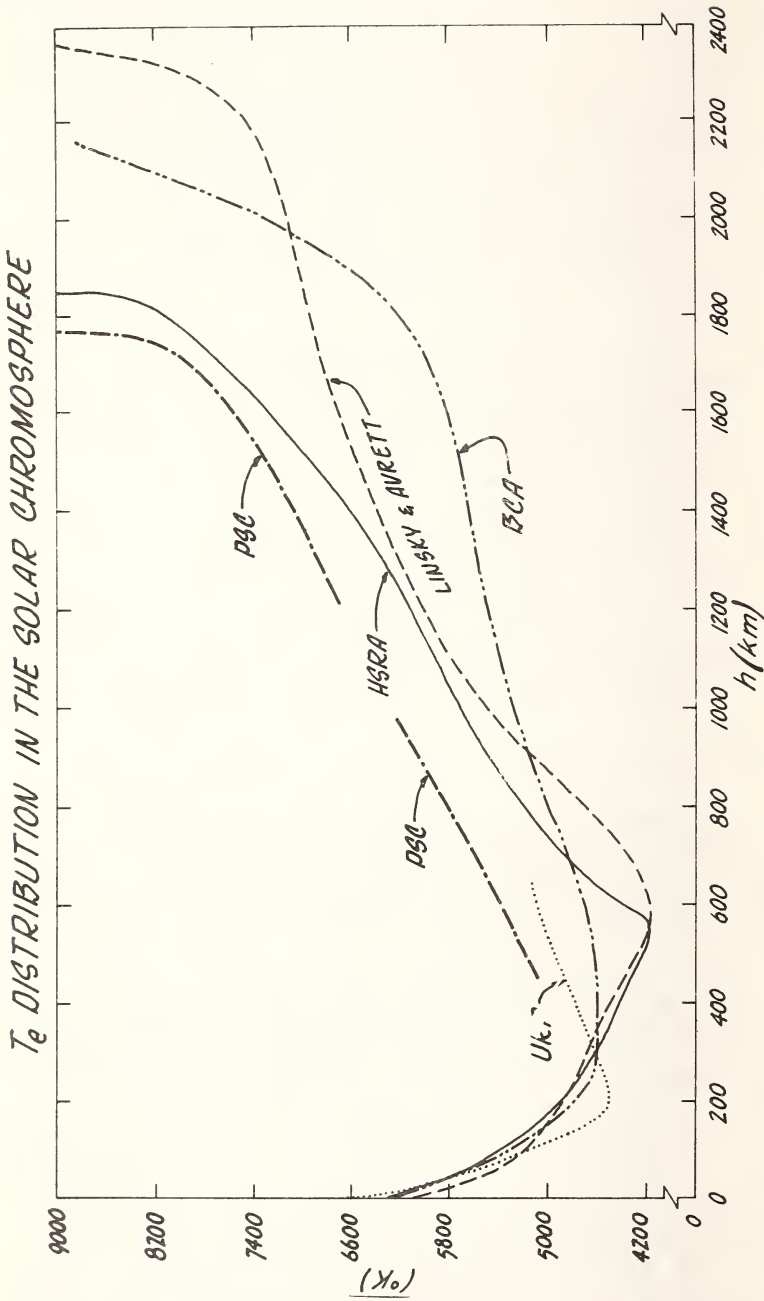


Figure 1. PSC - "Physics of the Solar Chromosphere" (Thomas and Athay 1961); URP - Utrecht Reference Photosphere; BCA - Bilderberg Continuum Atmosphere; HSR - Harvard-Smithsonian Reference Atmosphere; Linsky and Avrett (1970). In placing the PSC model on the same scale, we

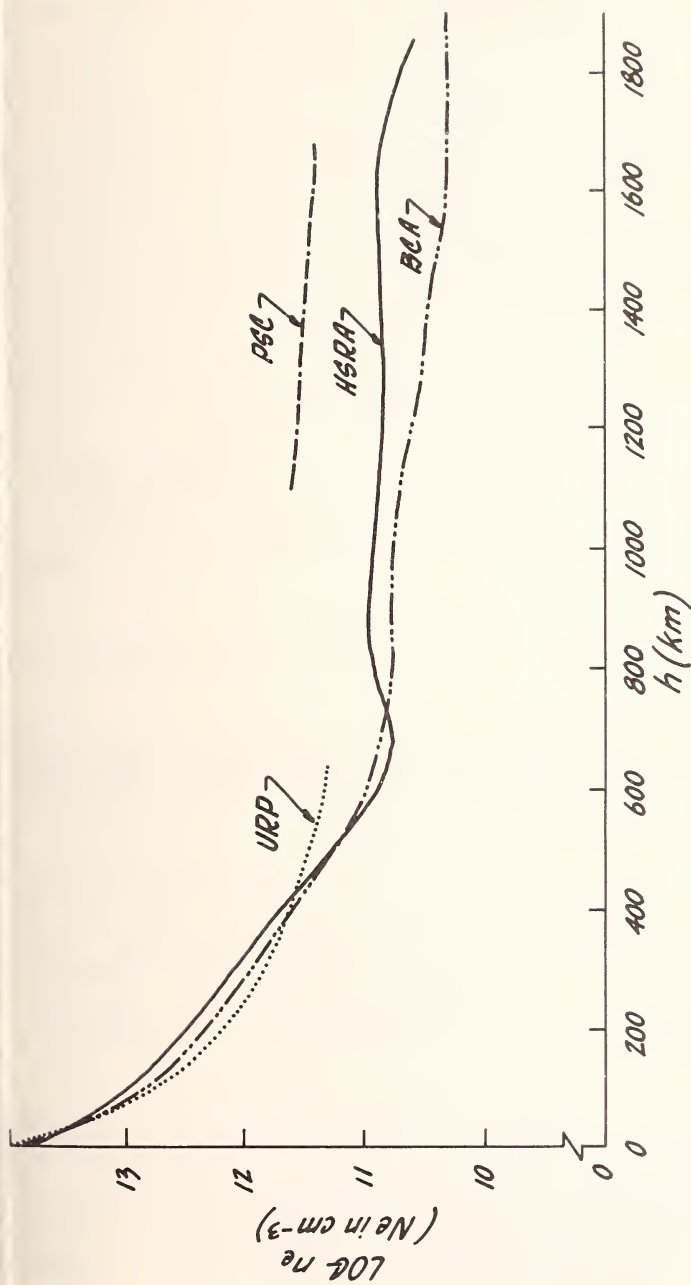


Figure 2. PSC - "Physics of the Solar Chromosphere" (Thomas and Athay 1961); URP - Utrecht Reference Photosphere; BCA - Bilderberg Continuum Atmosphere; HSRRA - Harvard-Smithsonian Reference Atmosphere. Height zero is at $r_{5000} = 1$. In placing the PSC model on the same scale, we have shifted its height zero by 410 km.

n_H DISTRIBUTION IN THE SOLAR CHROMOSPHERE

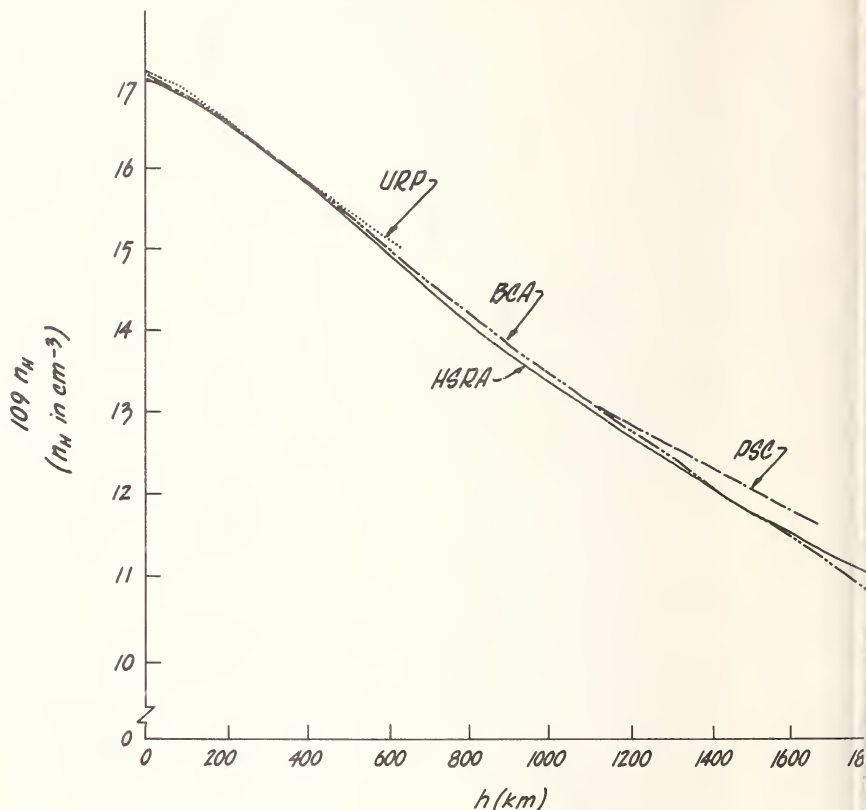


Figure 3. PSC - "Physics of the Solar Chromosphere" (Thomas and Athay 1961); URP - Utrecht Reference Photosphere; BCA - Bilderberg Continuum Atmosphere; HSRA - Harvard-Smithsonian Reference Atmosphere. Height zero is at $\tau_{5000} = 1$. In placing the PSC model on the same scale, we have shifted its height zero by 410 km.

given point. Because the source function is thus "controlled" by photoionization rather than by the local value of T_e , the population of the Balmer ground state increases and with it the importance of self-absorption effects. Thus both empirical analysis and theoretical computation indicated an over rather than an underpopulation of the energy levels, as had been implied in earlier investigations. The change came, however, from

rying Menzel's original approach to its logical conclusion.

In contrast to the above extension of Menzel's collision-free approach, the interpretation of the disk profiles of such lines as H and K of Ca^+ and Mg^+ (Jefferies and Thomas 1959) extended the approach followed in the analysis of the Lyman eclipse data. This presents an application of the third effect of the boundary on the microscopic processes, greater energy collisional than in radiative excitation, which reflects a coupling between departures from radiative equilibrium and LTE-R. However, we found that, as with the photoionization effect for the Balmer lines, this collisional effect was manifested through the source and sink terms in the transfer equation for the line and not, as in LTE-R, directly in the source function. As both collisionally controlled and collision-free treatments of the disk spectrum could be incorporated into the same general framework (Thomas 1957; Jefferies and Thomas 1959 et seq.; Thomas 1965; Jefferies 1968). In a rough sort of way, this uncouples the departures from the various classical assumptions. The non-LTE approach gives the general form of the source function

$$\text{source function} = \frac{\text{radiation field considered} + \text{source terms}}{1 + \text{sink terms}}$$

together with expressions for the source and sink terms and functions of the state parameters. To determine the permitted range in values of these state parameters and the influence of the source and sink terms, we study departures from hydrostatic equilibrium, radiative equilibrium, and spherical symmetry.

Integration of theoretical investigations

Just as the various observational anomalies could be grouped into four classes, so the different theoretical investigations can be brought together into two categories. Those in the first category, which has been called the "new spectroscopy" (Thomas 1965), aim at classifying the types of source and sink terms that exist and identifying them with the kinds of profiles of H lines and continua they produce in different atmospheres. As such, this approach is concerned with what appears to be the unsystematic distribution of excitation with height. The investigations in the second category aim at determining those factors that fix the val-

ues of the state parameters and hence at selecting those components of the source and sink terms that control the source function in any given situation. This approach is concerned with the absolute level of excitation and ionization, the density distribution, and possibly the departure from spherical symmetry. The first approach has been developed to a considerable extent; the second is in a less advanced stage.

(a) *The new spectroscopy.* This approach arose from attempts to systematize the methods for predicting the kind of profile expected of a given line or continuum in a given atmosphere. It consists of classifying the various transitions, ions, and atmospheres according to the physical processes controlling the source function. Such a classification is essential in identifying those atmospheric parameters about which information can be obtained from the analysis of a given spectral line or continuum.

In LTE, the spectroscopic behavior of a small volume element depends only on the local values of temperature, density, and chemical composition; except for the effect of electron scattering, it does not depend on the radiation field. The observed spectrum depends only on the distribution of temperature throughout the atmosphere. Density and composition determine the atmospheric region, hence the range in T_e , that is observed in the line or continuum of a given ion. Thus for a fixed chemical composition but an unspecified distribution of temperature and density, the relation between the location of a volume element and its spectroscopic state is two dimensional. But if to the assumption of LTE, we add the other assumptions of the classical model, we force both the temperature and density to decrease monotonically outward. Then the relation between the position of a volume element and its spectroscopic state is one dimensional. In this case, a sequence of lines and continua arranged according to their depth of formation would show a monotonic change in excitation, and conversely.

Without the assumption of LTE, the spectroscopic behavior of a small volume element depends not only on the local values of the temperature, density, and chemical composition, but also on the radiation field. The radiation field, in turn, depends on the physical properties of the surrounding atmospheric regions, in particular on the distribution of source and sink terms. The kind of source and sink terms that control a given line or continuum will depend on the properties of both the ion and the atmosphere. Hence there is no longer a one-to-one correspondence between the excitation of a

ine and its depth of formation, nor do the usual criteria for excitation level necessarily apply. For example, absorption lines with emission cores (collision dominated) may arise in the same atmospheric regions as absorption lines without emission cores (of which some are photoionization dominated). Thus the apparently random behavior of excitation with height - an important feature of the chromospheric anomaly - reflects simply the dependence of the spectroscopic state of a volume element on its environment and on the ionic configuration of the gas. The aim of the new spectroscopy is to develop systematic methods for introducing order where there appeared to be none. We study the apparent excitation level as a function of position in an atmosphere in which the distributions of T_e , n_e , and chemical composition are specified.

We first determine whether there are atmospheric regions in which collisions dominate over radiative processes in all transitions. If so, these regions are in TE-R. In most stars, any such regions occur only in the deepest photospheric layers; for some stars, they may occur throughout most of the photosphere; but they never occur in a chromosphere. In those atmospheric regions that are not collision dominated, there are, then, transitions with source functions that depend on the radiation field in the transition. Thus the distribution functions are coupled to the radiation field, and it is necessary to specify the details of this coupling. These details will depend on whether the atmospheric region produces its own radiation field in the given transition, i.e. on whether its optical thickness is greater or less than about one in the transition. If less than one, the source function is controlled by the external radiation field, and we study the region producing this field: for example, in all but the Lyman region, the radiation field in a planetary nebula is produced by the central star. If, however, the optical depth in the transition is greater than one - as occurs often in the solar chromosphere and the cores of all strong lines on the disk - the radiation field is determined by the distribution of source and sink terms. The aim then is to identify these terms and hence the processes, collisional or radiative, that fix them for the particular transition in a given atmosphere.

Since, in general, the ion must be treated as a whole, and since the source and sink terms for its various lines and continua may be coupled, it is often difficult to isolate individual processes. To use a line as a diagnostic tool for the atmosphere, we must obtain either an algebraic expression for the source and sink

terms or a sufficient number of numerical solutions to distinguish the significant processes in fixing these terms. Many "devices" such as the equivalent two-level atom (Thomas and Athay 1961) have been introduced to facilitate the algebraic approach, but whichever approach is used, the formulation in terms of source and sink terms enables us to place collision-controlled source functions, photoionization-controlled source functions, and various mixtures of the two all in the same framework. In the solar atmosphere, the prototypes of these three kinds of source functions are, respectively, the Ca II lines, the Balmer lines, and the Lyman lines. In other atmospheres, the behavior can be quite different. The prototypes have, however, enabled us to check the general structure of the theory and to verify, theoretically and empirically, the influence of the four boundary effects on the microscopic processes.

Thus the new spectroscopy tells us what governs the partition of energy and hence the type of spectrum for a given atmosphere. But to study the detailed variation in the behavior of the lines and continua across the spectral sequence, we need to know the distribution of state parameters in each class of atmosphere. The purpose of analyzing the observations is not to determine the partition of energy in a prescribed atmosphere, but to determine the properties of the atmosphere simultaneously with the partition. The development of methods to do this without preconditioning the result has followed two lines: one empirical, exemplified by the analysis of solar eclipse data; the other theoretical.

(b) *An empirical approach to state parameters.* This is an extension of Menzel's approach to a quantitative analysis of the solar chromosphere from eclipse observations of the hydrogen lines and continua. The aim is to obtain an empirical distribution of electron temperature, density (which is essentially the hydrogen concentration), ionization, and excitation, and thus infer the energy input, momentum input, and partition of energy. In order to do this, we require the distributions of T_e , n_H , n_e , n_p , and b_j for all energy levels j . Observations in two continua plus lines, a knowledge of the relative abundances of metals to hydrogen, and a theory for b_1 and b_2 of hydrogen make the problem determinate. In constructing an applicable theory, it is essential that the expressions for b_1 and b_2 be independent of any assumptions on the input of momentum and energy and that they include all relevant radiation fields, which in practice means the Lyman, Balmer, and

Paschen continua and H_{α} . The chromosphere is transparent in the Balmer and Paschen continua, but the transfer problem in the Balmer lines and in the Lyman continuum must be included. This treatment showed for the first time the effect of this coupled transfer solution on b_1 and b_2 , hence on the empirical determinations of T_e . The model obtained from this analysis is included in Figures 1, 2, and 3.

The conclusions of the 1961 analysis most relevant to this paper are as follows: (1) Because the values of T_e , b_1 , b_2 , and the Lyman continuum radiation are strongly coupled, each depending on an analysis of the atmosphere as a whole, the coupling in the tests for radiative equilibrium and LTE-R stand out. Departures from radiative equilibrium occur as low as 500 km (below this height the temperature distribution is not sufficiently reliable for us to draw definite conclusions). Departures from LTE-R occur in all the observed regions. (2) The physical reliability of the results is confirmed by comparison with independent data. The intensity of the Lyman continuum predicted from the empirical model is within a factor of two of the observed value. He I and He II lines are observed just where the model shows a steep rise in T_e to some value exceeding $10,000^{\circ}\text{K}$. (3) The analysis breaks down at the start of this abrupt rise in T_e . Empirically, the combined He I and Balmer continua require a geometrically inhomogeneous structure in the region where He I appears. Theoretically, the assumption of detailed balance in the Lyman lines is questionable in the same region. These conclusions on the Lyman continuum have been confirmed recently by Noyes and Kalkofen (1970) who used data in the rocket UV. By treating the Lyman lines and some lines of C II, Avrett, Vernazza, and Chipman (1970) have re-examined and improved the theory in the region of the steep rise in T_e .

The Standard Reference Models included in Figures 1, 2, and 3 are an amusing contrast to our empirical model. No account has been taken of eclipse data. The assumption of hydrostatic equilibrium has been applied to what appears to be a freehand extrapolation of $T_e(h)$ in the region $\tau_5 \leq 0.05$. Non-LTE effects have been either neglected entirely or included in a patchwork, non-consistent fashion. The original justification for constructing such models was that a standard model would provide a means whereby various theories of line formation could be compared. However, it was perhaps inevitable that once published, these models were accepted as valid representations of the Sun. The construction of numerically accurate but physically incon-

sistent models is in direct contrast to the approach of the Menzel school. It is interesting that these reference models appear to be approaching the 1961 model, which, while it will certainly be modified in detail, seems to be holding up quite well.

(c) *A theoretical approach to state parameters: population and transfer effects.* The new spectroscopy gives the spectroscopic state of a small element of gas for a given distribution of state parameters. An empirical analysis, such as that described in the previous section, suggests how we might obtain these distributions when we have the range of observations available for the Sun. The question remains of how to obtain them under less favorable conditions. With the exception of certain eclipsing systems, this must be done theoretically.

The values of the state parameters are in general fixed by a combination of transfer processes and local interactions. A solution of the transfer problem throughout the atmosphere provides a value for the transfer quantity at a point, e.g. the energy in the radiation or velocity field; the interaction with the local population of energy levels gives a value for the energy absorbed. Interactions among the energy levels determine the final partition of this absorbed energy. Although these steps are coupled, we can obtain a clearer physical picture by isolating the physical processes and quantities that determine the character of each step. For example, for a grey atmosphere in LTE-I and radiative equilibrium, J_ν is determined by the distribution of T_e . To a first approximation, T_e is fixed by the local value of the integrated J_ν . Thus J_ν is coupled to the distribution of T_e , but neither T_e nor J_ν is coupled to the ν -dependence of J .

We attempt to isolate the above steps by separating what we call population and transfer effects. Thus far we have applied our formulation only to the determination of T_e . In doing so, we have distinguished between changes in the local value of T_e due to changes in the energy supply, which we call transfer effects, and changes in the value of T_e due to changes in the relative importance of the microscopic processes fixing the populations, which we call population effects. For radiative equilibrium and a one-level atom, we have expressed the kinetic energy of the photo-recombining electrons, which depends on T_e alone, as the product of two factors: (1) the rate at which energy is supplied to the electron continuum per photoionized electron, and (2) the number of photoionizations per recombination. The first factor depends on

the energy transferred and controls the transfer effects; the second depends on the populations and controls the population effects. It is the behavior of the population factor that determines the explicit dependence of T_e on the process determining the ionization equilibrium. For this reason we have called it the temperature control bracket. For a multilevel atom, we take the weighted average of the photoionized and photorecombined electrons in each continuum. The weighting factor is the product of the temperature control bracket and the relative numbers of photorecombinations or photoionizations in each continuum. Thus far, the applications of this approach have been only exploratory. We believe, however, that it will give the same physical insight into those factors that determine the values of the state parameters as the new spectroscopy gave into identifying types of observed line profiles with classes of source and sink terms.

III. A GENERAL STELLAR MODEL

The interpretation of the solar chromosphere anomaly in terms of the physical processes associated with a transition region suggests that the conclusions of Section II on atmospheric structure and diagnostics are not peculiarly solar but relate more generally to stellar atmospheres. These conclusions may be summarized as follows, corresponding roughly to the classes of observed chromospheric anomalies. (1) The observed disk spectrum is formed in an atmospheric region that extends to far greater heights than that predicted by the classical model, which represents at most the deepest layers of the atmosphere. (2) The major contrast between the spectrum predicted by our method and that by the classical approach is that our method predicts a non-uniform variation of excitation with height in the atmosphere. This corresponds on the one hand to a diversity in the types of source functions, which is associated with differing source and sink terms, and on the other hand to the diversity in non-radiative energy supplies and departures from hydrostatic equilibrium and spherical symmetry. (3) To understand the complete structure of this extended region, it is necessary to allow for departures from all the classical assumptions successively with increasing height. The details can be expressed in terms of population and transfer effects: the former is associated with departures from LTE-R near the boundary, the latter with the production

of a chromosphere. (4) The initiation of any horizontal inhomogeneities by atmospheric instabilities introduces the possibility that any effect associated with a variation in height may also occur in the horizontal direction.

We suggest that just as with the Sun, what appears to be anomalous in stellar spectra is actually the key to the structure of the atmosphere. "Peculiar" spectra are then seen to indicate not something out of the ordinary but simply accentuated features of atmospheric structure common to all stars. The extreme peculiar spectra, known as "symbiotic", represent an enhancement of the same combination of high and low excitation effects already encountered in the solar chromosphere. This suggestion again reflects an early idea of Menzel's, which has been overlooked in recent years. The details of his idea differ from ours, but the basic physical point is the same.

A. *Menzel on Symbiotic Stars*

Symbiotic stars are those whose spectra include both high and low excitation lines and continua. Many years ago, a number of people, including Menzel, suggested that the obvious interpretation was in terms of binary stars, one hot, one cool. Subsequently Menzel modified this picture by suggesting that such stars were not in fact binaries but single stars divided into two regions: a central, hot nucleus surrounded by an extended, cool atmosphere supported by a combination of radiation pressure, turbulence, and stellar rotation. If the atmosphere were optically thin, the photosphere would be formed close to the hot nucleus, and we might observe a Wolf-Rayet type spectrum. If, on the other hand, the atmosphere were optically thick, the photosphere would be formed near the outer boundary, and the continuum would mimic that of a red giant. He elaborated this model to suggest that a single rotating star could produce both a hot and a cool continuum. The equatorial regions of the atmosphere, distended by rotation, would be optically thick, so the photosphere would be formed in the outer, cooler regions, whereas the polar regions would be optically thin, so one would see the hot continuum characteristic of the stellar nucleus.

We suggest that Menzel was correct in attributing symbiotic spectra to a single star rather than a multiple system. We would, however, alter the details of his model and greatly extend the number of stars to which it applies. Our picture is the following: All

stars are symbiotic, the differences being only a matter of degree, reflecting the relative importance of the classical and non-classical regions of the atmosphere in producing the observed spectrum. The symbiotic properties arise in two ways. In stars without transfer effects, and therefore without chromospheres, they originate in population effects. In this case, the high and low excitation lines cannot be associated with any distinct regions. In stars with transfer effects, and thus with chromospheres, there will be a height asymmetry in ionization, which will, in fact, be the reverse of that suggested by Menzel but in the direction of that suggested by one of us for Wolf-Rayet stars (Thomas 1950) and by Mrs. Payne-Gaposchkin for the Sun (1956 unpublished). You will recall her remark that on the basis of rocket UV spectra alone, she would classify the Sun as a WC6 star, a remark that suggested a similarity in the origin of the two spectra. Thus from disk observations, at least one star, the Sun, appears to be a cool star as seen in the visual spectrum, which originates in the lower atmospheric regions, and a hot star as seen in the UV, which originates in the upper regions. The principle is the same as Menzel's: symbiosis reflecting the schizophrenia of a single star. The reversal of the hot and cold regions comes from experience with Menzel's favorite star, the Sun, and follows the direction that he himself took in exploring the He I and He II anomaly. He can hardly object to this change in detail.

B. A General Stellar Atmosphere

In the deepest layers of the atmosphere, we have a region represented by the classical model. Here LTE-R is established by the predominance of collisions over every other kind of excitation process. The source function is fixed by T_e , which is in turn fixed by either radiative or quasi-static convective energy transport. As we move higher in the atmosphere, collisional processes decrease relative to radiative, and eventually we reach a point where radiative processes dominate. Here we may still have LTE-R in limited spectral regions provided the important radiative processes maintain a homogeneous radiation field. Effectively this means that no radiation can be observed in these transitions, but other transitions, to which these are coupled, can be observed. On this basis, we impose conditions on the maximum value of T_e and the minimum value of density, hence of gravity and momentum supply,

for the existence of an observable LTE-R region (Gebbie and Thomas 1971). It cannot be assumed a priori, however, that this region represented by the classical model can in fact be observed.

Above the region represented by the classical model, we must allow for departures from any or all the classical assumptions. Whether departures from LTE-R occur can be computed in terms of density and optical depth, if we know the distribution of state parameters. Thus, as we have stressed, we must investigate both population and transfer effects, either empirically or theoretically or both. In one atmosphere, we may have only population effects; that is, we may have departures from LTE while the other classical assumptions remain valid. In another atmosphere, with transfer effects, several of the assumptions may break down simultaneously.

If in the region above that described by the classical model, there are only population effects, we call it a non-classical photosphere. Here T_e may rise to some maximum value limited by the value of T_{eff} . The possible presence of several kinds of source and sink terms may give rise to the apparent anomalies in excitation reflected in the disk spectra.

If, on the other hand, this region has both population and transfer effects, we call it a chromosphere. (We do not distinguish between a chromosphere and corona.) Here T_e will rise to a value limited only by the input of non-radiative energy. Our understanding of this process is not yet sufficient to predict this maximum value of T_e in terms of the observed characteristics of a star. Thus the chromosphere is characterized by the presence of transfer effects, of $dT_e/dh > 0$, and of $T_e > T_{eff}$.

We now consider how we might establish at least the existence of a chromosphere from the observations. From the continuum formed in the deepest atmospheric levels, we can try to fix the general excitation level of the spectrum. This corresponds roughly to the effective temperature of the classical model. We then try to estimate the variation of excitation level with height using as our criteria the diversity of the spectra. If this excitation level exceeds that of the limit set by population effects alone, we conclude that transfer effects are contributing and that we have a stellar chromosphere.

For example, from the visual continuum of the Sun, we obtain an excitation level of about 5800°K for the regions represented by the classical model. Moving outward through the regions in LTE-R, T_e decreases to some

ning less than 4700°K - current estimates favor a value of about 4300°K . In the non-LTE regions, population effects could raise T_e to $5300 - 5500^{\circ}\text{K}$ in radiative equilibrium (Gebbie and Thomas 1970). The observation of He I in the disk spectrum by itself suggests an excitation level close to $10,000^{\circ}\text{K}$. The central emission cores of $\text{Ca}^+ \text{H}$ and K tend to confirm that the excitation level rises above the limit set by population effects alone. The rocket UV and radio spectra also support this conclusion. Thus from disk spectra alone, we infer the presence of transfer effects and hence of a chromosphere. Until we obtain a satisfactory treatment of the aerodynamic problem, we must, of course, determine the final model empirically.

Another example is the Wolf-Rayet stars. From the visual continuum alone, we infer an excitation level of some $40,000^{\circ}\text{K}$, give or take $10,000^{\circ}\text{K}$. Yet from the line spectrum in the visual region, we infer excitation conditions corresponding to some $200,000^{\circ}\text{K}$. Again we infer the presence of transfer effects and a chromosphere.

These examples can be extended to other stars as well as various stages of novae and binary systems consisting of an extended supergiant and a small hot companion. We believe this provides a picture of how Menzel's original ideas on the solar chromosphere, flavored by suggestions on symbiotic spectra and passed through the strainer of non-LTE diagnostics, have led to suggestions for a general model for a stellar atmosphere.

ACKNOWLEDGMENT

We are indebted to J-C. Pecker for continuous interchanges on the ideas in this paper and to Alice Levine for valuable advice on the expression of them.

BIBLIOGRAPHY

- Thay, R.G., Billings, D.E., Evans, J.W. and Roberts, W.O. 1954, *Ap. J.*, 120, 94.
Thay, R.G. and Menzel, D.H. 1956, *Ap. J.*, 123, 285.
Vrevelt, E.H., Vernazza, J. and Chipman, E. 1970, presented at the "Second Workshop on Orbiting Solar

- Observatories" at Goddard Space Flight Center, December 2-4, 1970 as reported in *Sky and Telescope*, 41, 268, 1971.
- Bilderberg Continuum Atmosphere, Gingerich, O. and de Jager, C. 1968, *Solar Physics*, 3, 5.
- Bilderberg Continuum Atmosphere, Revised, Gingerich O. 1969, as reported at AAS Solar Physics Meeting, Pasadena.
- Cayrel, R. 1963, *C. R.*, 257, 3309.
- Cillie, G.G. and Menzel, D.H. 1935, *Harvard Observatory Circular* No. 410.
- Dunn, R.B. 1960, Thesis, Harvard.
- Edlèn, B. 1942, *Zs. f. Ap.*, 22, 30.
- Evans, J.W., Roberts, W.O. and Thomas, R.N. 1950-51, unpublished planning documents for HAO 1952 eclipse expedition.
- Gebbie, K.B. and Thomas, R.N. 1970, *Ap. J.*, 161, 229.
- Gebbie, K.B. and Thomas, R.N. 1971, *Ap. J.*, in press.
- Goldberg, L. and Menzel, D.H. 1948, *Harvard Observatory Monograph*, No. 7.
- Harvard Smithsonian Reference Photosphere, Gingerich, O., Noyes, R.W., Kalkofen, W. and Cuny, Y. 1971, *Solar Physics*, submitted.
- Henze, W. 1968, Thesis, University of Colorado.
- House, L.L. 1961, Thesis, University of Colorado.
- Jefferies, J.T. 1968, *Spectral Line Formation* (Waltham Massachusetts: Blaisdell Publishing Company).
- Jefferies, J.T. and Thomas, R.N. 1959 et seq., *The Source Function in a Non-Equilibrium Atmosphere* (series), *Ap. J.*, 129, 401, et seq.
- Linsky, J.L. and Avrett, E.H. 1970, *P.A.S.P.*, 82, 169.
- Menzel, D.H. 1931, *Pub. Lick Obs.*, 17, Part 1.
- Menzel, D.H. 1937 et seq., *Physical Processes in Gaseous Nebulae* (series), *Ap. J.*, 85, et seq., 3.
- Menzel, D.H. 1947, A. Cressy Morrison Prize I, New York Academy of Sciences.
- Mihalas, D. 1970, *Stellar Atmospheres* (San Francisco: W.H. Freeman and Company).
- Noyes, R.W. and Kalkofen, W. 1970, *Solar Physics*, 15, 120.
- Pottasch, S.R. and Thomas, R.N. 1959, *Ap. J.*, 130, 94
- Pottasch, S.R. and Thomas, R.N. 1960, *Ap. J.*, 132, 19
- Roberts, W.O. 1945, *Ap. J.*, 101, 136.
- Thomas, R.N. 1948 et seq., *Superthermic Phenomena in Stellar Atmosphere* (series), *Ap. J.*, 108, 130, et seq.
- Thomas, R.N. 1949, *Ap. J.*, 109, 480.
- Thomas, R.N. 1951 et seq., *Thermodynamic Structure of the Outer Solar Atmosphere* (series), *Ap. J.*, 111, 165, et seq.

- Thomas, R.N. 1957, *Ap. J.*, 125, 260.
- Thomas, R.N. and Athay, R.G. 1961, *Physics of the Solar Chromosphere* (New York: Interscience Publishers).
- Thomas, R.N. 1965, *Non-Equilibrium Thermodynamics in the Presence of a Radiation Field* (Boulder: University of Colorado Press).
- Utrecht Reference Photosphere, Heintze, J.R.W., Hubenet, H. and de Jager, C. 1964, *B.A.N.*, 17, 442.

THE CORONA

J. B. Zirker

*Hawaii Institute of Geophysics
University of Hawaii*

INTRODUCTION

This paper discusses some recent trends in the study of the solar corona. Progress in this field has been accelerating steadily during the past decade, partly as a result of new observations (especially in the EUV and XUV) and partly because of improved understanding of coronal atomic processes. Rather than try to review the literature exhaustively, a task beyond the scope of this short work, I have selected three topics that illustrate current interests in the quiet corona. They are: the relation of coronal forms to the magnetic field, the physical state of the gas, and the mass (and energy) balance.

These topics form a chain of successively higher abstractions: it is natural to begin to study the solar atmosphere by describing its structures and their evolution; later one is concerned with a quantitative interpretation of its radiation, and this leads to the determination of gas density, temperature, and composition. Later still, we seek an understanding of the phenomena in terms of basic transport processes. In a more rational world, the development of coronal physics might have followed this simple linear progression. In fact, each area of study (form, constitution, and process) is under active investigation today, and our knowledge of them will advance rapidly in the next few years.

FORM

Solar astronomers have suspected for many years that coronal forms arise from the interaction of the coronal magnetic field and the electrically conducting gas. The idea occurred to the earliest eclipse

observers who interpreted polar plumes as evidence of a general dipole magnetic field. Trajectories of falling prominence material (McMath, Menzel, Dunn, Roberts, and Corral) suggested the influence of a guiding magnetic field over active regions. Arches and rays, visible in the forbidden iron line $\lambda 5303$ in coronal enhancements, suggested tubes of magnetic flux outlined by the gas (Lyot, Dunn, Dollfus). The similarity between the migration patterns through the sunspot cycle of large-scale photospheric magnetic field regions (studied principally by the Mt. Wilson group), prominence filaments, and coronal streamers, is indirect evidence for the close association of forms and fields. The idea is certainly plausible and is widely accepted but has not, until recently, been tested.

Unfortunately, direct measurements of coronal magnetic fields are few and rough: some of the best estimates come from radio observations of very low spatial resolution (Newkirk 1967). It is important, therefore, to try to use photospheric magnetic field measurements to estimate at least the direction of coronal fields.

H. U. Schmidt (1964) devised a numerical technique applicable to this and other problems. He showed how to calculate a potential field above a surface on which the normal field component is known. Newkirk and Utschuler have extended the Schmidt method to magnetic observations covering the whole disk. They have compared (1970) white-light observations of large-scale coronal structures with calculated magnetic field lines.

In general, the correspondence between field lines and coronal forms is good. Helmet streamers appear over "magnetic arcades" that link bipolar magnetic regions. Coronal condensations apparently coincide with open-field configurations. Filaments separate field regions of opposite polarity. Polar plumes, as expected, coincide with open-field lines. The potential field approximation is evidently sufficient to outline the gross features of the corona, even though it is based upon observations averaged over a month.

To my knowledge, no one has applied the potential field method for a comparison with smaller features of the corona, such as the arches and rays visible in coronal enhancements. Dunn (1971), who has summarized a decade of coronal green line observations of enhancements, has drawn attention to the importance of the footpoints of individual arches. Presumably, some special physical property distinguishes footpoints of illuminated arches. An extension of Newkirk and Utschuler's work to these arches may help to isolate the footpoints in the chromosphere.

D. Rust (1970) has carried out this kind of comparison for a loop-prominence system. Individual loops can be identified with individual flux tubes. However, it has not been explained why only certain tubes in the field radiate strongly.

Applications of this method to coronal active regions can lead to a useful unraveling of their interior structure, provided the potential field approximation is valid there. Figure 1 shows one of the remarkable X-ray photographs of the corona obtained by the American Science and Engineering (ASE) group with a rocket-borne grating-incidence telescope. Active regions seem to consist of a tight, sharply defined, hot core and a cooler halo, as viewed in 10 \AA to 60 \AA . Occasionally, arches that connect distant active regions are visible in the X-ray photographs. Other X-ray structures, so far not identified with chromospheric features, are also present in the quiet corona. Comparisons of these forms with the computed field lines should help to elucidate both.

Up to the present time, observations of large-scale structures in white light have been limited mainly to occasional glimpses during solar eclipses, with supplementary limb data of limited radial extent coming from ground-based K-Coronameter observations. As a result, we probably know more about the evolution of these coronal structures on a time-scale comparable with the solar cycle than over a period of a month. Similarly, although active regions in the corona have been followed by a succession of Orbiting Solar Observatory (OSO) experiments in the EUV and XUV, these observations have generally lacked the spatial resolution to permit a detailed comparison with the magnetic field. These limitations may soon be relieved by experiments to be flown on OSO-H and the Apollo Telescope Mount mission. The latter, in particular, includes an externally occulted coronagraph (the High Altitude Observatory experiment) capable of following the evolution of coronal streamers throughout a month or more; the ASE group will fly a grazing incidence telescope, which will record the structure and evolution of the corona over the disk with 5 arc-second resolution. We may expect fruitful comparisons of these new data with further magnetic field calculations.

Hopefully, it will be possible in the near future to measure, rather than calculate, coronal magnetic fields. A Babcock type of magnetograph at the High Altitude Observatory has detected circular polarization in the coronal green line (Harvey 1968) but with low signal to noise ratio. More sensitive coronal polarimetry

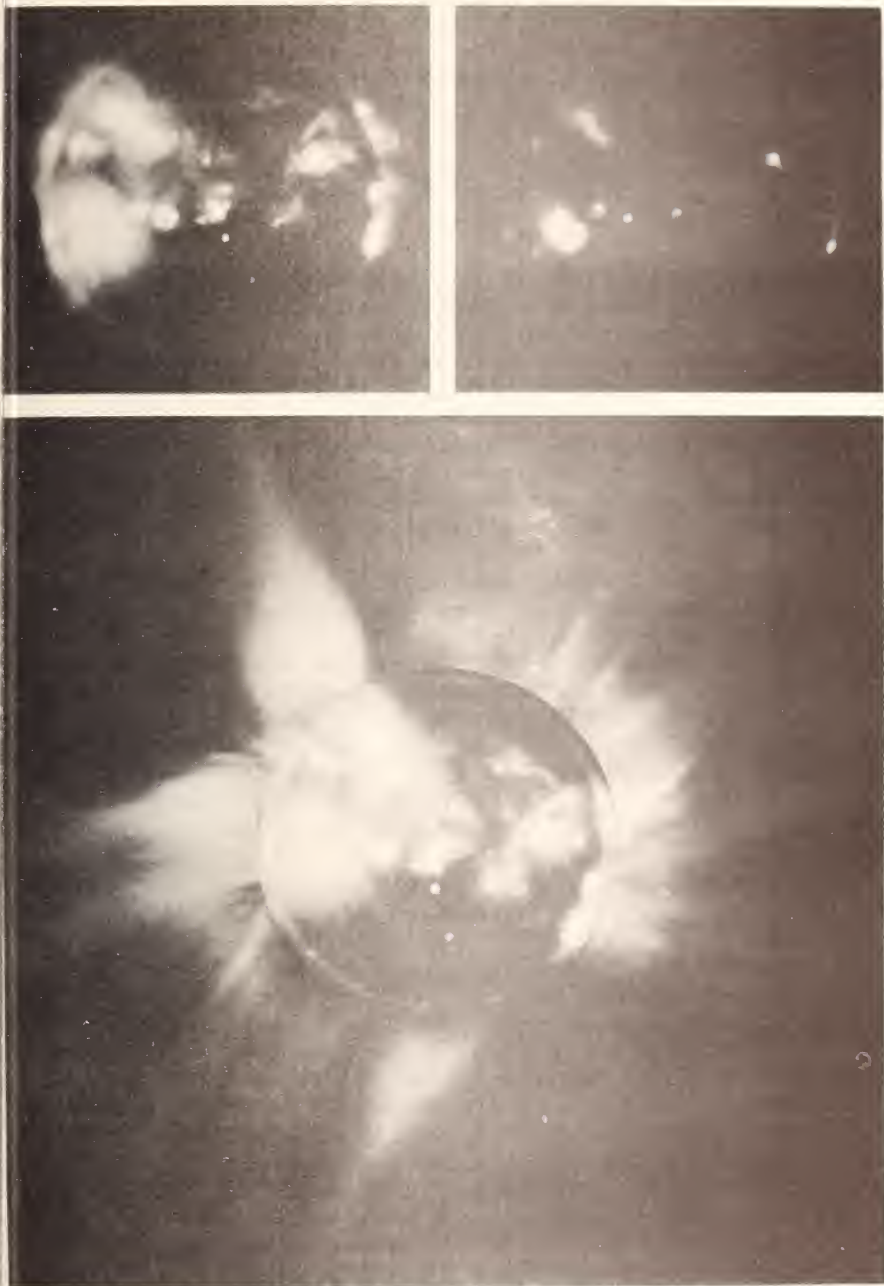


Figure 1. The corona on March 7, 1970. The large panel is a composite, showing the white-light corona at the limb (photographed by the High Altitude Observatory expedition) and the x-ray corona on the disk (photographed by the American Science and Engineering group).

eters are now under development at the High Altitude Observatory and the University of Hawaii, and one is in use at the Pic Du Midi Observatory (Charvin 1970).

PHYSICAL CONSTITUTION

The determination of the physical state of the coronal gas has been a long-standing objective of solar astronomers. We wish to find the distribution of temperature, density, composition and, if possible, velocity and magnetic field. To this end, observations covering the entire electromagnetic spectrum have been gathered and analyzed. Unfortunately, the corona is optically thin throughout much of its spectrum (even in the permitted lines) so that the distribution of physical parameters along a line of sight is difficult to find.

In the past, some investigators have met this difficulty by constructing non-geometric models to represent their observations. For example, we show in Figure 2 the distribution of emission measure $[\int n_e^2 dV]$ with coronal temperature in an active region, as determined from XUV line spectra by Batstone et al. (1970). Their observations have low spatial resolution a limitation that, coupled with the low intrinsic opacity of the gas, permits them only to find the amount of material at each of several discrete temperatures.

This type of representation, originally applied by Pottasch (1964), has been extended by Athay (1966) and Dupree and Goldberg (1967) to observations of permitted lines arising in the quiet corona within the temperature range $10^5 - 10^6$ °K.

If the corona is assumed to be spherically symmetric and isobaric, the emission measure versus temperature distribution can be interpreted as a height distribution of temperature (or density). The resulting temperature distribution is nearly discontinuous, suggesting the concept of an interface between the chromosphere and corona. Moreover, the inferred temperature gradient is consistent with a constant downward flux of heat, conducted from corona to the chromosphere. The assumption of constant heat flux has been incorporated in subsequent models of coronal active regions (Noyes et al. 1970).

Alternatively, some assumption of geometrical symmetry can be introduced to interpret observations from an active region. Figure 3 shows the hemispheri-

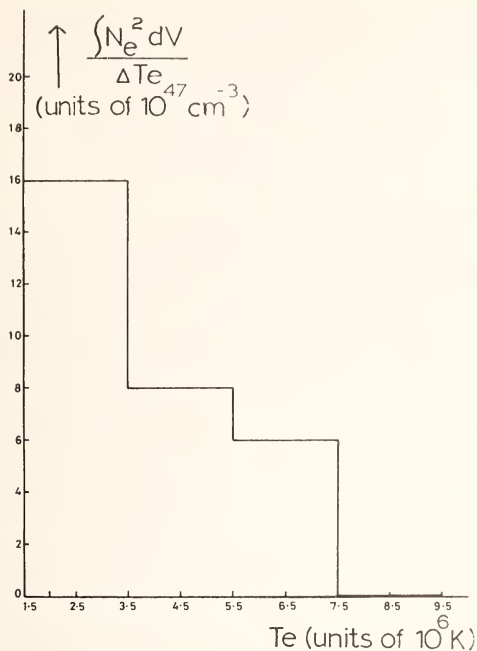


Figure 2. The distribution of emission measure as a function of temperature in a coronal active region (Batstone et al. 1970).

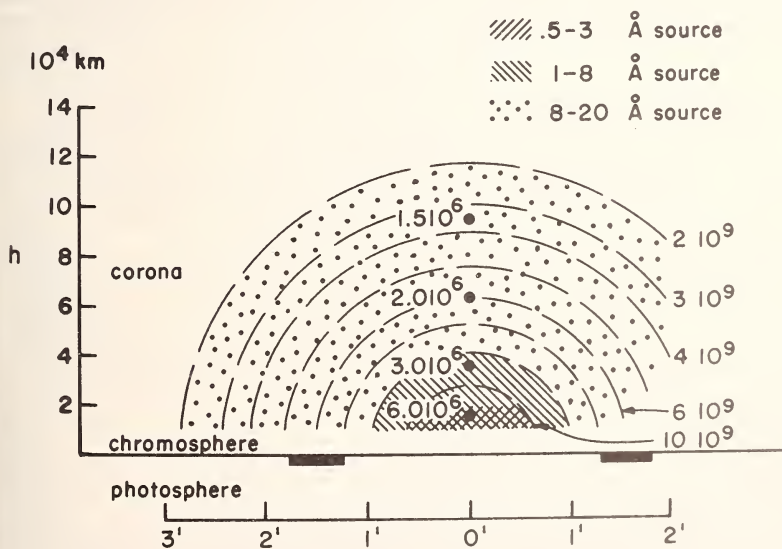


Figure 3. Model for a coronal active region, based upon XUV fluxes (Landini and Monsignori-Fossi 1971).

cal model suggested by Landini and Monsignori-Fossi (1971) to represent their XUV fluxes. Note that high temperature and high density are associated in this model. Similar results have been found from EUV observations by Boardman and Billings (1969).

High resolution filtergrams in the visible or XUV show, however, that the active corona, at any rate, is asymmetrical and inhomogeneous: arches, loops, rays, and filamentary structure abound in enhancements. As the spatial resolution of spectroscopic observation improves, it will become feasible to isolate individual fine structure against the sky or the disk, and to apply more directly analyses like the previous ones.

Recently, intensive efforts have been made to find and apply diagnostic methods specifically designed to determine the local value of electron density and temperature. These methods generally rely on line ratios from a single ion or related ions. One method that initially yielded useful results was devised by Gabriel and Jordan (1969). For ions in the helium iso-electronic sequence, they showed that the ratio of the forbidden ($^3S - ^1S$) to inter-combination ($^3P - ^1S$) line intensities is sensitive to electron density. Table 1 shows the results found by Rugge and Walker (1970) when they applied the method of Gabriel and Jordan to their XUV spectra of active regions. Very high densities are predicted by this method, the density increasing, moreover with the electron temperature of the region. These preliminary results have been modified by a subsequent redetermination of the lifetime of the 3S state

TABLE 1
LINE RATIOS AND PREDICTED DENSITIES
20 MARCH 1969

Ion	Approx. temp. of line formation $10^6 \text{ }^\circ\text{K}$	0604 UT $N_e \text{ (cm}^{-3}\text{)}$
O VII	1.8	2×10^8
Ne IX	3.5	1.5×10^{10}
Al XII	7.3	2×10^{11}
Si XIII	8.9	3.5×10^{11}
S XV	12.2	4×10^{12}

From H.R. Rugge and A.B.C. Walker, 1970, *Astron. and Ap.*, 5, 4.

Dupree (1971) has developed a similar diagnostic for electron density, using the lines from beryllium-like ions (CIII, OV) which appear in the spectrum of the temperature transition region

$$10^5 < T < 2.5 \times 10^5 \text{°K} .$$

The intensity ratio of the $^3P - ^3S$ line and the $^1P - ^1S$ line is moderately sensitive to electron density. Typical electron densities inferred from OSO IV and OSO VI data are 10^{10}cm^{-3} for quiet regions, 10^{11}cm^{-3} for active regions, and $5 \times 10^{11} \text{cm}^{-3}$ in a flare.

The optical forbidden lines can also be analyzed in this fashion. Figure 4 shows the variation of selected line ratios with electron density (Zirker 1970). Each pair of lines arises from transitions within the ground configuration of a particular ion, which is labeled on the curve. Each of the ions shown is abundant over only a limited range of temperature. Fe XI is present mainly between 1.2 and $1.7 \times 10^6 \text{°K}$, and Ni XV between 2.2 and 10^6°K . Thus it is possible to determine from a line ratio the electron density of material that lies within a narrow temperature range in the line of sight. Fisher (1971) has applied this technique to the study of a coronal enhancement observed with the coronagraph in Hawaii. Figure 5 shows the derived density at two temperatures, as a function of position across the enhancement. Jefferies, Orrall and Zirker (1971) have developed a general formulation of the method and applied it to eclipse observations of coronal enhancements.

In order to find suitable diagnostic methods, reliable calculations for the excitation and ionization equilibrium of a wide variety of coronal ions are required. These, in turn, rest ultimately on a knowledge of atomic transition rates and collision cross sections. The latter, particularly, are still very sparse. Considering the effort (and expense) invested in obtaining adequate observations, especially from satellites, it is unfortunate that so little effort is expended in calculating atomic parameters.

A series of satellite experiments, to be flown in the near future, should provide new and excellent spectroscopic data for the determination of coronal models. Among these we might mention the Harvard and Naval Research Laboratory instruments on board ATM and the Goddard spectrometer on OSO-H. The interface with the chromosphere will be studied by the High Altitude Observatory and Paris experiments on OSO-I. Intensive

Line Ratios

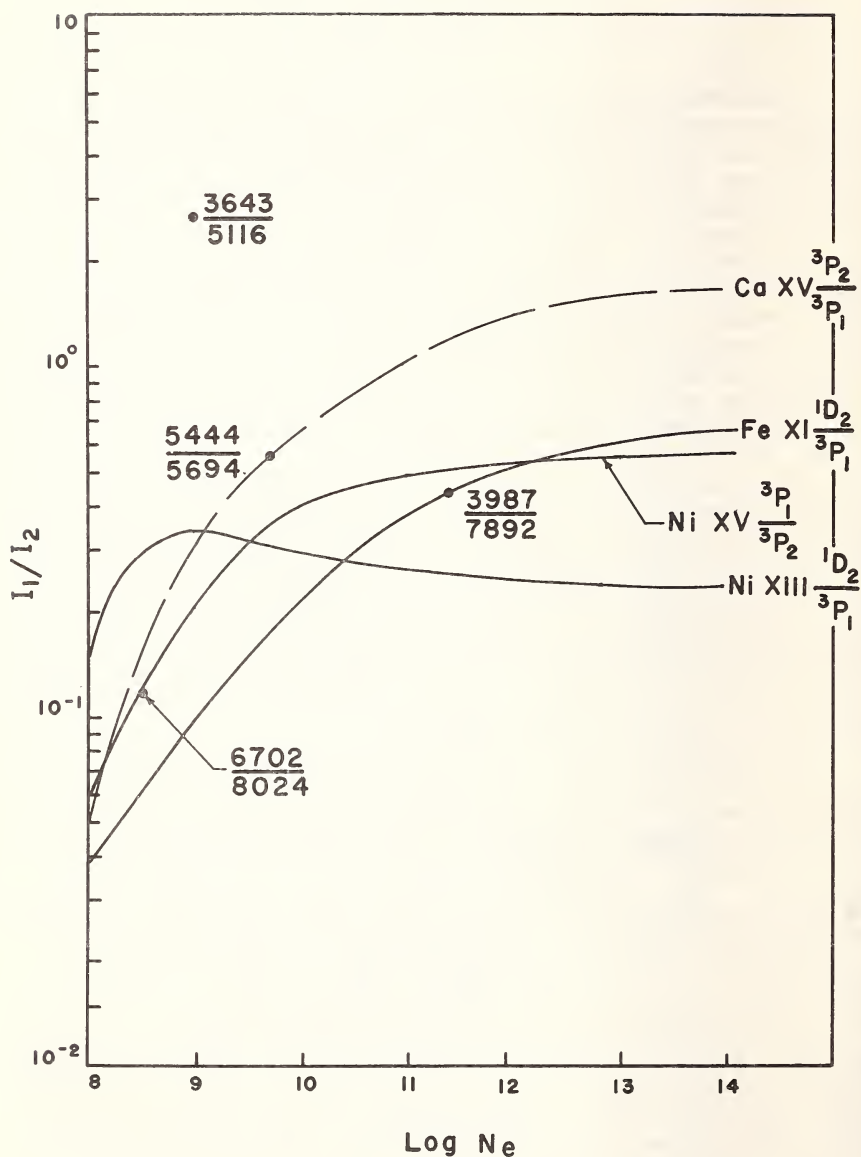


Figure 4. Electron density variation of optical forbidden line ratios (Zirker 1970).

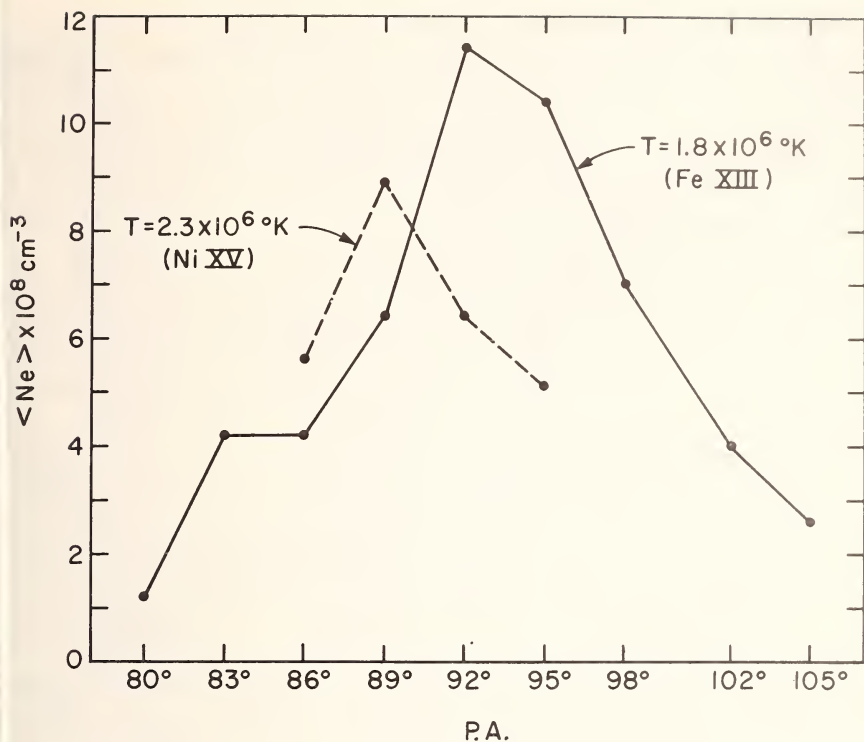


Figure 5. Electron density in a coronal enhancement, as determined from optical forbidden line ratios (Fisher 1971).

efforts to observe coronal regions on the limb will continue at several ground-based observatories.

MASS AND ENERGY BALANCE

One of the ultimate objectives of coronal research is to understand how the observable atmospheric phenomena arise from the transport of mass and energy. The basic ideas in the theory of the coronal energy balance have been recognized for over 30 years; however, the details have changed continuously. Heating is thought to accompany the dissipation of some form of mechanical wave energy that propagates out of the solar convective zone. Cooling occurs by the combined effects of radiation, heat conduction and convection (i.e. in the solar wind).

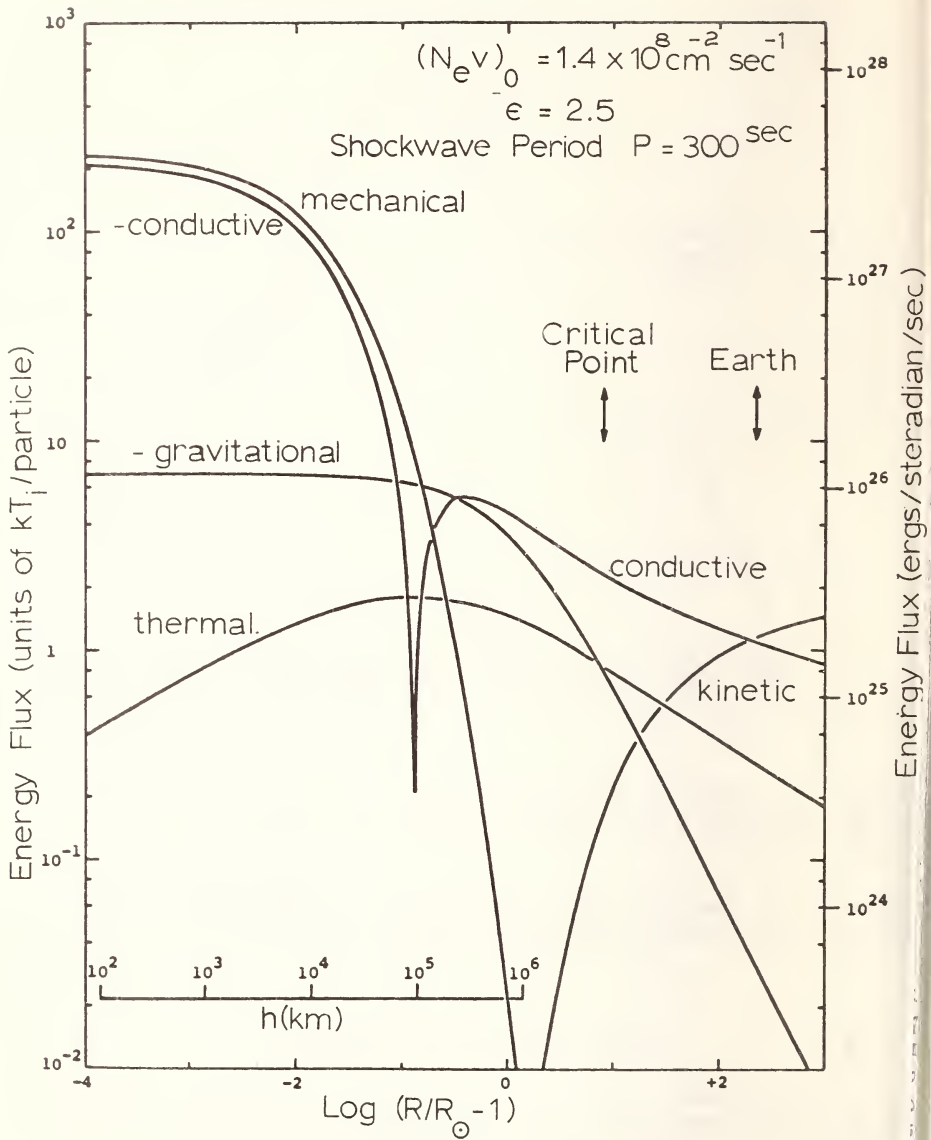


Figure 6. Height variation of different energy densities in a spherical, shock-heated corona (Kopp 1967).

One of the main uncertainties is the type of wave motion responsible for the heating. Sound (or shock) waves have been examined most thoroughly. Figure 6 shows some results drawn from R. Kopp's thesis (1967),

in which the equilibrium of a spherically-symmetric corona, heated by shock waves, is considered. The figure shows the height variation of the different types of energy present. Kopp's models predict very reasonable values for the maximum coronal temperature and the radial distribution of density, although only three free parameters (shown at the top of the figure) determine a model.

Pneuman and Kopp (1970) have recently considered the equilibrium of a helmet streamer, taking into account the pressure due to its magnetic field. Few observations are available to check the model, but it predicts a reasonable density enhancement of the streamer with respect to its surroundings.

Such models certainly reproduce the main characteristics of the observable corona. However, they give a poor description of the phenomena at the temperature transition zone. Moreover, they ignore the internal circulation of gas within the corona and consider only the net flow that escapes in the solar wind. More complete models are needed, but can only be attempted after a number of questions are settled observationally.

For example, Athay (1971) has pointed out that the "observed" downward heat flux from the corona is too large to be dissipated by radiation in the chromosphere, even though the latter radiates at maximum efficiency. Kuperus and Athay (1967) have suggested that a fraction of the corona heat flux is absorbed in the generation of macroscopic gas motions within the temperature interface. They ask whether chromospheric spicules are produced as a consequence of this coupling of the heat flux and gas motion.

Kopp and Kuperus (1968) have developed ideas along the same lines. They also seek to balance the observed radiative and heat flux terms in the interface. They postulate a plausible two-dimensional distribution of magnetic field, which, at chromospheric levels is concentrated mainly on the borders of the supergranulation cells, but at coronal heights is approximately uniform and radial. Such a field would channel a sizeable fraction of the downward heat flux into the borders, where it presumably drives macroscopic motions and is lost eventually in some (unexplained) radiative processes. Most of the observed radiation from the interface would arise from the regions overlying the interiors of the supergranulation cells, where the temperature gradient is less precipitous.

At the moment, then, the sinks of coronal energy in the chromosphere have not been identified observa-

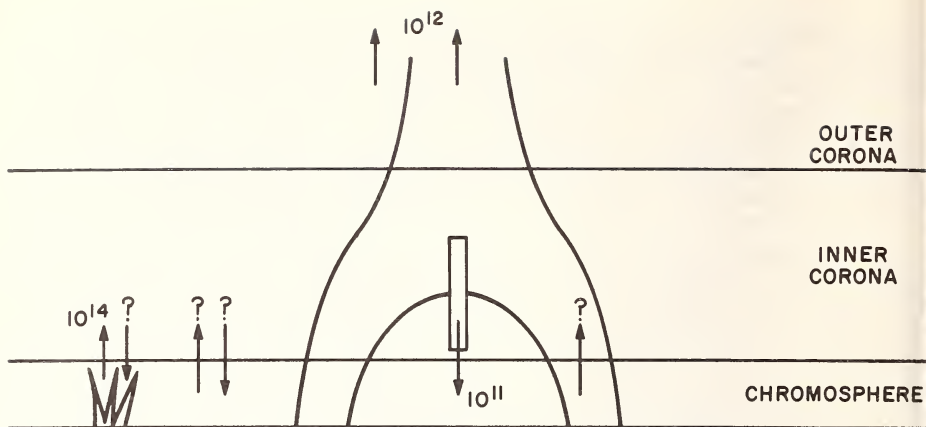


Figure 7. Elements in the mass balance of the corona (schematic).

tionally, although reasonable possibilities have been suggested. Moreover, a variety of wave motions (slow mode, Alfvén, fast mode, ion-cyclotron and gravity) still remain as plausible means for transferring energy upward. Critical observations could help to sort out the possibilities.

The sources and sinks of coronal mass are also uncertain. Figure 7 is a sketch illustrating our ignorance. The numbers attached to the different solar features represent total mass fluxes (over the whole Sun). For example, the upward motion of spicules (far left) represents a mass flux of order 10^{14} g/sec.

Only 1% of this flux is required to balance the eventual losses from the Sun in the solar wind (10^{12} g/sec). However, appreciable mass transfer may also occur at the interface away from spicules; for example, Howard (1971) has detected coherent downward motion in regions with dimensions of the order of a solar radius.

Mass flow within a helmet streamer prominence (center of Figure 7) can only be estimated crudely from solar wind observations near the Earth. Solar wind models (such as that of Pneuman and Kopp 1970) indicate that the net outward flux of mass might be very difficult to detect in the inner portions of the streamer: hydrostatic equilibrium seems to prevail to a good approximation, and only at several radii does the wind velocity reach the sonic point. However, these calculations are based on a rather simple model for the way in which the base of the streamer is heated and on the

assumption that interstreamer magnetic fields exceed the streamer field strength. Conceivably, the actual observational situation may be more favorable than implied by these models.

Clearly, to make further headway with the study of the corona's mass and energy balance, better observations are required. Velocity and density must be mapped in the coronal interface with a spatial resolution sufficient to resolve at least the supergranulation boundaries and preferably individual spicules. The High Altitude Observatory and University of Paris experiments planned for OSO-I are designed to attack this problem. The flux of heat conducted downward must be mapped in two dimensions over the solar surface and preferably in height. This will require a determination of the vector gradient of temperature - no small observational problem. Possibly the Harvard experiment aboard the ATM will supply some of this data. Transients in velocity, density or temperature, if detectable, could provide evidence on the types of waves that carry mechanical energy into the corona. The equilibrium of the corona in open and closed magnetic field regions needs to be compared. Mass fluxes through quiet-scent prominences need to be better defined since they may constitute an important internal cycle of coronal mass.

In summary, we have seen that an important trend in coronal research today is to combine diverse observations from the entire electromagnetic spectrum in order to attack a few major questions. Within the near future, new coordinated observations can be made that will bear directly on the solution of these major problems.

REFERENCES

- Athay, R.G. 1966, *Ap. J.*, 145, 784.
Athay, R.G. 1971 in *Physics of the Solar Corona*, ed. C. Macris (Dordrecht, Holland: Reidel Publishing Co.).
Batstone, R.M., Evans, K., Parkinson, J.H. and Pounds, K.A. 1970, *Solar Physics*, 13, 387.
Boardman, W.J. and Billings, D. 1969, *Ap. J.*, 156, 731.
Harvin, P. 1970, paper given at IAU Symposium 43 on Solar Magnetic Fields, Paris, France.

- Dunn, R.B. 1971, in *Physics of the Solar Corona*, ed. C. Macris (Dordrecht, Holland: Reidel Publishing Co.).
- Dupree, A. 1971, paper given at AAS Meeting Nov. 17-19 1971, Huntsville, Alabama.
- Dupree, A. and Goldberg, L. 1967, *Solar Physics*, 1, 22
- Fisher, R.R. 1971, *Solar Physics*, in press.
- Gabriel, A. and Jordan, C. 1969, *M.N.R.A.S.*, 145, 241.
- Harvey, J. 1968, *Astron. J.*, 73, S 63.
- Howard, R. 1971, *Solar Physics*, 16, 21.
- Jefferies, J.T., Orrall, F.Q., and Zirker, J.B. 1971, paper submitted to *Solar Physics*.
- Kopp, R. 1967, Doctoral dissertation, Harvard University.
- Kopp, R. and Kuperus, M. 1968, *Solar Physics*, 4, 212.
- Kuperus, M. and Athay, R.G. 1967, *Solar Physics*, 1, 36
- Landini, M. and Monsignori-Fossi, B.C. 1971, *Solar Physics*, in press.
- Newkirk, G. 1967, *Ann. Rev. Astro and Ap.*, 5, 213.
- Newkirk, G. and Altschuler, M.D. 1970, *Solar Physics*, 13, 131.
- Noyes, R., Withroe, G.L. and Kirschner, R.P. 1970, *Solar Physics*, 11, 388.
- Pneuman, G.R. and Kopp, R. 1970, *Solar Physics*, 13, 17
- Pottasch, S. 1964, *Space Science Reviews*, 3, 816.
- Rugge, H.R. and Walker, A.B.C. 1970, *Astro and Ap.*, 5, 4.
- Rust, D. 1970, paper given at IAU Symposium 43 on Solar Magnetic Fields, Paris, France.
- Schmidt, H.U. 1964, in "NASA Symposium on Physics of Solar Flares," NASA Spec. Publ. No. 50, ed. W. Hess.
- Zirker, J.B. 1970, *Solar Physics*, 11, 68.

THE CHEMICAL COMPOSITION
OF THE PHOTOSPHERE AND THE CORONA

George L. Withbroe
Harvard College Observatory

1. INTRODUCTION

The problem of determining the chemical composition of the solar atmosphere has attracted the attention of astronomers for over forty years. Knowledge of the chemical abundances in the Sun and other astronomical objects, such as the Earth, moon, meteorites, stars and planetary nebulae is important to several areas of astronomy and astrophysics in the development of (1) reliable models for the interiors and atmospheres of the Sun and stars, (2) nucleogenesis theories, and (3) theories describing the formation and subsequent evolution of the solar system, stars, and stellar systems.

Studies of the Sun are particularly useful because the solar spectrum can be observed over a very broad wavelength range with high spectral resolution. In addition, due to the relative nearness of the Sun to the Earth, we can attack the problem of the solar chemical composition with a greater variety of techniques than is possible with other stars. Information on the solar chemical abundances can be derived from observations of the photosphere, chromosphere, corona, solar wind, and solar cosmic rays. This paper discusses the chemical composition of the photosphere and corona.

Quantitative analysis of the chemical composition of the solar atmosphere was initiated by Henry Norris Russell in 1929. He determined photospheric abundances of 56 elements and 6 molecules from intensities listed in the Rowland atlas and a simple photospheric model in which it was assumed the absorption lines originate in a reversing layer located above the photospheric layers producing the continuum; and the reversing layer is characterized by a uniform temperature and pressure.

Soon after Russell's pioneering work appeared in print, Donald H. Menzel (1931) published his classic study of the solar chromosphere. This massive work

discusses in detail the theory of line formation and its application to the quantitative analysis of chromospheric flash spectra. Among the many valuable contributions contained in Menzel's paper is the first determination of the chemical composition of the chromosphere. Using a method of analysis similar to the one Russell applied to the photosphere, Menzel derived chromospheric abundances for 20 elements.

In the years that followed, Menzel, his students, and associates continued working on the problem of solar abundances. Two of these students, Lawrence H. Aller and Leo Goldberg, have been particularly influential and active in this field. In 1943 they published some of the results obtained by Menzel and his associates, and in 1960, along with Edith A. Müller, they published what has become the standard reference work on solar abundances (Goldberg, Müller, and Aller 1960), hereafter referred to as the GMA abundances. This very thorough analysis of 42 elements made use of new solar observations, new f -values, a photospheric model based on continuum limb-darkening observations, and a precise theoretical treatment of the line formation for both weak and moderate strength lines with different ionization and excitation potentials. Over the past 30 years, Menzel, Goldberg, and Aller have stimulated the interest of numerous students and associates in the solar-abundance problem.

Other important work of historical interest that preceded the GMA analysis is that of Strömgren, Unsöld, and Claas. In 1940 Strömgren pioneered the modern approach to abundance analysis by developing a photospheric model in which the temperature, gas pressure, and electron pressure were given as a function of optical depth. For the first time the abundance of each element could be derived relative to hydrogen, since the equivalent width of a line depends upon the ratio of the line to the continuous-absorption coefficient, where the continuous absorption is produced by negative hydrogen ions as discovered by Wildt in 1939.

Unsöld in 1948 and Claas in 1951 performed extensive abundance analyses based on curve-of-growth techniques. Unsöld used a simplified solar model that neglected the effects of temperature and pressure gradients on the formation of lines with different excitation and ionization potentials; Claas used a more sophisticated model that included these effects.

In the decade since the publication of the GMA analysis, numerous individuals, too many to mention by name, have been active in photospheric abundance work. The basic techniques have not changed much except for

the treatment of lines in crowded sections of the spectrum. In the more sophisticated analyses, abundances are generally derived from such lines by computing short sections of the spectrum so as to take into account the influence of lines neighboring on the profile of the line under investigation.

2. THE PHOTOSPHERIC IRON ABUNDANCE

The most important recent work on photospheric abundances is the revision of the iron abundance. For a number of years one of the outstanding problems of solar physics was the order of magnitude discrepancy between the photospheric and coronal abundances of iron. However, starting in the mid 1960's, evidence began appearing which indicated that the photospheric abundance was incorrect. The first evidence was provided by the identification of the forbidden Fe II lines in the photospheric spectrum. The work of Swings and his associates (Swings 1965, 1966; Grevesse and Swings 1969; Nussbaumer and Swings 1970) in this area has been particularly important. They found that in order to account for the presence of the [Fe II] lines, the photospheric iron abundance an order of magnitude larger than the value determined from the permitted Fe I and Fe II lines was required.

Soon after the [Fe II] results became available, evidence for large systematic errors in the permitted Fe I and Fe II oscillator strengths began appearing with the publication of new measurements by Huber and Hobey (1968), Grasdalen et al. (1969), Whaling et al. (1969), Garz and Kock (1969), Wolnik et al. (1970), Bascheck et al. (1970), Bridges and Wiese (1970), Martinez-Garcia et al. (1970), Huber (1971), Wolnik et al. (1971) and others.

Of special significance were the results of the Kiel group whose new laboratory oscillator strengths for the permitted Fe I and Fe II lines (Garz and Kock 1969; Bascheck et al. 1970) and subsequent solar analyses (Garz et al. 1969a, 1969b; Bascheck et al. 1970) resulted in a photospheric iron abundance in good agreement with the photospheric value determined from the [Fe II] lines and the coronal value.

Some of the reported photospheric iron abundances are listed in Table I.* The values are on a logarithmic scale where the hydrogen abundance, $\log N_H$, is set

*Tables I-VI are on pages 136-144.

equal to 12.00. The most reliable values are in the bottom third of the list beginning with the [Fe II] results of Grevesse and Swings (1969). The abundance most consistent with recent revisions of the permitted line oscillator strengths and recent abundance determinations from the permitted and forbidden lines of both Fe I and Fe II is $\log N_{\text{Fe}} = 7.4 \pm 0.3$. The assigned error limits take into consideration the small systematic differences between the recent oscillator strength determinations and the uncertainties in the photospheric models and line-damping constants. As will be shown later, a photospheric iron abundance of $\log N_{\text{Fe}} = 7.4$ is in fairly good agreement with the coronal value.

3. PHOTOSPHERIC ABUNDANCES

Table II summarizes some recent results on the chemical composition of the photosphere. The "adopted" photospheric abundances are values selected from a variety of references too numerous to cite. The sources of the adopted values are given in column 7. For comparison with the adopted values, the GMA values are given in column 3, and meteoritic values are given in column 5. The meteoritic values are scaled such that $\log N_{\text{Si}} = 7.55$. These abundances were determined from a class of carbonaceous chondrites that might be representative of the primordial material out of which the solar system was formed and hence might have a composition similar to that of the Sun. The differences between the photospheric and meteoritic abundances are given in column 6.

For the first 20 elements the agreement between the solar and meteoritic values is very good, except for lithium and chlorine. Lithium can be destroyed by burning in the solar interior, which may explain why the solar values are so low. For chlorine, both the solar and meteoritic values are uncertain. The solar value is based on only one line, while the meteoritic value is questionable because chlorine is a highly volatile element.

For the elements with atomic numbers between 20 and 40 the agreement between the adopted values and meteoritic abundances is better than the GMA results particularly for the iron group. There are still a few discrepancies, however, and in such cases these solar values may be questioned because of uncertainties in the oscillator strengths or because the element is

represented by only a few lines, which might be blended. The same statement holds for apparent discrepancies in elements with atomic numbers above 40. Note the significant increase in the number of elements whose solar abundances have been determined since 1960.

Although there are a number of elements for which the relative solar and meteoritic abundances exceed 0.3 dex ($0.3 \text{ dex} = 10^{0.3}$), it is premature at this time to conclude that the meteoritic and solar abundances are either the same or different. For one reason or another, solar abundances of most of the discrepant elements may be in error.

How reliable are these photospheric abundances? There are three basic sources of error: (1) inadequate theory of line formation; (2) inadequate models for the temperature and density structure of the photosphere; and (3) inadequate atomic data, especially oscillator strengths and, to a lesser extent, damping constants.

Almost all photospheric abundance determinations are based on the assumption of LTE; that is, it is assumed that excitation and ionization of atoms in the photosphere are governed by the Boltzmann and Saha equations, respectively, with the excitation and ionization temperatures at any point in the atmosphere being set equal to the local electron temperature. Müller (1966) reviewed work on this subject and concluded that departures from LTE do not significantly affect abundances determined from equivalent widths of weak and moderate-strength lines. Some of the more recent evidence for departures from LTE that have shown up in analyses of equivalent widths (cf. Jefferies 1966, Withbroe 1969a) can now be attributed to systematic errors in the oscillator strengths used in the analyses (cf. Huber and Tobey 1968, Garz and Kock 1969).

Müller has also discussed the influence of uncertainties in the assumed photospheric models and damping constants and concluded that the uncertainties in these parameters produced errors in the abundances no larger than 0.3 dex.

With the exception of elements that are represented by only a few lines which may be blended, the principal source of uncertainty in the photospheric abundances stems from doubts about the reliability of the oscillator strengths. The most widely used oscillator strengths for abundance work are still those of Corliss and Bozmann (1962), which unfortunately contain a number of systematic errors (Warner and Cowley 1967; Zwann 1967; Huber and Tobey 1968; Wolnik et al. 1968, 1969, 1970, 1971; Grasdalen et al. 1969; Whaling et al. 1969;

Garz and Kock 1969; Bridges and Wiese 1970; Martinez-Garcia et al. 1970; Takens 1970; Huber 1971; and others). Consequently any abundances based on the original Corliss and Bozmann oscillator strengths may be in question. Several elements between atomic numbers 20 and 40 and most elements with atomic numbers greater than 40 fall into this category. Corrections to the Corliss and Bozmann oscillator strengths will be published in the near future by the National Bureau of Standards. This should improve the situation.

5. CORONAL ABUNDANCES

Coronal abundances have been determined from two types of data: forbidden-line observations made from the ground and extreme ultraviolet (XUV) observations made from above the Earth's atmosphere. We will consider the forbidden-line results first.

The emission lines in the visible spectrum of the corona have been observed for over 100 years during numerous solar eclipses, and during the past 30 years on a more routine basis thanks to the development of the coronagraph. The identification by Grotrian in 1939 and by Edlén in 1942 of the coronal-emission line belonging to forbidden transitions of highly ionized atoms provided astronomers with their first opportunity to determine the chemical composition of the corona.

Observations in which abundances are derived from coronal emission lines usually consist of equivalent-width measurements where the intensity of the emission line is directly compared to the intensity of the continuum at the same wavelength. The intensity of the line depends upon the chemical abundance of the element producing the line, the fraction of atoms in the appropriate stage of ionization, the line excitation mechanism, and the density of the corona. The corona density can be inferred from the intensity of the continuum, which is produced by scattering of photospheric radiation by coronal electrons. The ionization can be determined from the relative intensities of lines produced by different ions of the same element. Excitation is generally computed theoretically by assuming equilibrium and taking into account the various processes that can populate and depopulate the relevant atomic levels.

The pioneering work on the chemical composition of the corona was performed in 1948 by Woolley and Allen, who determined the coronal abundances of Ar, Ca, Fe,

nd Ni. Their abundances, along with values from other investigators, are given in Table III. With the exception of Nikolskii's, all of the iron values are in good agreement. The adopted values for iron and the other elements are given in the last column. Before averaging, all of Nikolskii's values were systematically raised to agree better with the absolute scale defined by the other investigators. Pottasch (1964b) has discussed various sources of systematic errors in forbidden-line analyses and concluded that the systematic errors are on the order of 0.3 dex.

With the advent of rockets capable of carrying instrumentation above the ultraviolet-absorbing layers of the Earth's atmosphere, the XUV portion of the solar spectrum became accessible to observation. The solar UV spectrum contains the coronal resonance lines, including lines of several elements whose line emissions have not been observed in the visible. The first UV solar spectrum was obtained in 1946 by the U.S. Naval Research Laboratory using an instrument launched on a V-2 rocket. Since then numerous solar XUV experiments have been flown on suborbital and orbiting vehicles.

Ivanov-Kolodny and Nikolskii (1961, 1962), Pottasch (1963a, 1964b, 1967), Athay (1966), and others have developed techniques for determining relative coronal abundances from XUV observations. The intensity of an XUV line depends upon the abundance of the parent element, the fraction of atoms in the ionization state producing the line, and the electron density in the layer of the atmosphere where the line is produced. Since atoms in a given state of ionization are abundant over only a small range of temperatures, XUV lines will be formed in the layer of the atmosphere where formation of the appropriate stage of ionization is most strongly favored. By comparing the relative intensities of lines coming from different chemical elements but produced by ions formed in the same atmospheric layer, one can determine relative abundances.

To determine absolute abundances (abundances relative to hydrogen) from XUV data it is necessary to determine the electron density in the atmospheric layer where the lines are formed. Two techniques have been used. One (Pottasch 1963a; Dupree and Goldberg 1967; Heimers 1970) is based on solar radio-brightness temperatures, which depend on the run of temperature and density in the solar atmosphere. The other (Withbroe 1970, 1971) utilizes measurements of the intensity of the coronal white-light continuum of K-corona caused by scattering of photospheric light by coronal electrons.

Table IV lists the relative coronal abundances derived by different investigators. The abundances are given on a linear scale relative to the silicon abundance, which is set at 100. Generally there is agreement within a factor of 2 to 3 (0.3 to 0.5 dex), the major exception being iron where there is an order of magnitude difference. The best determination of the Si/Fe ratio is that of Jordan and Pottasch (1968) who obtained a value of unity, which is the value adopted here. The data of Athay (1966) and Dupree and Goldberg (1967) can be represented by a Si/Fe ratio of unity. The "adopted" values are the relative abundances that the author believes best represent the XUV results.

Table V places these abundances on a scale relative to hydrogen, based on data from several sources. As indicated earlier it appears that the Fe/Si ratio is unity and, therefore, the most reasonable estimate for the coronal silicon and iron abundance is 7.5 on the normal logarithmic scale. The higher values found by Pottasch (1963a, 1964b, 1967) and Withbroe (1970) are less reliable than the other results. The absolute scale for the adopted values is accurate to ± 0.5 dex.

Table VI summarizes the coronal results of Table III for forbidden lines and Tables IV and V for the XU lines. There is a systematic difference in scale between the two sets of abundances, with the forbidden lines giving abundances about 0.3 dex higher on the average. I arbitrarily split the difference to obtain the adopted coronal values. For comparison the differences between these abundances and the adopted photospheric and meteoritic values are also given. In general, the agreement is good except for potassium and cobalt. However, on the basis of the overall agreement between the coronal, photospheric, and meteoritic values, I would like to suggest that at least for these elements a useful working hypothesis would be that the values for these three sets of abundances are equal.

6. SUMMARY

Tables II and VI contain the adopted chemical compositions of the photosphere and corona. From the discussion of the results presented in these tables we summarize the following major points:

1. As shown in Table II, we are gradually building a fairly complete picture of the composition of the solar photosphere for the first 92 elements.

2. The problem of the solar iron abundance appears to have been largely resolved by recent work. Further analysis will probably not change the photospheric value adopted here by more than ± 0.3 dex.
3. The photospheric and coronal abundances are equal to within a factor of 2 (0.3 dex). Since the systematic errors in the abundances are of this magnitude, it seems reasonable to adopt the hypothesis that the two sets of abundances are equal until there is better evidence to the contrary.
4. There are some large discrepancies between the solar and meteoritic abundances for a number of elements, but because of uncertainties in the oscillator strengths, line identifications, or blending problems that may affect the discrepant solar values, it is premature to conclude that these two sets of abundances differ significantly.
5. There is still a need for better measurement of oscillator strengths for a number of elements whose abundances are based on measurements of questionable reliability. This is probably the outstanding problem remaining in solar abundance studies.

ACKNOWLEDGMENTS

I wish to thank Professor L. Goldberg and Dr. R. N. Thomas for the invitation to participate in the Menzel Symposium. I am indebted to Professor L. H. Aller and Professor L. Goldberg who stimulated my interest in the solar-abundance problem. This work was supported in part by the National Aeronautics and Space Administration through contract NAS-5-9274 and grant NGL-22-007-006.

TABLE I
SOME REPORTED PHOTOSPHERIC IRON ABUNDANCES

Ions	Investigators	Values*
Fe I	Russell (1929)	7.70
Fe I	Goldberg and Aller (1943)	6.99
Fe I	Unsöld (1948)	7.72
Fe I	Claas (1951)	7.62
Fe I	Weidemann (1955)	7.01
Fe I	Goldberg et al. (1960) (GMA)	6.57
Fe I	Leftus (1963)	6.76
Fe I	Baschek et al. (1963)	6.18
Fe II	Baschek et al. (1963)	6.78
Fe I	Teplitskaya and Vorobeva (1964)	6.78
Fe I	Müller and Mutschlecner (1964)	6.70
Fe I	Warner (1964)	6.81
Fe I	Goldberg et al. (1964)	6.54
Fe I	Aller et al. (1964)	6.57
Fe II	Aller et al. (1964)	6.59
[Fe II]	Swings (1965)	7.80
[Fe II]	Swings (1966)	7.40
Fe I	Müller (1967)	6.80
Fe I	Withbroe (1967)	6.85
Fe II	Warner (1968)	6.51
Fe I	Withbroe (1969a)	6.80
[Fe II]	Withbroe (1969b)	7.63
Fe I	Grevesse (1970)	6.61
Fe II	Grevesse (1970)	6.72
[Fe II]	Grevesse and Swings (1969)	7.50
Fe I	Garz et al. (1969)	7.60
Fe I	Rogerson (1969)	6.85
Fe II	Baschek et al. (1970)	7.63
Fe I	Cowley (1970)	7.00
Fe I	Takens (1970)	7.48
Fe I	Ross (1970)	7.20
[Fe II]	Nussbaumer and Swings (1970)	7.50
Fe I	Richter and Wulff (1970)	7.55
[Fe I]	Grevesse et al. (1971)	7.50
Fe I	Martinez-Garcia and Whaling (1971)	7.45

*Log $N_A+12.0$ where A is the abundance of the element relative to hydrogen.

PHOTOSPHERIC CHEMICAL COMPOSITION

At. #	Element	Photosphere		Abundances		Sources of Adopted Photospheric Values	Comments ²
		GMA	Adopted	Meteor. (Urey 1967)	Δ Meteor. ¹ & Adopted Photos.		
1	H	12.00	12.00				
2	He						
3	Li	0.96	0.60	3.25	2.65	Grevesse (1970) Engvold et al. (1970)	N, f, b, t
4	Be	2.36	1.06			Traub, Roseler (1971) Hauge, Engvold (1968)	I, f, b, t
5	B		≤ 2.80			Grevesse (1968)	N, f, t, λ
6	C	8.72	8.57			Grevesse (1968) Lambert (1968)	N, M, F, t, λ
7	N	7.98	8.06			Grevesse (1970) Lambert (1968)	N, M, t, λ
8	O	8.96	8.83			Grevesse (1970) Lambert (1968) Grevesse (1970)	N, M, F, t, λ
9	F		4.56	4.92	0.36	Müller et al. (1968) Hall, Noyes (1969)	M, f, λ
10	Ne		(7.45)			Coronal value ³	
11	Na	6.30	6.24	6.36	0.12	Lambert, Warner (1968a) Holweger (1971)	N, t
12	Mg	7.40	7.54	7.57	0.03	Lambert, Warner (1968c) Holweger (1971)	N, I, t
13	Al	6.20	6.40	6.48	0.08	Lambert, Warner (1968a)	N, t, λ
14	Si	7.50	7.55	7.55	0.00	Lambert, Warner (1968b)	N, I, t
15	P	5.34	5.43	5.56	0.13	Lambert, Warner (1968a)	N, t

Table II (continued)

16	S	7.30	7.21	7.25	0.04	Lambert, Warner (1968a) Swings et al. (1969)	N,F,t,ℓ
17	Cl		5.65	4.79	0.86	Lambert, Mallia (1968b)	N,f,t
18	Ar		(6.65)			Coronal value ³	
19	K	4.70	5.05	5.13	0.08	Lambert, Warner (1968a)	N,t,ℓ
20	Ca	6.15	6.33	6.42	0.09	Lambert, Warner (1968c) Lambert et al. (1969b)	N,I,F,t,ℓ
21	Sc	2.82	3.07	3.09	0.02	Warner (1968)	N,I,t,ℓ,e
22	Ti	4.68	4.74	4.91	0.17	Grevesse (1970)	N,ℓ
23	V	3.70	4.10	4.02	-0.08	Grevesse (1970)	N,ℓ,e
24	Cr	5.36	5.70	5.63	-0.07	Grevesse (1970)	N,I,ℓ
25	Mn	4.90	5.20	5.50	0.30	Grevesse (1970)	N,ℓ
26	Fe	6.57	7.40	7.50	0.10	(See Text)	N,I,F,ℓ,t
27	Co	4.64	4.50	4.91	0.41	Holweger, Oertel (1971) Garz (1971)	N,ℓ,e
28	Ni	5.91	6.28	6.24	-0.04	Grevesse (1970)	N,F,ℓ,t
29	Cu	5.04	4.45	4.32	0.13	Schmidt (1961) Aller (1968)	N,ℓ,e
30	Zn	4.40	4.42	4.53	0.11	Lambert et al. (1969a)	N,ℓ
31	Ga	2.36	2.84	3.26	0.42	Lambert et al. (1969a)	N,f,b,ℓ
32	Ge	3.29	3.32	3.69	0.37	Lambert et al. (1969a)	N,f,b,t
33	As						
34	Se			3.50			
35	Br			2.78			
36	Kr						
37	Rb	2.48	2.63	2.36	-0.27	Lambert, Mallia (1968a)	N,f,b,ℓ
38	Sr	2.60	2.82	2.93	0.11	Lambert, Warner (1968c)	N,I,ℓ,t
39	Y	2.25	1.62	2.21	0.59	Krueger et al. (1968) Aller (1968)	I,t
						CMA. Aller (1965) ⁴	N,I,ℓ,e

Table II (continued)

41	Nb	1.95	2.30				Wallerstein (1966)		N,b,ℓ,e
42	Mo	1.90	1.90				GMA; Aller (1965) ⁴		N,b,f,ℓ,e
43	Tc						Aller (1968)		N,b,f,ℓ,e
44	Ru	1.43	1.57				Aller (1968)		N,b,ℓ,e
45	Rh	0.78	1.55				Grevesse et al. (1968)		N,b,ℓ,e
46	Pd	1.21	1.57	2.17	0.60		GMA; Müller (1968) ⁵		N,b,ℓ,e
47	Ag	0.14	0.67	1.53	0.86		Aller (1968)		N,b,f,ℓ
48	Cd	1.46	1.97	1.93	-0.04		Lambert et al. (1969a)		N,b,f,t
							Aller (1968)		N,b,f,t
49	In	1.16	1.71	0.78	-0.93		Lambert et al. (1969a)		N,b,f,ℓ
50	Sn	1.54	1.71	1.81	0.10		Lambert et al. (1969a)		N,b,f,ℓ
51	Sb	1.94	0.75	1.13	0.38		Aller (1968)		N,b,f,ℓ,e
52	Te			1.61					
53	I								
54	Xe								
55	Cs		≤1.79	1.11	≥-0.68		Stellmacher, Wiehr (1969)		N,ℓ,t,e
							Grevesse (1970)		
56	Ba	2.10	1.80	2.22	0.42		Aller (1968)		I,ℓ,t
							Lambert, Warner (1968c)		
57	La		1.81	1.11	-0.70		Grevesse, Blanquet (1969)		I,ℓ,e
58	Ce		1.64	1.62	-0.02		Grevesse, Blanquet (1969)		I,ℓ,e
							Canfield (1969)		
59	Pr		1.63	0.78	-0.85		Grevesse, Blanquet (1969)		I,ℓ,e
60	Nd		1.82	1.44	-0.38		Grevesse, Blanquet (1969)		I,ℓ,e
61	Pm		absent				Grevesse, Blanquet (1969)		
62	Sm		1.66	0.91	-0.75		Grevesse, Blanquet (1969)		I,ℓ,e
63	Eu		0.49	0.51	0.02		Grevesse, Blanquet (1969)		I,b,ℓ,e
64	Gd		1.12	1.15	0.03		Grevesse, Blanquet (1969)		I,b,ℓ,e
65	Tb			0.42					
66	Dy		1.11	1.11	0.00		Grevesse, Blanquet (1969)		I,b,ℓ,e

Table II (continued)

67	Ho	0.50							
68	Er	0.76	0.89	0.13	Grevesse, Blanquet (1969)	I, b, f, λ , e			
69	Tm	0.43	0.09	-0.34	Grevesse, Blanquet (1969)	I, b, λ , e			
70	Yb	0.81	0.87	0.06	Grevesse, Blanquet (1969)	I, b, f, λ			
71	Lu	0.84	0.09	-0.73	Grevesse, Blanquet (1969)	I, b, f, λ , e			
72	Hf								
73	Ta								
74	W	2.57			Grevesse et al. (1968)	λ , e			
75	Re		0.25						
76	Os	0.75	1.34		Grevesse et al. (1968)	λ , e			
77	Ir	2.21	1.24		Grevesse et al. (1968)	N, λ , e			
78	Pt		1.75						
79	Au	0.32	0.91	0.59	Aller (1968)	N, f, b, λ , e			
80	Hg	≤ 3.00	2.61	≥ -0.39	Lambert et al. (1969a)	N, b, f, t			
81	Tl	≤ 0.20	0.81	≥ 0.61	Lambert et al. (1969a)	N, b, f, λ			
82	Pb	1.87	1.75	-0.12	Lambert et al. (1969a)	N, b, λ			
					Grevesse (1969)				
83	Bi	≤ 0.80	0.78	≥ -0.02	Grevesse (1969)	N, b, f, λ			
84	Po								
85	At								
86	Rn								
87	Fr								
88	Ra								
89	Ac								
90	Th	0.82	-0.02	-0.84	Grevesse (1969)	I, f, b, λ , t			
91	Pa								
92	U	$0.60 \leq$	-0.50	≥ -1.10	Grevesse (1969)	I			

¹Assumes $\log N_{Si} = 7.55$ ²N = abundance determined from lines of neutral atom

-I = abundance determined from lines of ionized atom

Table II (continued)

M = abundance determined from lines of molecule

F = abundance determined from forbidden lines

f = abundance determined from fewer than four lines

b = possible blending problems

ℓ = laboratory oscillator strengths

t = theoretical oscillator strengths

e = possible significant errors in the oscillator strengths

³Adopted value given in Table VI minus 0.1

⁴GMA; Aller (1965) GMA abundances as revised by Aller (1965)

⁵GMA; Müller (1967, 1968) GMA abundances as revised by Müller (1967, 1968)

TABLE III
CORONAL ABUNDANCES FROM FORBIDDEN LINE DATA

At.#	Element	Reported Values				Adopted Values*
		Woolley, Allen (1948)	Pottasch (1964a)	Nikolskii (1967)	Other	
1	H	12.00	12.00	12.00	12.00	12.00
16	S		7.10			7.10
18	Ar	5.00	7.10	6.30		7.00
19	K		5.90			5.90
20	Ca	6.30	6.80	6.10		6.60
24	Cr		6.00			6.00
25	Mn		5.70			5.70
26	Fe	7.80	7.87	7.30	7.85†	7.85
27	Co		5.60	4.80		5.50
28	Ni	6.40	6.72	6.00		6.55

*In the case of Nikolskii (1967), 0.55 was added to the values before averaging.

†Other Fe values (the average is 7.85):

7.86 (Pottasch 1963)	8.00 (Shkolovskii 1950a,b)
7.70 (Jordan 1966b)	7.60 (Suzuki & Hirayama 1964)
7.80 (Malville 1967)	≥7.00 (Jefferies & Orrall 1966)
8.00 (Dupree 1968)	7.90 (Eddy & Malville 1967)

TABLE IV
XUV CORONAL ABUNDANCES RELATIVE TO Si

At.#	Element	Reported Values			
		Pottasch (1964b,67)	Jordan, Pottasch (1968)	Athay (1966)	Dupree, Widing, Goldberg Sandlin (1967) (1968)
1	H	1000000			
2	He	200000			
6	C	1000		1900	1200
7	N	120		340	
8	O	500		1300	2900
10	Ne	70		100	≤500
11	Na	4		7.5	
12	Mg	60		100	250
13	Al	4		6.3	
14	Si	100	100	100	100
15	P	0.8		0.7	
16	S	40		62	
18	Ar				
20	Ca	3			
26	Fe	100	100	12	12
28	Ni	9	10*		20

*Originally measured by Jordan (1966a)

TABLE V
ABSOLUTE XUV CORONAL ABUNDANCES*

Investigators	Values Reported	
	XUV & Radio Data	XUV & K-Coronameter Data
tasch (1963,1964b,1967)	log N _{Si} =8.0	
ree, Goldberg (1967)	log N _{Si} =7.5	
pert (1967)	log N _{Fe} =7.35	
hbroe (1970)		log N _{Si} =7.7
hbroe (1971)		log N _{Si} =7.5
mers (1970)	log N _{Si} =7.56	
Value adopted: log N _{Si} = log N _{Fe} = 7.5		

TABLE IV
(continued)

Reported Values					
Polkskii (1969)	Withbroe (1970)	Reimers (1970)	Withbroe (1971)	Dupree (1971)	Adopted Values*
100000					3200000
300000					5100000
667				1000	1200
100	290			430	280
2000	1000		1300	1700	1400
100		85	80	79	84
6.7			8	5.4	6
133	98	200	80	85	100
10			7	10	7
100	100	100	100	100	100
					0.7
33				58	53
10					10
13		4			5
67		112		56	100
6.7					10

TABLE VI
CORONAL CHEMICAL COMPOSITION

At. #	Element	Forbid. Lines	XUV	Abundances			
				Δ Forbid. & XUV	Adopted Coronal	Δ Coronal & Photos.	Δ Coronal & Meteor. *
1	H	12.00	12.00		12.00		
6	C		8.60		8.75	0.18	
7	N		7.90		8.05	-0.01	
8	O		8.60		8.75	-0.08	
10	Ne		7.40		7.55		
11	Na		6.30		6.45	0.21	0.09
12	Mg		7.50		7.65	0.11	0.08
13	Al		6.30		6.45	0.05	-0.03
14	Si		7.50		7.65	0.09	0.10
15	P		5.30		5.45	0.02	-0.11
16	S	7.10	7.20	-0.10	7.15	-0.05	-0.10
18	Ar	7.00	6.50	0.50	6.75		
19	K	5.90			5.75	0.70	0.62
20	Ca	6.60	6.20	0.40	6.40	0.07	-0.02
24	Cr	6.00			5.85	0.15	0.22
25	Mn	5.70			5.55	0.35	0.05
26	Fe	7.85	7.50	0.35	7.67	0.27	0.27
27	CO	5.50			5.35	0.85	0.44
28	Ni	6.55	6.50	0.05	6.53	0.25	0.29

REFERENCES

- ller, L.H. 1965, *Advances in Astronomy and Astrophysics*, 3, ed. Z. Kopal (New York: Academic Press), 1.
- ller, L.H. 1968, *Proc. Astron. Soc. Australia*, 1, 133.
- ller, L.H., O'Mara, B.J., and Little, S. 1964, *Proc. Nat. Acad. Sci.*, 51, 1238.
- thay, R.G. 1966, *Aströphys. J.*, 145, 784.
- aschek, B., Garz. T., Holweger, H., and Richter, J. 1970, *Astron. Astrophys.*, 4, 229.
- aschek, B., Kogel, W.H., and Traving, G. 1963, *z.f. Astrophys.*, 56, 282.
- ridges, J.M. and Wiese, W.L. 1970, *Astrophys. J.*, 161, L71.
- anfield, R.C. 1969, *Astrophys. J.*, 157, 425.
- laas, W.J. 1951, *Rech. Astron. Obs. Utrecht*, 12, 1.
- orliss, C.H. and Bozman, W.R. 1962, *U.S. Nat. Bur. Stand. Monograph* 53.
- owley, C. 1970, *Astrophys. Letters*, 5, 149.
- upree, A.K. 1968, Doctoral Thesis, Harvard University.
- upree, A.K. 1971, *Bull. Amer. Astron. Soc.*, 3, 246(A).
- upree, A.K. and Goldberg, L. 1967, *Solar Phys.*, 1, 229.
- ddy, J.A. and Malville, J.M. 1967, *Astrophys. J.*, 150, 289.
- dlén, B. 1942, *z.f. Astrophys.*, 22, 30.
- ngvold, O., Kjeldseth Moe, O., and Maltby, P. 1970, *Astron. Astrophys.*, 9, 79.
- arz, T. 1971, *Astron. Astrophys.*, 10, 175.
- arz, T., Holweger, H., Kock, M., and Richter, J. 1969a, *Astron. Astrophys.*, 2, 446.
- arz, T. and Kock, M. 1969, *Astron. Astrophys.* 2, 274.
- arz, T., Kock, M., Richter, J., Baschek, B., Holweger, H., and Unsöld, A. 1969b, *Nature*, 223, 1254.
- oldberg, L. and Aller, L.H. 1943, *Atoms, Stars, and Nebulae* (Philadelphia: Blakiston Co.).
- oldberg, L., Kopp, R.A., and Dupree, A.K. 1964, *Astrophys. J.*, 140, 707.
- oldberg, L., Müller, E.A., and Aller, L.H. 1960, *Astrophys. J. Suppl.*, 5, 1.
- rasdalen, G.L., Huber, M., and Parkinson, W.H. 1969, *Astrophys. J.*, 156, 1153.
- revesse, N. 1968, *Solar Phys.*, 5, 159.
- revesse, N. 1969, *Solar Phys.*, 6, 381.
- revesse, N. 1970, *Mem. Acad. Roy. Belg.*, 39, 1.
- revesse, N., Blanquet, G., and Boury, A. 1968, *Origin and Distribution of the Elements*, ed. L.H. Ahrens (Oxford: Pergamon Press), 177.

- Grevesse, N. and Blanquet, G. 1969, *Solar Phys.*, 8, 5.
- Grevesse, N., Nussbaumer, H., and Swings, J.P. 1971, *Mon. Not. Roy. Astron. Soc.*, 151, 239.
- Grevesse, N. and Swings, J.P. 1969, *Astron. Astrophys.* 2, 28.
- Grotrian, W. 1939, *Naturwissenschaften*, 27, 214.
- Hall, D.N.B. and Noyes, R.W. 1969, *Astrophys. Letters*, 4, 143.
- Hauge, O. and Engvold, O. 1968, *Astrophys. Letters*, 2, 235.
- Holweger, H. 1971, *Astron. Astrophys.*, 10, 128.
- Holweger, H. and Oertel, G. 1971, *Astron. Astrophys.*, 10, 434.
- Huber, M. 1971, *Shock Tube Spectroscopy Laboratory Report No. SR-34* (Cambridge: Harvard College Observatory).
- Huber, M. and Tobey, F.L., Jr. 1968, *Astrophys. J.*, 152, 609.
- Ivanov-Kholodny, G.S. and Nikolskii, G.M. 1961, *Soviet Astron. A.J.*, 5, 31.
- Ivanov-Kholodny, G.S. and Nikolskii, G.M. 1962, *Geomagnetism i Aeronomyia*, 2, 425.
- Jefferies, J.T. 1966, *Abundance Determinations in Stellar Spectra*, ed. H. Hubenet (New York: Academic Press), 207.
- Jefferies, J.T. and Orrall, F.Q. 1966, *Astrophys. J.*, 145, 231.
- Jordan, C. 1966a, *Mon. Not. Roy. Astron. Soc.*, 132, 463.
- Jordan, C. 1966b, *Mon. Not. Roy. Astron. Soc.*, 132, 515.
- Jordan, C. and Pottasch, S.R. 1968, *Solar Phys.*, 4, 104.
- Krueger, T.K., Aller, L.H., Ross, J., and Czyzak, S.J. 1968, *Astrophys. J.*, 152, 765.
- Lambert, D.L. 1968, *Mon. Not. Roy. Astron. Soc.*, 138, 143.
- Lambert, D. L. and Mallia, E.A. 1968a, *Mon. Not. Roy. Astron. Soc.*, 140, 13.
- Lambert, D.L. and Mallia, E.A. 1968b, *Solar Phys.*, 5, 181.
- Lambert, D.L., Mallia, E.A., and Warner, B. 1969a, *Mon. Not. Roy. Astron. Soc.*, 142, 71.
- Lambert, D.L., Mallia, E.A., and Warner, B. 1969b, *Solar Phys.*, 7, 11.
- Lambert, D.L. and Warner, B. 1968a, *Mon. Not. Roy. Astron. Soc.*, 138, 181.
- Lambert, D.L. and Warner, B. 1968b, *Mon. Not. Roy. Astron. Soc.*, 138, 213.

- Lambert, D.L. and Warner, B. 1968c, *Mon. Not. Roy. Astron. Soc.*, 140, 197.
- Lambert, D.L. and Swings, J.P. 1967, *Solar Phys.*, 2, 34.
- Leftus, V. 1963, *Bull. Astron. Inst. Csl.*, 14, 155.
- Malville, J.M. 1967, *Astrophys. J.*, 148, 229.
- Martinez-Garcia, N. and Whaling, W. 1971, *Amer. Phys. Soc. Meeting*, New York, N.Y.
- Martinez-Garcia, M., Whaling, W., Mickey, D.L., and Lawrence, G.M. 1970, Orange AID Preprint OAP-288, Calif. Inst. Tech., Pasadena, Calif.
- Menzel, D.H. 1931, *Pub. Lick Obs.*, 17, 1.
- Müller, E.A. 1966, *Abundance Determination in Stellar Spectra*, ed. H. Hubenet (New York: Academic Press), 171.
- Müller, E.A. 1967, *Solar Physics*, ed. J.N. Xanthakis (New York: Interscience), 33.
- Müller, E.A. 1968, *Origin and Distribution of the Elements*, ed. L.H. Ahrens (Oxford: Pergamon Press), 155.
- Müller, E.A., Baschek, B., and Holweger, H. 1968, *Solar Phys.*, 3, 125.
- Müller, E.A. and Mutschlechner, J.P. 1964, *Astrophys. J. Suppl.*, 9, 1.
- Neupert, W.M. 1967, *Solar Phys.*, 2, 294.
- Nikolskii, G.M. 1967, *Soviet Astron. A.J.*, 10, 915.
- Nikolskii, G.M. 1969, *Solar Phys.*, 6, 399.
- Nussbaumer, H. and Swings, J.P. 1970, *Astron. Astrophys.*, 7, 455.
- Pottasch, S.R. 1963a, *Astrophys. J.*, 137, 945.
- Pottasch, S.R. 1963b, *Mon. Not. Roy. Astron. Soc.*, 125, 543.
- Pottasch, S.R. 1964a, *Mon. Not. Roy. Astron. Soc.*, 128, 73.
- Pottasch, S.R. 1964b, *Space Sci. Rev.*, 3, 816.
- Pottasch, S.R. 1967, *Bull. Astron. Inst. Neth.*, 19, 113.
- Reimers, D. 1970, submitted to *Astron. Astrophys.*
- Richter, J. and Wulff, P. 1970, *Astron. Astrophys.*, 9, 37.
- Rogerson, J.B. 1969, *Astrophys. J.*, 158, 797.
- Ross, J.E. 1970, *Nature*, 225.
- Russell, H.N. 1929, *Astrophys. J.*, 70, 11.
- Schmidt, T. 1961, *z.f. Astrophys.*, 53, 273.
- Shklovskii, I.S. 1950a, *Crimean Astrophys. J.*, 5, 86, 109.
- Shklovskii, I.S. 1950b, *Crimean Astrophys. J.*, 6, 105.
- Stellmacher, G. and Wiehr, E. 1969, *Astrophys. Letters*, 3, 91.

- Strömgren, B. 1940, *Festschrift für Eli Strömgren* (Copenhagen: Munskgaard), 218.
- Suzuki, T. and Hirayama, T. 1964, *Publ. Astron. Soc. Japan*, 16, 58.
- Swings, J.P. 1965, *Ann. d'Astrophys.*, 28, 703.
- Swings, J.P. 1966, *Ann. d'Astrophys.*, 29, 371.
- Swings, J.P., Lambert, D.L., and Grevesse, N. 1969, *Solar Phys.*, 6, 3.
- Takens, R.J. 1970, *Astron. Astrophys.*, 5, 244.
- Teplitskaya, R.B. and Vorobeva, V.A. 1964, *Soviet Astron. A.J.*, 7, 778.
- Traub, W. and Roseler, F.L. 1971, *Astrophys. J.*, 163, 629.
- Unsöld, A. 1948, *z.f. Astrophys.*, 24, 306.
- Urey, H.C. 1967, *Quart. J. Roy. Astron. Soc.*, 8, 23.
- Wallerstein, G. 1966, *Icarus*, 5, 75.
- Warner, B. 1964, *Mon. Not. Roy. Astron. Soc.*, 127, 413.
- Warner, B. 1968, *Mon. Not. Roy. Astron. Soc.*, 138, 229.
- Warner, B. 1969, *Observatory*, 89, 107.
- Warner, B. and Cowley, C.R. 1967, *J. Quant. Spect. Radiative Transfer*, 7, 751.
- Weidemann, V. 1955, *z.f. Astrophys.*, 36, 101.
- Whaling, W., King, R.B., and Martinez-Garcia, M. 1969, *Astrophys. J.*, 152, 389.
- Widing, K.G. and Sandlin, G.D. 1968, *Astrophys. J.*, 152, 545.
- Wildt, R. 1939, *Astrophys. J.*, 89, 295.
- Withbroe, G.L. 1967, *Shock Tube Spectroscopy Laboratory Report No. SR-17* (Cambridge: Harvard College Observatory).
- Withbroe, G.L. 1969a, *Solar Phys.*, 9, 19.
- Withbroe, G.L. 1969b, *Astrophys. J.*, 156, 1177.
- Withbroe, G.L. 1970, *Solar Phys.*, 11, 42.
- Withbroe, G.L. 1971, *Solar Phys.*, in press.
- Wolnik, S.J., Berthel, R.O., and Carnevale, E.H. 1969, *Astrophys. J.*, 157, 1969.
- Wolnik, S.J., Berthel, R.O., and Wares, G.W. 1970, *Astrophys. J.*, 162, 1037.
- Wolnik, S.J., Berthel, R.O., Larson, G.S., Carnevale, E.H., and Wares, G.W. 1968, *Phys. Fluids*, 11, 1002.
- Wolnik, S.J., Berthel, R.O., and Wares, G.W. 1971, *Astrophys. J.*, 166, L31.
- Wooley, R.v.d.R. and Allen, C.W. 1948, *Mon. Not. Roy. Astron. Soc.*, 108, 292.
- Zwann, C. 1967, *Bull. Astron. Inst. Netherlands*, 19, 1.

III

GASEOUS NEBULAE

*Chairman: James G. Baker
Harvard College Observatory*

I've just discovered that astronomy
is a science that requires a little
less than no-place accuracy.

Leland Cunningham



OPTICAL LINE SPECTRUM

S. J. Czyzak

*Perkins Observatory
The Ohio State and
Ohio Wesleyan Universities*

and

T. K. Krueger

*General Physics Laboratory
Wright-Patterson Air Force Base*

I. INTRODUCTION

In his introduction to *Selected Papers on Physical Processes in Ionized Plasmas* (1962), Professor Donald H. Menzel points out that for the astronomer, hydrogen is the most important element in the universe. It constitutes 90% of all atoms. However, the 9% of helium and the remaining 1% of the atoms also play an important role in unraveling the mysteries of the universe. Thus, in the field of astrophysics, the study of the elements and their spectra, i.e. line intensities and continua, is fundamental to the understanding of the physical processes that take place in stars, nebulae, and galaxies.

Professor Menzel considered this aspect of astrophysics sufficiently important that in 1935 he and C. L. Pekeris started a study of hydrogen. In 1937 he initiated a thoroughgoing study of the various types of physical processes occurring in highly ionized gases, which included radiative and collisional interactions of the various atoms. For the next decade, he and his co-workers pursued this effort intensively. The results of this first phase of the work are well known through the series of publications entitled "Physical Processes in Gaseous Nebulae".

The work at Harvard did more than improve and extend the earlier investigations of Zanstra, Ambarzumian, Plaskett, Carroll, and Menzel on hydrogen and helium spectra, and those of Bowen, Condon, and

Pasternack on forbidden-line spectra. It inspired investigations on forbidden-line strengths by Garstang and Aller, Ufford and Van Vleck; on collision strengths by Seaton and his collaborators; and on the physics of gaseous nebulae by some of Menzel's original collaborators, e.g. Goldberg and Aller, and also by Osterbrock and his associates, Seaton and his team, Peimbert, and many others.

The continued effort of many scientists has enabled us to explain today at least some of the physical processes in gaseous nebulae.

The incentive to seek accurate measurements of spectral-line intensities was largely provided by the precise predictions of Menzel's theoretical work. His important contributions include: (1) absorption coefficients and hydrogen-line intensities (with Pekeris); (2) the theory of recombination (with Baker); (3) forbidden line strengths (with Shortley, Aller, and Baker); (4) the first quantum mechanical calculations of collision strengths (with Hebb); (5) the first quantitative treatment of the Bowen fluorescent mechanism.

In spite of the tremendous effort by Professor Menzel and other scientists, there is still no completely adequate interpretation of optical line spectra.

II. THE PROBLEM OF MEASURED INTENSITIES

As is well known, line intensities in gaseous nebulae may be obtained by spectrophotographic and spectrophotoelectric methods. Generally, both methods are employed because each has certain advantages in estimating various line intensities. In the spectrophotographic method one can use a slit spectrograph, a slitless spectrograph, or narrow band filters to evaluate, respectively, the line intensities of the nebula, the spectrum of the central star, and the radiation in specific regions. With these one can then make appropriate comparisons, all of which are essential to a satisfactory evaluation of the spectrum. Also, by varying the exposure one can obtain graded intensities and thus the opportunity of measuring not only strong lines but also weak ones.

The present photoelectric methods enable us to obtain an "integrated" intensity for the various spectral lines from the entire nebula in both the blue and visible regions. In particular, this method gives excellent confirmation of the strong and medium intensity spectral lines. By a combination of photographic

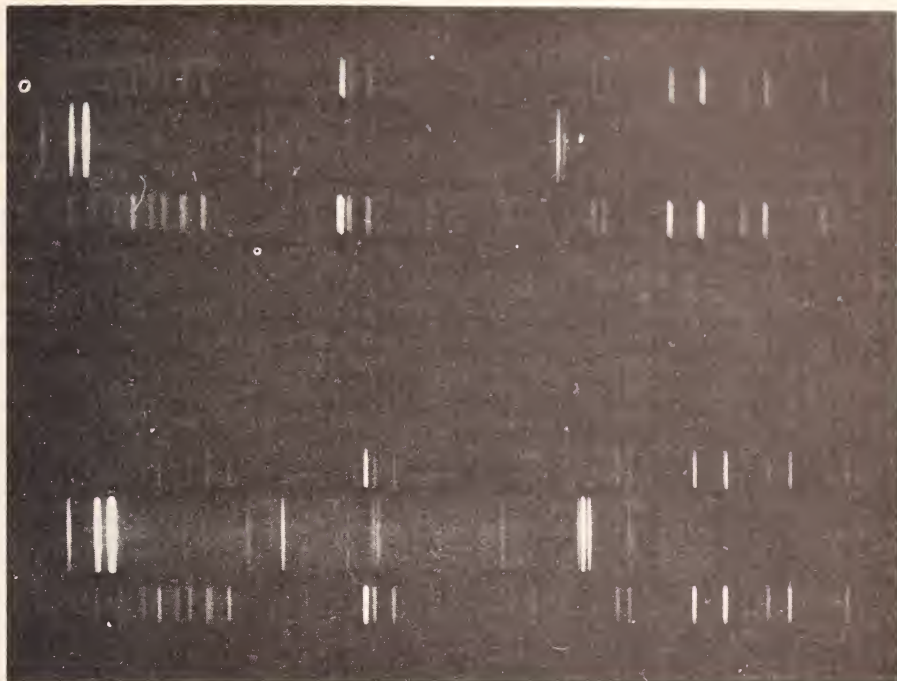


Figure 1. Spectrograms of NGC 3587 taken at the Perkins 72" telescope of The Ohio State and Ohio Wesleyan Universities at the Lowell Observatory, Flagstaff, Arizona. These spectrograms were taken by G. Boeshaar, S. J. Czyzak and Kent Ford. Exposures were 30 minutes and 145 minutes duration.

and photoelectric means, one can then obtain a more detailed analysis of a particular spectrum, i.e. the former can be used to obtain weak line intensities through long exposures, and the latter can be used to obtain strong and medium lines.

More recently the innovation of the image tube has been helpful in spectral analysis. Here too, by using a slit spectrograph and off-set guiding, one can obtain spectrograms of high and low excitation regions separately. The great advantage with the image tube is the relatively short exposure time necessary to obtain useful results. Figure 1 shows two spectrograms of NGC 3587 for the region $\lambda 4800$ to $\lambda 7500$, at two different exposures, which were done with Dr. Kent Ford's image tube at the 72-inch telescope at Flagstaff, Arizona.

We use all these methods in order to gather the

data necessary to determine the spatial distribution of ions and atoms. However, we still face certain difficulties in the measurement of our line intensities. Generally, the measured intensities are good to $\pm 10\%$ for the strong lines, $\pm 20 - \pm 40\%$ for the medium intensity lines, and for the weak lines the uncertainty may be as high as 100%.

Much of the problem in assessing the line intensities is due to irregularities within the nebula itself. If the structure of the nebula is reasonably uniform, so that the line intensities in particular regions or condensations can be measured, then it is quite feasible to explain the general structure of a nebula, for example, IC 418. If, on the other hand, the structure is irregular and local condensations are present throughout, then one obtains more or less integrated intensities rather than intensities representing specific regions only. In these cases a satisfactory explanation of the structure is very unlikely. Two examples of such a complex structure would be NGC 6543 and NGC 1514.

Considerable improvement has been made over the years in the techniques used for spectral investigation of nebulae; however, we have not yet reached the stage where we can make accurate detailed studies of the regions in which the ions occur. This is not to imply that there has not been any success in identifying regions in which some of the ions are formed, but this depends upon the degree of symmetry and size of the nebula. For example, for stellar types it is not feasible, and we have been able to obtain only integrated intensities for the spectral lines, i.e. the regions of high and low excitation cannot be isolated for spectral analysis. In summary, our present combination of techniques allows us to arrive at a reasonably good estimate of the ionization distribution and structure for some of the nebulae.

III. THEORETICAL CONSIDERATIONS IN LINE INTENSITY MEASUREMENTS

In gaseous nebulae, we are concerned with the following kinds of lines:

- (1) permitted lines (electric dipole radiation) that arise from photoionization and recombination;
- (2) forbidden lines (magnetic dipole and electric quadrupole radiation) which arise when electrons that have been collisionally excited to metastable levels of

a configuration cascade to the lower levels of the same configuration;

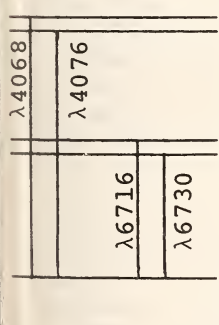
(3) fluorescent lines (Bowen 1934), which arise in high excitation nebulae when O^{+2} ions absorb HeII (Ly α) radiation and when N^{+2} ions absorb one of the fluorescent OIII lines.

Accurate intensity measurements are important for all of these lines because we have an accurate theory with which to interpret them, thanks to Menzel's pioneer work, which has been amplified and extended in recent years. One might truthfully say that the theory is ahead of the observations in many instances; for example, critical lines are often weak and difficult to measure accurately.

A proper account of the above three mechanisms would require more space than is available and has been given in the literature by many writers. Therefore, we shall confine our attention to one illustrative problem, the excitation of the forbidden lines of ionized sulfur because they appear in many nebular filaments.

Now that reliable atomic parameters are available, at least so we believe, the relevant forbidden lines become correspondingly more useful for the diagnostics of nebular plasmas, i.e. for deducing densities and temperatures of the individual condensations or filaments in which these lines originate.

The basic equations of statistical equilibrium for the five levels of [SII] may be written in the following manner:



The diagram shows energy levels for SII. The top level is labeled $2P_{\frac{1}{2}, \frac{3}{2}}$ and has two sub-levels with wavelengths $\lambda 4068$ and $\lambda 4076$ indicated. Below this is the $2D_{\frac{3}{2}, \frac{5}{2}}$ level, with sub-levels at $\lambda 6716$ and $\lambda 6730$. The bottom level is $4S_{\frac{3}{2}}$.

$$N_e q_{mn} + N_e \sum_{m=2=n}^5 N_n q_{mn} + \sum N_m A_{mn} =$$

$$N_n \left\{ N_e \sum_{m=n-1}^5 q_{mn} + \sum_{m<n} A_{mn} \right\}$$

with $n = 2, 3, 4, \text{ \& } 5$

where q_{mn} = the rate of collisional excitation of upper level n to lower level

$$q_{mn} = 8.62 \times 10^{-6} \frac{\Omega(m, n)}{\omega_m T^{1/2}} e^{-\chi_{mn}/kT} e^{-\chi_n/kT}$$

q_{nm} = the rate of collisional de-excitation of level n to level $m = 8.62 \times 10^{-6} \frac{\Omega(m,n)}{\omega_n T^{1/2}}$,

Ω = the collision strength for electron impact excitation to level n from level m .

A_{mn} = the total transition probability, which is due to the sum of the magnetic dipole and electric quadrupole contributions in the [SII] problem, that is, $A^{(M)}(J,J') + A^{(Q)}(J,J')$ where

$$A^{(M)}(J,J') = \frac{3.532 \times 10^4}{(2J+1)} \bar{\nu}^3 S^{(M)}(J,J')$$

$$A^{(Q)}(J,J') = \frac{2.648 \times 10^3}{(2J+1)} \bar{\nu}^5 S^{(Q)}(J,J') ,$$

where $\bar{\nu}$ is the frequency in wavenumbers.

The equations involving the q 's are based on the following two assumptions: (1) electron velocities can be represented by a Maxwellian distribution, and (2) the energy change is small over the range under consideration.

From the above expressions we see that it is essential to have accurate S 's and Ω 's. Both quantities, except in the case of the magnetic dipole contribution for S , depend very strongly on the wave functions, and until relatively recently this was one of the main "stumbling blocks" in obtaining accurate A 's and Ω 's.

Today, these wave functions are calculated by the Hartree-Fock Self-Consistent Field Method developed by Charlotte Froese-Fisher, Roothaan and his co-workers, Mayers and Hirsch, and others. These highly sophisticated programs are the result of the expansion and improvement of the early pioneer work of Hartree and his students (Garstang, Douglas, Mayers and Froese-Fisher), and Fock.

Here also it is essential to mention Bates, Lowdin, Hylleraas, Dalgarno, Layzer, H. Kelly, and others in connection with their fundamental work on atomic structure. For it is the advancement and developments in

atomic structure that significantly contributed to the solution of the problems encountered in calculating atomic parameters.

The intensity ratio

$$r_1 = \frac{I(\lambda 6716)}{I(\lambda 6730)}$$

of [SII] is particularly useful for getting a good estimate of the density N_e if $0.5 < r_1 < 1.15$. This is because the solutions of the equilibrium equations for the five levels of the ground state configuration lead to values of r_1 that, when plotted as a function of $\log x$ (where $x = 10^{-2} N_e / \sqrt{T_e}$), give curves lying very close together (Figure 2) and nearly vertical for $0.75 < t < 1.5$ (where $t = 10^{-4} T_e$). Since this is the approximate range of T_e in planetary nebulae, the value of x and hence N_e for an assumed T_e should be fairly good, especially since the line intensities, $\lambda 6716$ and $\lambda 6730$, are well measured. For example, consider NGC 7662 for which Weedman (1968) reports an $r_1 = 0.62$. If one assumes $T_e = 10,000^\circ$, then $N_e = 1.04 \times 10^4 / \text{cm}^3$. If, on the other hand, one assumes either $T_e = 7500^\circ \text{K}$ or $T_e = 15,000^\circ \text{K}$, the spread in N_e is $1.00 \times 10^4 < N_e < 1.00 \times 10^4$. Consequently, it is seen that r_1 can be used to give N_e to within 5 to 10%, and this would certainly be at least as reliable as the measurement of r_1 and the atomic parameters used to predict it. Thus, it certainly can be said that the use of r_1 gives reliable results for N_e provided, of course, that the measured line intensities are reliable, as is the case for the $\lambda 6716$, $\lambda 6730$ lines in [SII].

The ratio r_1 cannot, however, tell us much about the temperature, and for a good estimate of T_e we must therefore consider other intensity ratios. One set of lines that could be used is $\lambda 4068$ and $\lambda 4076$, the ratio between their sum and that of $\lambda 6716$ and $\lambda 6730$ being sensitive to T_e . However, there is an observational problem in that the $\lambda 4068$ and $\lambda 4076$ lines are blended with those of Hg, so that they cannot always be used. However, $\lambda 4068$ is often sufficiently free from Hg contamination that an estimate of the line intensity can be made, and the ratio

$$r_2 = \frac{I(\lambda 4068)}{I(\lambda 6716) + I(\lambda 6730)}$$

is generally used. But the intensity of the $\lambda 4068$ line

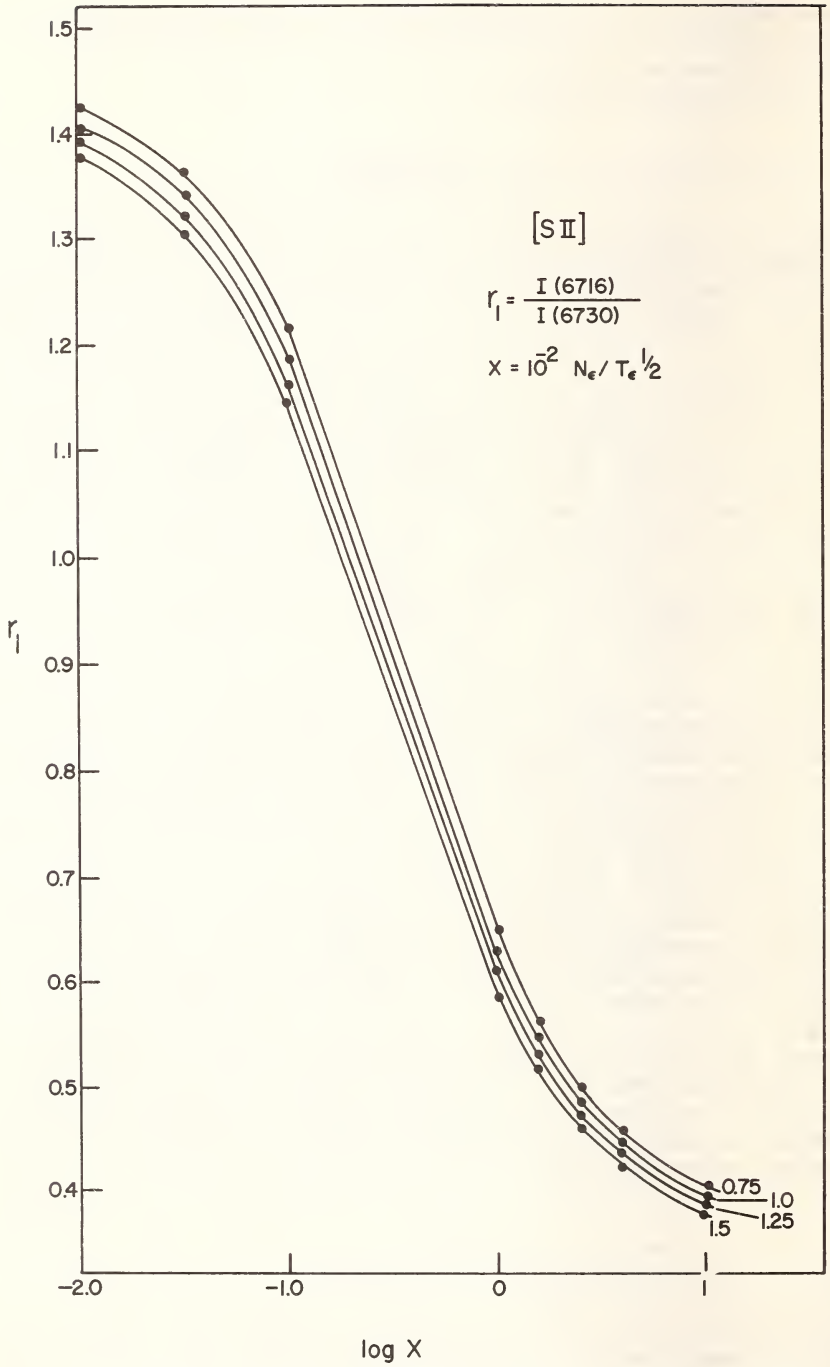


Figure 2. Theoretical curves for the intensity ratio, r_I .

weak and therefore much less accurately measured than those in r_1 . This leads to results that can be inconsistent. Consider again NGC 7662. If one takes the measured value of r_2 and uses the theoretical curves r_2 vs. $\log x$ (Figure 3) to obtain x for values of T_e in the range $7500^\circ < T_e < 15,000^\circ$, and if one then uses this value of x with the value of N_e obtained from r_1 to find T_e , one finds that this T_e is nowhere near the T_e of the curve in Figure 3, regardless of which curve is used. The difference may be as much as

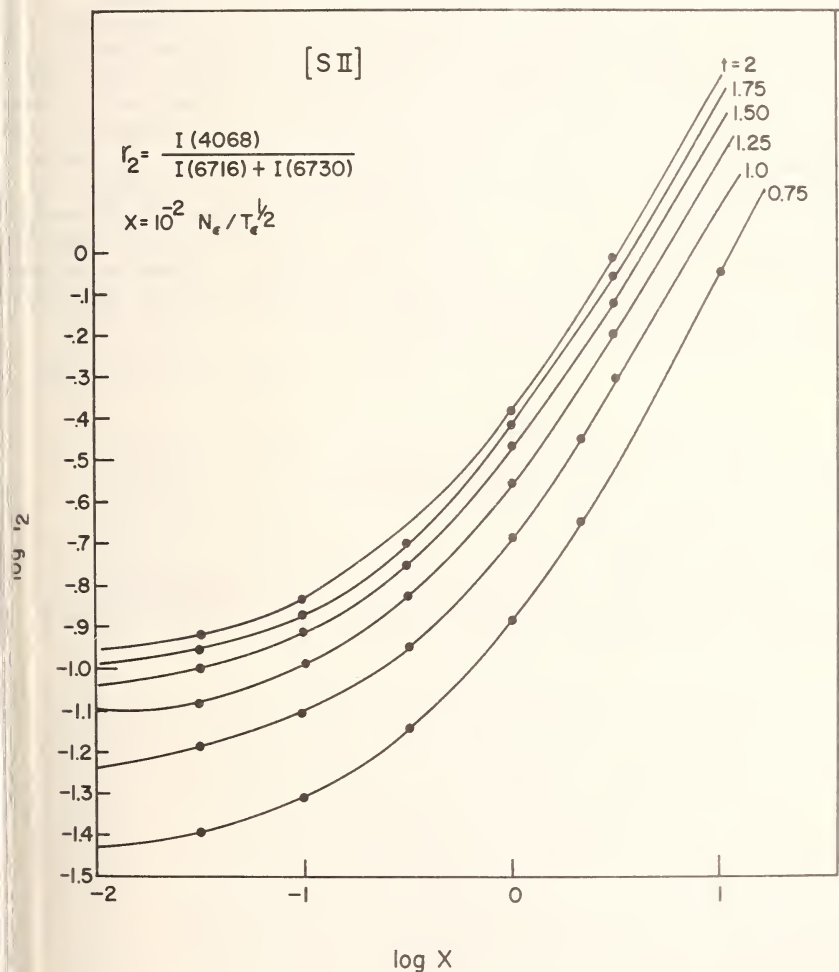


Figure 3. Theoretical curves for the intensity ratio, r_2 .

an order of magnitude. Or, if one computes T_e by using a different ion, as for example the [OIII] ratio $I(\lambda 4363)/I(N_1+N_2)$ and uses r_2 to obtain N_e , the resulting value of N_e will usually be higher than that obtained from r_1 . The difference may be as much as a factor of 1.5 to 2.

IV. CONCLUSION

Today, while we have certain spectroscopic data (mostly in the blue region), it is quite apparent that additional data in the visual and infrared regions are required. The discrepancies in N_e and T_e as determined by the r_1 and r_2 ratios confirm this. While the $\lambda 4076$ and $\lambda 4076$ values in [SII] are highly desirable in our calculations, the mercury contamination (blending) in a number of instances precludes their use. It is also necessary to get additional data for other lines, namely, those of [ClIII], [ArIV], and other $2p^q$ and $3p^q$ ($q = 2, 3, 4$) ions. With accurate intensity ratios and atomic parameters, the study of the structure and ionization distribution can be carried out in greater detail and with greater confidence.

REFERENCES

- Bowen, I.S. 1934, *P.A.S.P.*, 46, 146.
Menzel, D.H. 1962, *Selected Papers on Physical Processes in Ionized Plasmas* (New York: Dover)
Weedman, D.W. 1968, *Ap. J.*, 153, 49.

CHEMICAL COMPOSITION OF TYPICAL PLANETARY NEBULAE

Lawrence H. Aller

University of California, Los Angeles

When we attempt to determine the chemical composition of a gaseous nebula from its bright-line spectrum, we know at the outset that there exist tremendous deviations from local thermodynamic equilibrium, and that we must invoke the detailed mechanism appropriate to the excitation of each line. In fact, the prime objective of the original program embodied in the series on "Physical Processes in Gaseous Nebulae" was the quantitative interpretation of the spectra of these objects; the last paper (Menzel and Aller 1945) was an attempt to assess their chemical compositions.

If we grant that the physical mechanisms of spectral-line and continuum excitation are understood, we have the following tasks:

1. Calculation of accurate atomic parameters, notably the Einstein A values and the collision strengths Ω (Hebb and Menzel 1940). Czyzak has mentioned this problem in the preceding paper.
2. Accurate measurement of line intensities and continuum data.
3. Allowance for the distribution of atoms of a given element among different ionization stages.

I cannot overemphasize the importance of a photometric calibration of line intensities measured by photographic photometry. We have tried to do this for the nebulae discussed in a series of papers "Spectrophotometric Studies of Gaseous Nebulae". Early photographic work had suggested a deviation of the Balmer decrement from theoretical predictions; later measurements showed a preponderance of Balmer decrements that tended to agree with theory. Joseph Miller (1971) has found a decrement for NGC 7027 that agrees with theory, and indeed a new series of spectrograms of this object with improved calibrations confirms this

result; so great care must be used in the measurement of weak lines.

Although "photoelectric accuracy" is the envy of all of us who work with the photographic plate, we must realize that there are certain tasks that can be done only by combinations of photographic and photoelectric photometry. A typical photoelectric measurement of a nebular spectrum line embodies an integration over the entire disk of the nebula - or a sizable region thereof. Thus

$$I_{PEP} = \int I(x,y) dA$$

while a photographic observation gives us

$$I_{ptg}(x,y) \Delta x \Delta y = \int_{y-\frac{1}{2}\Delta y}^{y+\frac{1}{2}\Delta y} \int_{x-\frac{1}{2}\Delta x}^{x+\frac{1}{2}\Delta x} I(x,y) dx dy .$$

Here Δx and Δy depend on the resolution of the photographic plate, the seeing, and the microphotometer system employed. Further,

$$I(x,y) = \int_{-\infty}^{+\infty} E(x,y,z) dz$$

where dz is the element of integration along the line of sight, whereas theoretical considerations always give us $E(N_e, T_e)$, which can vary from point to point x, y, z , within the nebula.

Consider, for example, the isophotic contours of NGC 6818, as shown in Figure 1. Photoelectric measurements would give the integrated intensity over the surface; photographic measurements would give intensities corresponding to a small area or a series of small areas taken along a line across the nebula. The ideal solution would be to use the photoelectric measurements in conjunction with the isophotic contours to interpolate the photographic intensity measurements.

So far we have not had sufficiently detailed information on isophotic contours of different ions to apply this technique to any complex nebula. At this point we need a large body of monochromatic photographs of

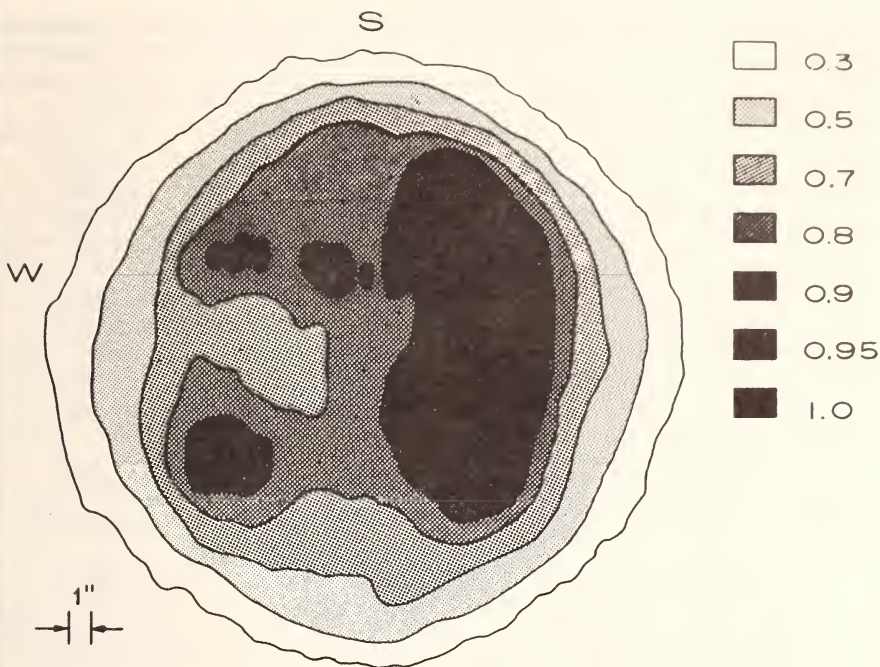


Figure 1. Isophotic contours of $\lambda 5007$ [OIII] in NGC 6818. These contours were traced with the Michigan Iso-photometer by Mrs. Nancy Boggess from a plate secured at the coude focus of the 100-inch telescope of the Hale Observatories. The approximate scale is indicated at the left. The numbers, 1.0, 0.95, 0.9, etc. give the logarithm of the intensity (surface brightness of the nebula). Loss of resolution is produced mostly by seeing and guiding errors.

nebulae, such as those obtained by Kent Ford and Vera Rubin (1971) and by M. F. Walker and G. E. Kron (1971).

At the present time there are two ways one can proceed. One is to concentrate attention on selected knots or filaments and analyze these in great detail. This procedure requires much observing time with a large telescope, but it may prove necessary for objects such as NGC 6543 or NGC 2392.

An alternate procedure, which has been applied by Peimbert and Costero (1969) to the Orion nebula, is to take the variations of density and temperature into account in a statistical sense. For example, different values of the electron temperature may be found from an analysis of the radio-frequency-continuum data (Mills and Shaver 1967) than from the forbidden lines of

[OIII]. A comparison of the Balmer jump with high members of the Balmer series may give another estimate, and so forth. These temperature differences represent a different weighting of different regions in the nebula, depending on the mechanism of emission involved. In an extended object such as Orion, one has little choice, but in a planetary nebula where individual knots and filaments can be recognized, it is to be hoped that one may have regions of fairly constant temperature and density.

Nevertheless, we cannot overemphasize the importance of these fluctuations, which Peimbert has clearly demonstrated must be taken into account. We must still face up to the problem of why these temperature fluctuations are so large. In a given nebula, they may range from 6000°K to 10,000°K.

Density fluctuations are also spectacular and occur in many planetaries. Some seventeen years ago (Aller 1954), I suggested that the observed spectrum of NGC 7027

...can be understood in terms of a nebula consisting of numerous filaments, knots, and tenuous regions, such that the density may range from perhaps less than 10,000 ions/cm³ to perhaps something like 200,000 ions/cm³...

Such large densities seemed unusual in planetaries (other than IC 4997) at that time, but Goldberg has presented a similar conclusion for NGC 7027 at this symposium.

A second problem is how to allow for the distribution of atoms among different ionization stages. Three procedures have been proposed:

1. Construction of empirical ionization curves
2. Allowance for a domination of the ionization of many ions by the ionized helium radiation field, and other empirical considerations
3. Detailed construction of models for nebulae

In the first method, originally employed by Bowen and Wyse (1939), one compares the ratios of ionic concentrations of various elements, e.g., employing the lines of [NeIII] and [NeIV], or [OII] and [OIII], or [ArIII] and [ArIV], and so forth. That is, one assumes that the degree of ionization depends only on the ionization potential and neglects the detailed deformations of the radiation field.

When this procedure is applied, one finds, for example, that the [NeIV] and [NeV] lines must be produced in much hotter regions than the [OIII] lines; otherwise one finds a strange dependence of chemical composition on excitation.

Seaton (1968) pointed out that one should employ a relation of the type

$$\frac{N(\text{HeII}) + N(\text{HeI})}{N(\text{HeI})} = \frac{N(\text{O})}{N(\text{OII}) + N(\text{OIII})}$$

since the ionization of oxygen is influenced by that of helium. That is, the second ionization potential of helium falls near the third ionization potential of oxygen, so unless HeII is present, there should not be sufficient radiation to ionize OIII to OIV.

If we employ this relation for the nebulae discussed in the spectrophotometry series and plot the oxygen/hydrogen abundance ratio against the excitation class of the nebula (Aller 1956), there is a large scatter but a very distinct relation between the maximum O/H ratio and the nebular excitation, in the sense that only high-excitation nebulae have large O/H ratios. That is to say, the O/H ratio depends on the excitation class. In these calculations we have assumed that the electron temperature is that given by the usual [OIII] line ratios. One suspects that the adopted model is oversimplified, and I have accepted the larger values of the O/H ratio as being more meaningful.

Of course there probably exists a large variation in the elemental abundance ratios, as indicated for example by the work of Kaler (1970). One is, however, suspicious of a dependence on excitation class. Clearly, one must employ models with appropriate temperature and density variations, as Peimbert and Costero have done for the Orion nebula.

By using the data published in the nebular photometry series, I find for helium

$$\text{Log } N(\text{He}) = A(\text{He}) = 11.09$$

with a spread of about 0.1. This value is deduced from the $\lambda 4686$ line of ionized helium and the $\lambda 4471$ and $\lambda 4026$ lines of HeI, interpreted with the aid of the theory developed by Robbins (1968).

The CII $\lambda 4267$ doublet is observed in a large number of nebulae. If we assume that this line is produced by recombination only, we may deduce the $(\text{C}^{++})/N(\text{H}^{+})$ ratio from the expression

$$\frac{(\text{C}^{++})}{(\text{H}^{+})} = 0.0060 T^{0.256} \frac{I(4267)}{I(4861)}, \quad 6300^{\circ}\text{K} < T_e < 20,000^{\circ}\text{K}$$

derived from the calculations by Bednarek and Clarke (1971). For $A(C) = 8.7$, $I(4267) \lesssim 0.8$. Indeed, since the $\lambda 4267$ line appears to be stronger than this in a number of nebulae, it must, as pointed out by Kaler (1971), be excited by line emission rather than by pure recombination.

There are a number of nebulae, among them NGC 7009, where the line is considerably weaker, and here it may actually be excited by recombination. For the time being, we adopt $A(C) = 8.7$ with the understanding that this is the roughest kind of guess rather than a determination.

The nitrogen abundance is difficult to estimate. The NIII lines cannot be used since they are excited by the Bowen fluorescent mechanism, and the NII lines are weak. A theory similar to that developed for CII might be employed, but here again we might be dealing with excitation by radiation from the central star. One can employ the ionization curve method or, what amounts to very nearly the same thing, assume $N(N+)/N(N) = N(O+)/N(O)$. The objection to this procedure is that on the photographs obtained with the best definition, filaments observed in [NII] tend to be "harder" in appearance than those observed in [OII]. If we apply this simplified procedure, restricting it to the lower excitation objects or to objects that show strong [NII] or [NI] lines even though they may show numerous high-excitation lines, we obtain

$$A(N) = 8.12 \pm 0.12;$$

but there is a big spread among the nebulae. For a single nebula, the dispersion $\sigma = 0.37$.

To estimate the oxygen abundance, I have favored the higher excitation objects, where the temperature derived from the [OIII] line ratios probably agrees more closely with that from the hydrogen spectrum. The average value is thus found to be

$$A(O) = 8.85 \pm 0.15.$$

The ionization pattern of neon probably mimics that of oxygen, whether one draws an ionization curve or employs Seaton's argument. Thus I compare neon and oxygen directly to find $A(Ne) = A(O) - 0.63$. Hence,

$$A(\text{Ne}) = 8.2 \pm 0.1.$$

I would be quite willing to agree with Kaler that planetaries probably show a large range in chemical composition, although these approximate methods probably do not give good estimates for the heavier elements in any one nebula.

For fluorine, sodium, and others, I still recommend, as working estimates, the figures given at the Tatranska Lomnica Symposium (Aller and Czyzak 1968):

$$A(\text{F}) = 4.9 \quad A(\text{S}) = 7.9 \quad A(\text{Ar}) = 7.0 \quad A(\text{Ca}) = 6.4$$

$$A(\text{Na}) = 6.6 \quad A(\text{Cl}) = 6.9 \quad A(\text{K}) = 5.7 .$$

All these approximations suffer from the fact that no proper account is taken of the modification of the radiation field by the nebular gases and of the consequent change of ionization with distance from the central star. One must construct a model for the nebula, in which the transfer equation and the equations of statistical equilibrium are solved throughout the nebular shell. At each point, then, the electron temperature and radiation field are obtained.

Such calculations have been undertaken by Williams (1968), by Flower (1968, 1969) and by Harrington (1969). It is, however, necessary to consider the inhomogeneities. A refined treatment in which account is also taken of the rarer elements, fluorine, sodium, sulfur, chlorine, argon, and others, is being developed by Mrs. Buerger at Ohio State University and will be applied to a number of nebulae.

ACKNOWLEDGMENT

This program was supported by the National Science Foundation Grant No. GP23, 460.

REFERENCES

- Aller, L.H. 1954, *Ap. J.*, 120, 401.
- Aller, L.H. 1956, *Gaseous Nebulae*, (London: Chapman & Hall), 66.
- Aller, L.H., and Czyzak, S.J. 1968, *Planetary Nebulae, I.A.U. Symposium 34*, eds. D. Osterbrock and C.R. O'Dell (Dordrecht, Holland: Reidel Publishing Co.), 209.
- Bednarck, T.A. and Clarke, W. 1971 in press.
- Bowen, I.S. and Wyse, A.B. 1939, *Lick Obs. Bull.*, 19, 1.
- Flower, D.R. 1968, *Planetary Nebulae, I.A.U. Symposium 34*, eds. D. Osterbrock and C.R. O'Dell (Dordrecht, Holland: Reidel Publishing Co.), 205.
- Flower, D.R. 1969, *M.N.R.A.S.*, 146, 171, 243.
- Ford, K. and Rubin, V. 1971 in press.
- Harrington, J.P. 1969, *Ap. J.*, 156, 903.
- Hebb, M.H. and Menzel, D.H. 1940, *Ap. J.*, 92, 408.
- Kaler, J.B. 1970, *Ap. J.*, 160, 887.
- Kaler, J.B. 1971 in press.
- Menzel, D.H. and Aller, L.H. 1945, *Ap. J.*, 102, 239.
- Miller, J.S. 1971, *Ap. J. Letters* in press.
- Mills, B.Y. and Shaver, P. 1967, *Australian Journal Physics*, 21, 95.
- Peimbert, M. and Costero, R. 1969, *Boletin No. 31 Obs. Tonantzintla, Tacubaya (Mexico)*.
- Robbins, R.R. 1968, *Ap. J.*, 151, 497.
- Seaton, M.J. 1968, *M.N.R.A.S.*, 139, 129.
- Walker, M.F. and Kron, G.E. 1971, quoted in *Planetary Nebulae*, by L.H. Aller (Cambridge, Mass.: Sky Publishing Corp.), Chap. 5.
- Williams, R.E. 1968, *Planetary Nebulae, I.A.U. Symposium 34*, eds. D. Osterbrock and C.R. O'Dell (Dordrecht, Holland: Reidel Publishing Co.), 190.

RADIO RECOMBINATION LINES

Leo Goldberg

Harvard College Observatory

J. P. Wild (1952) pointed out that transitions between levels of high quantum number in hydrogen would occur at radio frequencies, although he assumed they would overlap to form a continuum and would not therefore be observed as lines. In the solar flash spectrum, for example, Stark broadening at chromospheric densities terminates the Balmer series at about $n = 30$. In H II regions, however, where the density is about 10^4 cm^{-3} , Stark broadening is relatively insignificant for $n \lesssim 200$, and the line shapes are almost entirely determined by Doppler broadening.

A few years later, Kardashev (1959) calculated the theoretical intensities of hydrogen recombination lines with $\Delta n = 1$ and predicted that they ought to be observable in H II regions. Kardashev used a simple equation expressing the ratio of the central line temperature to the brightness temperature of the free-free continuum as a function of electron temperature and line frequency:

$$\frac{T_L}{T_C} = 6.5 \times 10^{-6} \frac{\nu}{T^{\frac{3}{2}}} . \quad (1)$$

For $T = 10,000^\circ\text{K}$, this expression predicts intensity ratios varying from 1% at 1500 MHz to 20% at 30,000 MHz. Kardashev also suggested that similar recombination lines of helium might be observed, but displaced toward higher frequencies by 123 km/sec as required by the slight difference in Rydberg constants.

In 1964, Kardashev's prediction was confirmed by observation, first in the USSR (Dravskikh and Dravskikh 1964) and shortly thereafter in the USA (Höglund and Mezger 1965). The first lines detected corresponded to transitions with $\Delta n = 1$. Such transitions from $n + 1$

to n are called $n\alpha$ lines, and by analogy with optical series, transitions from $n + 2$, $n + 3$, $n + 4$, $n + 5 \dots$ to the same lower level n are called $n\beta$, $n\gamma$, $n\delta$, $n\epsilon \dots$ lines. $n\alpha$ lines have now been observed in a large number of H II regions over a wide range of frequencies corresponding to principal quantum numbers as small as $n = 56$ and as large as $n = 253$. Transitions with $\Delta n = 2$ or more have also been detected. The corresponding helium lines have also been detected in many of these objects as well as another set of lines, which are almost certainly due to neutral carbon.

The intensities of radio recombination lines depend on the level populations, and therefore the departure coefficients b_n for the high levels are of interest. Since the b_n values must approach unity near the series limit, Kardashev argued that the level populations could be calculated from the Saha-Boltzmann equation. When the Kardashev equation is used for the determination of temperature, however, the values derived from the α -lines tend to be 30-40% smaller than optical determinations, for example from the ratio of forbidden line intensities. On the other hand, the β and higher-order lines yield temperatures more nearly in accord with optical values. Three possible explanations of the discrepancy have been debated among radio astronomers and theorists (Dupree and Goldberg 1970): (1) The assumption of thermodynamic equilibrium (TE) in the calculation of level populations is incorrect. (2) The optical determinations of electron temperature are in error, possibly due to inaccurate cross sections for the collisional excitation of forbidden lines. This explanation implies that the electron temperatures of H II regions are lower than previously assumed, by 30-40%, and also that some unexplained physical process is attenuating the intensities of the higher order lines. (3) The discrepancy is caused by inhomogeneities in the temperature and density of H II regions.

It now seems reasonably certain that the observations can be explained by a combination of departures from TE and density inhomogeneities. In H II regions, it is indeed true that the b_n values of high atomic levels are nearly unity, for example, $b_{100} = 0.9932$ for $T_e = 10^4 \text{K}$, $n_e = 10^4 \text{cm}^{-3}$ (Brocklehurst 1970). However, the most interesting consequence of departures from thermodynamic equilibrium is not the slight reduction in the absolute population of the levels, but the even smaller deviation of the ratio of populations from unity and its effect on the amount of stimulated emission, or negative absorption as I prefer to think of it. In his first paper in the famous series on physical

processes in gaseous nebulae, Professor Menzel (1937) pointed out that in gaseous nebulae, negative absorption reduced the line absorption coefficient not by the factor

$$1 - \frac{B_{mn}}{B_{nm}} \frac{N_m}{N_n} = 1 - e^{h\nu/kT} ,$$

but by

$$1 - \left(\frac{b_m}{b_n} \right) e^{h\nu/kT} ,$$

where B_{mn} and B_{nm} are the Einstein coefficients of negative and positive absorption, respectively, and where m is the upper and n the lower level of the transition. In H II regions, $h\nu$ is always $\ll kT$ throughout the radio frequency spectrum, and therefore the factor may be written

$$1 - \frac{B_{mn}}{B_{nm}} \frac{N_m}{N_n} = - \frac{(b_m - b_n)}{b_n} + \frac{b_m}{b_n} \frac{h\nu}{kT} , \quad (2)$$

$$\approx - \frac{d \ln b_n}{dn} \Delta n + \frac{b_m}{b_n} \frac{h\nu}{kT} .$$

When n is very large, ν is proportional to Δn and hence we can put $\Delta n = 1$ and $\nu = \nu_\alpha$. Before discussing the significance of this expression, I would like to show in Figure 1 how b_n is expected to vary with n , according to theoretical calculations by Brocklehurst (1970). Such calculations for high levels with $n > 40$ were first made by Seaton (1964) to demonstrate the effect of electron collisions on the populations of high levels. The rate at which electron collisions transfer atoms from one level with principal quantum number n to adjacent levels increases as n^4 . For the range of electron densities shown in Figure 1, collisions are unimportant in populating levels with $n < 20$, and the b_n values are accordingly independent of electron density. As n increases, collisions become effective at some value of n which depends on the electron

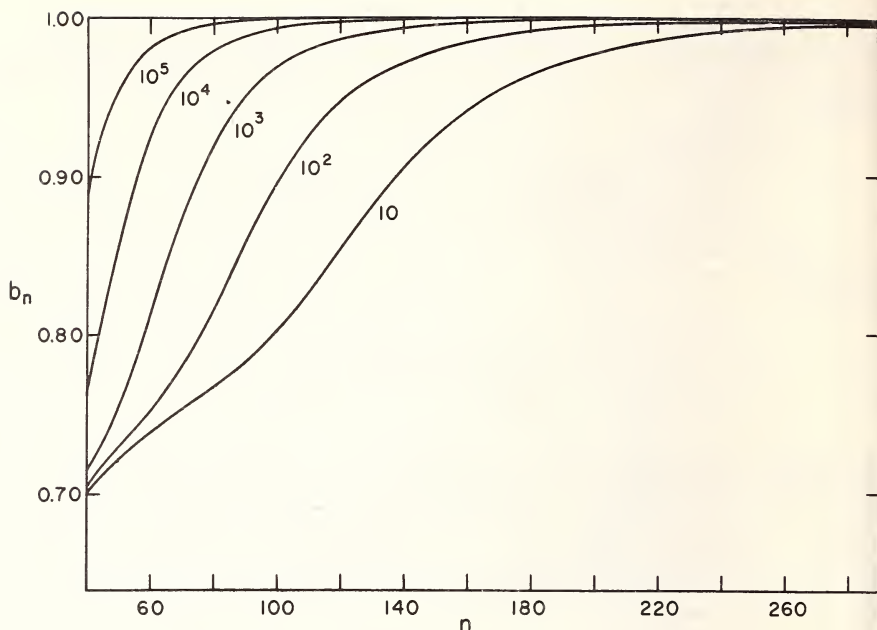


Figure 1. Departure coefficients b_n as a function of principal quantum number n for $T = 10,000^\circ\text{K}$ and $N_e = 10, 10^2, 10^3, 10^4$ and 10^5cm^{-3} .

density, after which the b_n values increase rapidly towards unity.

Seaton (1964) pointed out that the intensity per unit frequency longward of the series limit, in the region where the high series members overlap to form a continuum, is proportional to b_n , and that intensity measurements near the Balmer and Paschen limits in the spectra of gaseous nebulae might give important information on physical processes. Coincidentally, Seaton calculations were published at about the time radio recombination lines were first being observed and so had an entirely different and unintended application. The original calculations have since been superseded a whole series of more accurate ones, the latest of which are by Brocklehurst (1970).

Recently, we have used these calculations in conjunction with measurements of the spectra of Orion A and NGC 7027 obtained by J. L. Greenstein and I. S. Bowen with the 200-inch telescope (Goad, Goldberg, and Greenstein 1971) to derive values of the electron density in the two objects. The points plotted in Figure

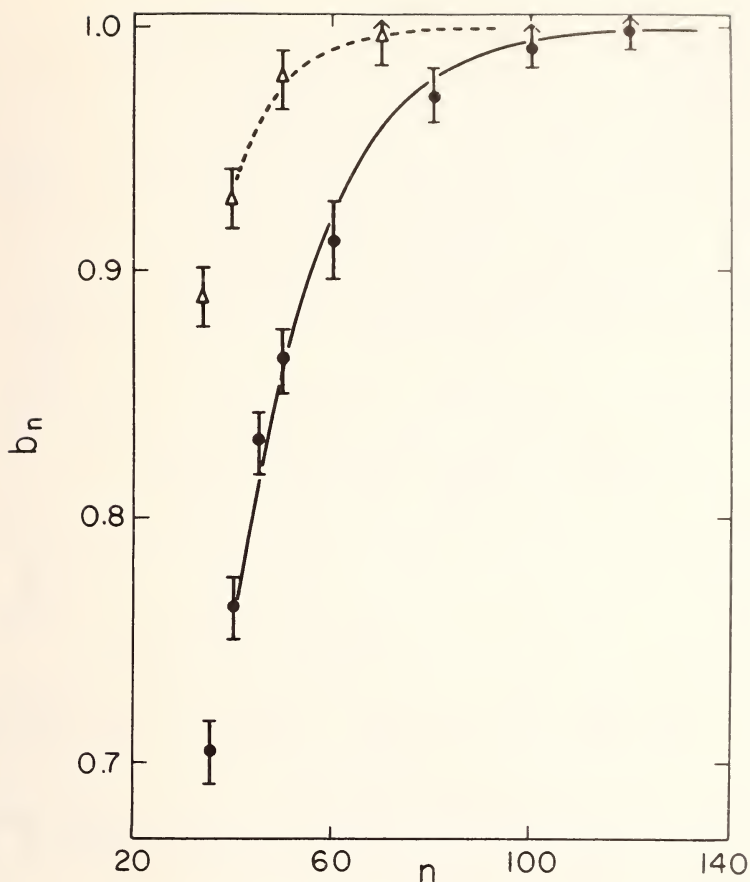


Figure 2. Experimental determination of departure coefficients b_n from intensity measurements near the Balmer limit in the spectra of NGC 7027 (open triangles) and NGC 1976 (Orion A) (filled circles). The curves are theoretical predictions for $T = 10,000^\circ\text{K}$, $N_e = 4 \times 10^5 \text{cm}^{-3}$ (NGC 7027) and for $T = 10,000^\circ\text{K}$, $N_e = 1 \times 10^4 \text{cm}^{-3}$ (NGC 1976). (Goad, Goldberg and Greenstein 1971).

2 are the empirical values of b_n derived from the spectra, whereas the curves are predicted from theory. For Orion A, the best fit is obtained with $T = 10,000^\circ\text{K}$ and $N_e = 1 \times 10^4 \text{cm}^{-3}$ and for NGC 7027, $T = 10,000^\circ\text{K}$ and $N_e = 4 \times 10^5 \text{cm}^{-3}$. The curves are relatively insensitive to temperature. The electron densities are in fairly good agreement with values derived by other methods (Saraph and Seaton 1970; Hjellming and Davies 1970).

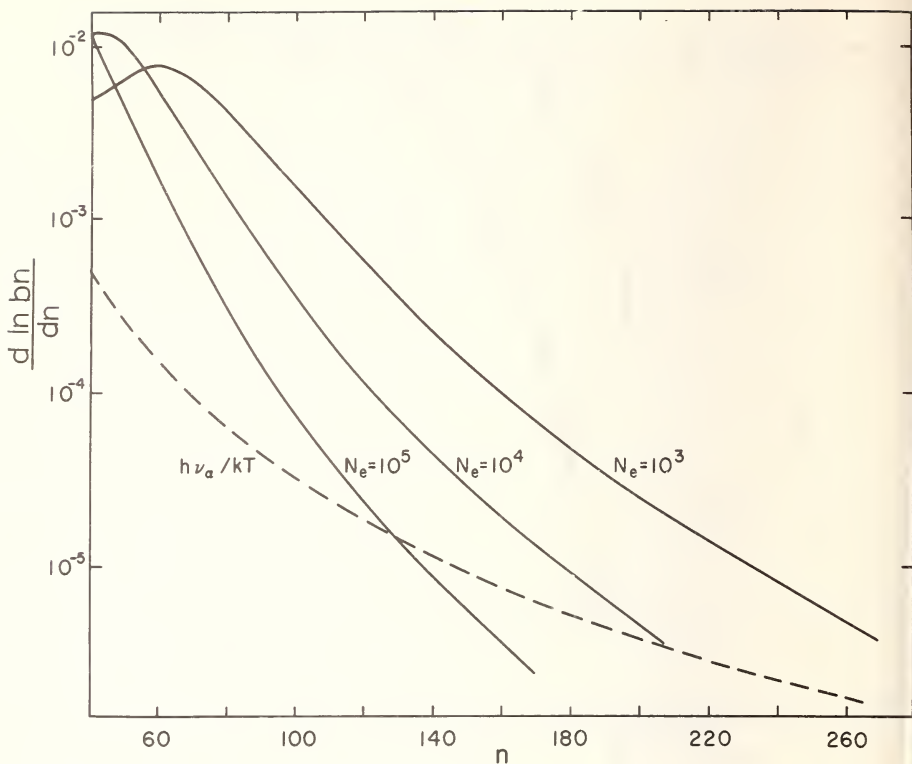


Figure 3. $d \ln b_n / dn$ (solid lines) and $h\nu_\alpha / kT$ (dashed line) as a function of principal quantum number n for $T = 10,000^\circ\text{K}$ and $N_e = 10^3, 10^4$ and 10^5cm^{-3} .

As shown in Figure 3, $d \ln b_n / dn$ is always positive and larger than $h\nu/kT$ over a large range of n . Accordingly, the line absorption coefficient is negative. As n increases, $d \ln b_n / dn$ passes through a maximum at some value of n depending on the electron density and then gradually decreases toward 0. For a given value of N_e , there is always a value of the principal quantum number, say n_0 , at which the $d \ln b_n / dn$ and $h\nu_\alpha / kT$ curves intersect and which increases with decreasing electron density. At this point, the populations of the upper and lower levels of the transition are equal; positive and negative absorption exactly balance, and the gas is optically thin to the line radiation, no matter how great the optical depth in the continuum. In Figure 1, the intersection occurs at $n = 130$ for $N_e = 10^5 \text{cm}^{-3}$, and at $n = 210$ for $N_e =$

10^4 cm^{-3} . To the left of the intersection point, the level populations are inverted and the line intensities may be amplified above their LTE intensities by partial maser action. The degree of amplification depends not only on the electron temperature and density but also on the optical depth in the continuum and therefore on the emission measure, but in the limit of very large optical depth, the intensity is independent of the emission measure (Dupree and Goldberg 1970). To the right of the intersection, the level populations are no longer inverted and approach their equilibrium values as n increases. Since the absorption is now positive, large optical depth in the continuum causes the lines to vanish.

Physically, the effect of inverting the level populations is to decrease the total absorption coefficient in the line plus continuum and thereby to decrease the optical depth and increase the source function. The theory has been well worked out, and extensive and detailed numerical calculations have been performed (Hjellming et al. 1969; Andrews and Hjellming 1969) for α , β , γ , δ , and ϵ lines in the range of quantum numbers from 40 to 220 and for a variety of combinations of temperature, electron density and emission measure. To be successful, the theory has to explain two anomalies that arose earlier in the interpretation of the data by TE theory. The first is that the α -line intensities are generally higher than predicted with optically determined temperatures, and the second is that the intensities of higher order lines were usually found to be weaker than expected relative to α -lines observed at nearly the same frequency. Qualitatively, both discrepancies could be explained by the non-LTE theory because higher order lines are amplified less than α -lines. The difficulty was that the required degree of amplification demanded somewhat higher electron densities and considerably higher emission measures for objects like Orion A than would have been expected from other types of optical and radio measurements. Hjellming and Churchwell (1969) seem to have explained this anomaly, however, by postulating that most of the recombination line radiation originates in small clumps of relatively high density. Since the intensity is weighted by the square of the electron density, the emission comes mostly from the clumps of high N_e and high emission measure. Various methods have been devised for the estimation of mean values of the nebular parameters by comparisons between theory and observation (Hjellming and Churchwell 1969; Goldberg and Cesarsky 1970; Hjellming and Gordon 1971).

TABLE 1
PARAMETERS OF H II REGIONS DERIVED FROM
RADIO RECOMBINATION LINES

Object	T (°K)	N_e (cm ⁻³)	E (pc cm ⁻⁶)
Orion A	10,000	2.5×10^4	1.26×10^7
M17	8,000	3.8×10^4	1.0×10^7
W3 (IC 1795)	11,000	7.7×10^4	4×10^7
W43	5900-8000	---	~6 $\times 10^6$
M16	~7250	---	~5 $\times 10^6$
NGC 2024	~7500	---	<2 $\times 10^6$

From R.M. Hjellming and R.D. Davies, 1970, *Astron. and Ap.*, 5, 53.

Table 1 shows mean values of the three parameters derived by Hjellming and Davies (1970) for a number of H II regions.

HELIUM LINES

Helium recombination lines have now been observed in more than fifteen H II regions, their radial velocities indicating they are formed in the same region as the hydrogen lines. The relative widths of the hydrogen and helium lines are a measure of the electron temperature, and their relative intensities may provide one of the best indicators of the helium abundance in the Galaxy. The ratio of intensities is in fact identical with the ratio of abundances if ionized hydrogen and singly-ionized helium occupy the same volume, since recombination theory predicts that departures from TE in the level populations will be the same for both hydrogen and helium. A recent summary by Churchwell (1970) classifies northern H II regions in three groups according to their ionized helium abundances as shown in Table 2. Optical determinations of ionized helium abundances in Group I objects, when they are available, agree with the radio results, but they also suggest that neutral helium adds 1-3% so that the total abundance ratio is about 10% by number. Theoretical calculations also suggest that the sizes of H⁺ and He⁺ regions are the same if the density is uniform and the ionizing stars are of sufficiently early type. Clumping of the gas, which has been inferred from the interpretation of the hydrogen lines, would increase

TABLE 2

ABUNDANCE RATIO IONIZED HELIUM TO IONIZED HYDROGEN
DERIVED FROM RADIO RECOMBINATION LINES IN H II REGIONS

Source	$N(\text{He}^+)/N(\text{H}^+)$
GROUP I	
IC 1795	0.077 ± 0.013
Orion A	0.083 ± 0.005
RCW 38	0.140 ± 0.030
Carina I	0.088 ± 0.042
RCW 57 I	0.088 ± 0.025
RCW 57 II	0.130 ± 0.034
PKS 1549-54	0.116 ± 0.057
PKS 1618-50	0.099 ± 0.038
NGC 6357	0.083 ± 0.012
W48	0.093 ± 0.037
W417	0.091 ± 0.008
W51	0.085 ± 0.010
GROUP II	
NGC 6334	0.059 ± 0.020
NGC 6357	0.054 ± 0.014
W43	0.057 ± 0.012
W49	0.061 ± 0.012
GROUP III	
W3gr	< 0.019
W6gr	< 0.041
W7gr	< 0.021
NGC 7538	< 0.060
W20R 21	< 0.111
NGC 2024	< 0.02

From E. Churchill, 1970, Thesis, University of Indiana.

the proportion of neutral helium, and therefore 10% is considered to be a lower limit. The ionizing stars believed to be associated with most of the Group II objects are very hot, and therefore it is conjectured that the Group II objects may exhibit an unusually high degree of clumping.

Among the Group III objects, NGC 2024 is known to

be a low excitation object. Recently, the helium lines 85α and 109α have been detected by Cesarsky (1971) who finds an abundance ratio to hydrogen of 0.017 - 0.020, which is within the upper limit given by Churchwell. Of the remaining objects, both DR 21 and NGC 7538 may have considerable He^{++} , but the small lower limits shown by the three galactic center sources have not been explained and may imply a real deficiency in the helium abundance toward the galactic center.

CARBON LINES

In addition to the hydrogen and helium lines, recombination lines of an element of higher atomic weight have been detected in seven H II regions at several frequencies from 1425 MHz to 10,527 MHz. There are three reasons why the element can probably be identified as carbon in a region in which the hydrogen is predominantly neutral:

(1) If the line is assumed to be carbon, the radial velocity frequently differs from that of the companion hydrogen line but is in much closer agreement with available measurements of the 21-cm absorption line.

(2) Carbon is the most abundant element with an ionization potential less than that of hydrogen.

(3) The central intensity of the carbon line in NGC 2024 is stronger relative to hydrogen than in any other H II region. Last year we observed the hydrogen 166α line with unusually high spectral resolution (Ball et al. 1970) and found a narrow component superposed on the profile but displaced from the line center by +5.0 km/sec, which agrees with the relative displacement of the carbon line to well within the experimental error. In other words, the separation of this line component from the carbon line is exactly the amount expected from the difference in Rydberg constants.

Recently, a similar component of the hydrogen line has been observed at three other frequencies in the same object, by Chaisson (1971) at 8 GHz (94α) and by Cesarsky (1971) at 10 GHz (85α) and 3.2 GHz (137α). The observations are summarized in Table 3. The radial velocities derived for both the hydrogen and carbon lines at the four frequencies are in good agreement. If we assume that the carbon is fully ionized and that its abundance relative to hydrogen is 4×10^{-4} , we can infer the fractional ionization of hydrogen in the H II region. The derived value of 2×10^{-4} is in satisfactory agreement with theoretical calculations on the

TABLE 3
C (H I), H (H I) AND H (H II)
LINE PARAMETERS IN NGC 2024

Line	T_L	V_{LSR} (km/sec)	$n(H+)/n(C+)$
H II 85 α	0.70 \pm 0.01	5.6 \pm 1	
H I 85 α	0.03 \pm 0.01	9.5 \pm 1	0.3 \pm 0.25
C I 85 α	0.11 \pm 0.01	10.0 \pm 1	
H II 94 α	0.42 \pm 0.01	5.0 \pm 0.2	
H I 94 α	0.024 \pm 0.01	9.1 \pm 1.5	0.8 \pm 0.6
C I 94 α	0.049 \pm 0.01	9.3 \pm 0.7	
H II 109 α	0.67 \pm 0.01	5.5 \pm 1	
H I 109 α	< 0.04	--	
C I 109 α	0.11 \pm 0.02	10.4 \pm 1	
H II 137 α	0.39 \pm 0.05	5.1 \pm 1	
H I 137 α	0.07 \pm 0.05	9.4 \pm 3	0.56 \pm 0.5
C I 137 α	0.18 \pm 0.05	10.3 \pm 0.7	
H II 157 α	0.16 \pm 0.03	3.2 \pm 1	
H I 157 α	0.075 \pm 0.04	8.2 \pm 1	0.68 \pm 0.5
C I 157 α	0.168 \pm 0.05	8.8 \pm 3	

Sources are given in the text.

ionization of H I clouds by low energy cosmic rays (Field et al. 1969).

It seems highly probable that the carbon lines are formed in cool, dense clouds or condensations in which the hydrogen is mostly neutral. The clouds also seem to be close to or embedded in H II regions. For example, no lines have been observed in non-thermal sources. But the exact physical parameters of the clouds are still unknown and the subject is controversial. The one thing that seems certain is that the lines are not formed in TE, because they appear in emission even when the brightness temperature of the background H II continuum is as high as several thousand degrees, despite the fact that the temperature of the line forming region is probably less than 100°K. Following a suggestion by Zuckerman and Palmer (1968), Mezger, Churchwell and Hjellming (Churchwell 1970) have proposed that the lines are formed in dense, cold condensations, which they identify with prestellar objects in

which $T_e = 12^\circ\text{K}$ and $n_H \sim 10^6 \text{ cm}^{-3}$. The high density is needed to keep the hydrogen neutral against the ionizing radiation field. In TE, the optical depths at the line center are \gg unity (on the order of 10^3) and would produce strongly saturated absorption lines. If TE is not assumed, the optical depth in the line may be expressed as $\tau = b_n \beta \tau_L^*$ (Goldberg 1968) where τ_L^* is the optical depth the line would have in TE and

$$b_n \beta = b_m \left(1 - \frac{kT_e}{h\nu_\alpha} \frac{d \ln b_n}{dn} \right) . \quad (3)$$

In the Mezger-Churchwell-Hjellming model, $b_n \beta$ must take on small positive values, in order to reduce the line absorption coefficient and thereby increase the source function so that the lines can appear in emission against the continuum of the background H II region.

Churchwell (1970) has shown that in condensations dense enough to maintain neutral hydrogen, the carbon will nevertheless be completely singly-ionized, but a more detailed treatment by Werner (1970) of the absorbing effects of dust shows that the carbon will remain neutral for hydrogen densities greater than about 10^3 cm^{-3} . However, the line might still be emitted from the outer periphery of the condensation.

Our own explanation of the carbon line (Dupree and Goldberg 1969) is based on the following argument. Strong 21-cm absorption is frequently observed against the background continuum of H II regions, and agreement in radial velocity and line width suggests that the carbon line is formed in the same region as the 21-cm line. Neutral hydrogen densities derived by Clark (1965) from Orion A observations of the 21-cm line are on the order of 100 cm^{-3} , which would correspond to an electron density of about 0.1 cm^{-3} at most. At such densities, level populations should be strongly inverted at quantum numbers of about 100, and only a slight amplification of the background H II continuum, by as little as 0.1%, would be sufficient to account for the observed line intensities. It must be realized however, that the number density is derived from the column density by assuming the cloud is roughly spherical. The true densities could be much greater if the cloud is highly flattened along the line of sight.

Theoretical calculations of departure coefficients

under conditions found in H I regions and high resolution mapping of the emitting sources are needed to clarify the mechanism of the carbon line emission.

REFERENCES

- Andrews, M.H., Hjellming, R.M. 1969, *Ap. Lett.*, 4, 159.
- Ball, J.A., Cesarsky, D., Dupree, A.K., Goldberg, L., and Lilley, A.E. 1970, *Ap. J.*, 162, L25.
- Brocklehurst, M. 1970, *M.N.R.A.S.*, 148, 417.
- Cesarsky, D. 1971, in preparation.
- Chaisson, E. 1971, in preparation.
- Churchwell, E. 1970, Thesis, University of Indiana.
- Clark, B.G. 1965, *Ap. J.*, 142, 1398.
- Dravskikh, A.F. and Dravskikh, Z.V. 1964, *Astron. Tsirk.*, 282, 2.
- Dupree, A.K. and Goldberg, L. 1969, *Ap. J.*, 158, L49.
- Dupree, A.K. and Goldberg, L. 1970, *Ann. Rev. Astron. and Ap.*, 8, 231.
- Field, G., Goldsmith, D.W. and Habing, H.J. 1969, *Ap. J.*, 155, L49.
- Goad, L., Goldberg, L. and Greenstein, J.L. 1971, paper presented at 134th Meeting Amer. Astr. Soc., Baton Rouge, La.
- Goldberg, L. 1968, *Interstellar Ionized Hydrogen*, ed. Y. Terzian (New York: W.A. Benjamin, Inc.).
- Goldberg, L. and Cesarsky, D. 1970, *Ap. Lett.*, 6, 93.
- Hjellming, R.M., Andrews, M.H. and Sejnowski, T.J. 1969, *Ap. Lett.*, 3, 111.
- Hjellming, R.M. and Churchwell, E. 1969, *Ap. Lett.*, 4, 165.
- Hjellming, R.M. and Davies, R.D. 1970, *Astron. and Ap.*, 5, 53.
- Hjellming, R.M. and Gordon, M.A. 1971, *Ap. J.*, 164, 47.
- Höglund, B. and Mezger, P.G. 1965, *Science*, 150, 339.
- Kardashev, N.S. 1959, *Astron. Zh.*, 36, 838.
- Menzel, D.H. 1937, *Ap. J.*, 85, 330.
- Saraph, H.E. and Seaton, M.J. 1970, *M.N.R.A.S.*, 148, 367.
- Seaton, M.J. 1964, *M.N.R.A.S.*, 127, 177.
- Werner, N.W. 1970, *Ap. Lett.*, 6, 81.
- Wild, J.P. 1952, *Ap. J.*, 115, 206.
- Zuckerman, B. and Palmer, P. 1968, *Ap. J.*, 153, L145.

INTERNAL MOTIONS AND KINEMATICS OF
PLANETARY NEBULAE

William Liller

Harvard College Observatory

The earliest astronomical reference to Donald Howard Menzel appears in *Harvard Bulletin* 773, written almost 50 years ago:

"Mr. D. H. Menzel has recently found approximately two thousand nebulae on ninety photographs made at Arequipa, with the 24-inch Bruce telescope...nearly 20,000 nebulae are now recorded...approximately twenty-five per cent have been found at the Harvard Observatory. (signed) H. Shapley, August 1, 1922."*

According to *Harvard Bulletin* 777, five of the new nebulae were in fact planetary nebulae, although actually only three were new. These are listed in the Perek-Kohoutek *Catalogue of Galactic Planetary Nebulae* as 322-2°1, 329-2°2, and 331-1°1. We feel it appropriate to show, in Figure 1, a reproduction of the first planetary discovered by young Mr. Menzel.

In a review article written only four years later, Menzel (1926) brashly attributed "the curious doubled lines" seen in the spectra of many planetary nebulae to the Doppler effect. Because he was the first to do so publicly, it is particularly fitting to review at this time the state of our knowledge of the internal motions and kinematics of planetary nebulae.

At the outset, we stress that 98 per cent of the mass in a planetary nebulae is contained in hydrogen and helium. Thus through collisions, heavier elements

*It should be noted that Professor Menzel frequently wrote popular articles on science (and science fiction) under various pseudonyms such as Don Home, Charles Howard, and Charles Dahama. Possibly, earlier papers exist but it would seem unlikely since neither Professor Menzel nor his secretary for more than 20 years, Miss Beaudoin, could recall such literary offerings.



Figure 1. Mz 1 alias 322-2°1, the first planetary nebula discovered by D. H. Menzel. Pencil drawing made from the photograph that appears in the Perek-Kohoutek Catalogue of Galactic Planetary Nebulae.

must quickly absorb the momentum carried by these two constituents and assume a velocity close to that of the surrounding atoms and ions. Different velocities derived from the radiation of different ions therefore reflect the stratification of these ions within the nebula and the dependence in some way of the velocity on distance from the central star.

Secondly, apparent outward (or inward) angular motion of the nebular edge may result from increased (or decreased) excitation and ionization. In the formula for the radius of the ionization or Strömgren sphere, we find such factors as the temperature and luminosity of the exciting star, and the density and composition of the intervening gas. Thus a nebula that grows steadily in angular extent may in fact be much larger than observed and may be undergoing internal changes that have nothing to do with the gas motions.

Basically, two techniques are available for investigating the kinematical structure of a planetary nebula: spectrography and astrometry. Each will be discussed now in some detail.

At a temperature of $10,000^{\circ}\text{K}$, the root-mean-square velocity of an oxygen atom is 3.2 km/s ; for hydrogen it is 4 times greater. A high resolution optical spectrograph can reach these velocities and resolve lines separated by even smaller amounts. The pioneering work of Campbell and Moore (1918) and the later work of O. C. Wilson (1950) and of Osterbrock and his associates (1966) have fully exploited the attainable photographic resolution. Increased efficiencies have come through the multi-slit technique used well on planetaries by Wilson (1958) and by G. Münch (1968). Fabry-Perot interferometry makes possible the precise measurement of numerous local velocities from one photographic plate, since wavelength shifts corresponding to around 1 km/s cause detectable distortions in the circular pattern produced by constructive interference at different orders. Some of the earliest experiments of Fabry (Fabry and Buisson 1911) used gaseous nebulae for study subjects. More recently Ring and his colleagues (Davies, Ring, and Selby 1964), Vaughan (1967), Courtès (1960), and Picmic (1971) have carried experimentation with interferometers to a high degree of sophistication.

Measurements of the increase in angular size of planetary nebulae have been made successfully by Latypov (1957), Liller (1957), Liller, Welther, and Liller (1966), and Chudovicheva (1964). Probably the best photographic material has been only partly reported (Liller and Liller 1968), and the final results are in preparation. In every instance, the pro-

cedure involved detailed comparison of old and new plates taken with the same instrument. Intervals between plates ranged up to 62 years (Crossley reflector, Lick Observatory) at plate scales as high as 5.0 arc seconds/mm (Mount Wilson 100-inch Cassegrain). The final mean errors attainable amount to a few tenths of an arc second per century, with the results never being larger than ten times this amount. While routine astrometric procedures are usually followed in the reduction, the plates have inherently several unique error sources. Included among these is the "spiky" distribution of energy in planetaries and the happenstance that singly ionized oxygen has a strong pair of lines in the near ultraviolet (3726, 3729 Å), and doubly ionized oxygen has a strong pair of lines in the green (4959, 5007 Å). Differing spectral response, caused by the conversion around 1930 from silver to aluminum for mirror coatings, and the improved emulsion sensitivity in the green, can affect the importance of these radiations and confuse the results. Fortunately, many discrete features such as sharp knots and filaments exist in planetaries, and the green nebular lines so dominate their spectra that they are monochromatic for all practical purposes.

O. C. Wilson's classic work (1950) reveals outward expansions of up to 57 km/s (NGC 2392), but even in this planetary zero velocities occur for quadruply-ionized neon, which is found only in the inner regions of the nebula. In general one finds a good linear correlation between outward velocity and monochromatic image diameter for radiations of differing levels of excitation and ionization, leading us to conclude that on the whole particles move outward with speeds that increase in proportion to distance from the center. The results for hydrogen are somewhat less well determined since these spectral lines are not as sharp as those from heavier ions. Such a phenomenon would be expected since the root-mean-square kinetic velocities of hydrogen atoms are always a sizeable fraction of the expansion velocities. The detailed line-shape studies of Osterbrock and his associates (Osterbrock, Miller, and Weedman 1966; Weedman 1968) reveal that lines of H, He II, [O III], and [N II] are wider than the expected thermal Doppler widths and therefore establish that significant mass motions exist within planetary nebulae. Moreover, these authors find that the distribution of emission with radial velocity has a rather well-defined peak, which suggests that the heavier ions make excellent markers in the general nebular wind.

Multi-slit observations have permitted Wilson (1958) and G. Münch (1968) to derive models for specific

nebulae; Wilson for NGC 7662 and Münch for NGC 6543. The latter nebula appears to consist of two spiral filaments, which are placed like opposing corkscrews emanating along the line of sight from the central star.

To reach nebulae of low surface brightness such as NGC 6853 (the "Dumbbell"), Bohuski, Smith, and Weedman (1970) employed a pressure-scanned Fabry-Perot interferometer tuned to H α and to singly ionized nitrogen at λ 6584. While the width of each of the nitrogen components averaged 14.5 km/s, comparable to the spectrographic results of Osterbrock et al. (1966), Bohuski et al. found the hydrogen line at the center of the nebula to present a broad profile of half width 75 km/s. They conclude that the hydrogen emission is spread throughout much of the nebula while the [N II] emission is restricted to a thin spherical shell.

A similar approach by Carranza, Courtès, and Louise (1968) to NGC 7293 (the "Helix") shows it to have a radial expansion velocity of 37.4 km/s in the light of [N II]. However, they were unable to fit a regular helical pattern to the observations.

The first apparently successful measurement of the increase in angular size of a planetary nebula was by Latypov, who found from astrograph plates (60"/mm plate scale) that the Ring Nebula (NGC 6720) expands at a rate of 0.9 ± 0.1 per century. However, Liller, Welther, and Liller (1966), using Crossley reflector plates (38.7"/mm) taken over a 62 year base line, were unable to confirm this result. More recent results by the Lillers (see Figure 2) give insight into the disagreement. The points plotted here were derived from Mount Wilson plates taken at the Cassegrain focus of the 60-inch and the Newtonian focus of the 100-inch telescopes, most of which show greater filamentary detail than do the Crossley photographs and presumably those taken with the Soviet astrograph. As might be expected, edges present complications in both the measurement and the analysis. The difficulty of measuring a diffuse edge is far greater than locating a diffuse filament, simply because of the asymmetry involved. Furthermore, seeing problems, changes in emulsion contrast, and possibly sensitivity differences can all add uncertainties that are difficult to evaluate. With the high plate scale and good seeing available with the Mount Wilson photographs, we find the new filament measures definitely superior to any other results. Expansion data for NGC 2392, 6818, and 7662 have already been published (Liller and Liller 1968); other results will appear soon in *Publications of the Astronomical Society of the Pacific*. In all, some 22 planetaries

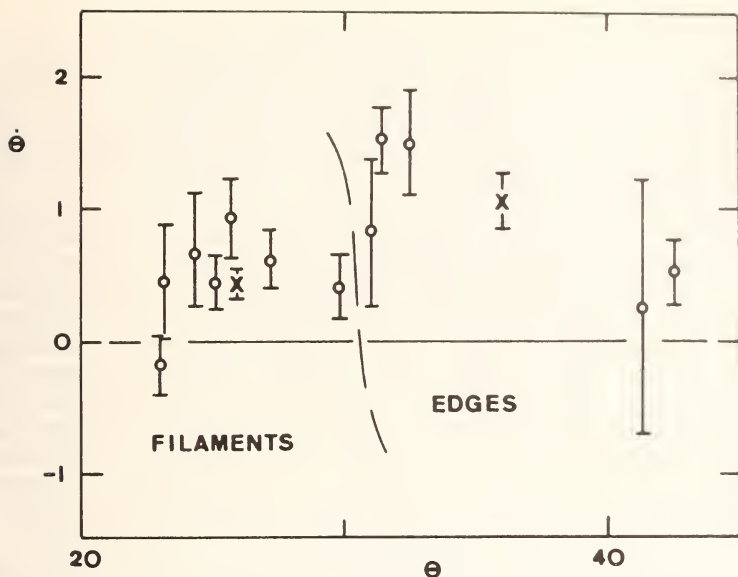


Figure 2. Radial expansion rate in arc seconds per century as a function of radius for NGC 6720 (the Ring Nebula). The error bars are twice the mean error in length; the x's mark the weighted means of filament and edge measures. From Mount Wilson photographs.

have now been studied with Mount Wilson plates by Mrs. Liller and myself.

From a comparison of the spectrographic and astrometric results, one can draw limited conclusions about the distances of planetary nebulae, since for a spherically symmetric object the distance

$$d = \frac{100 V_R}{4.74 \dot{\theta}} \text{ parsecs}$$

where V_R is the outward velocity of the gas and $\dot{\theta}$ is the angular motion perpendicular to the line of sight measured in arc seconds/century. The problem is in identifying the appropriate $\dot{\theta}$ and V_R since both usually have a spread of values, which depend on the distance from the central star. Another possible source of error is an asymmetry, which would cause the gas in one plane of the nebula to move outwards with a velocity different from that of the gas in another plane. Liller, Welther, and Liller (1966) have, nonetheless,

made a general analysis of distance scales and find that for optically thin nebulae, Shklovsky's (1956) distance scale appears most reliable, while for all other planetaries the Minkowski (1965) distance scale is best. These results have recently received confirmation from Heywood Smith Jr. (1971).

Another valuable use for the results of motion studies is to test and evaluate models of planetary nebulae such as those described by Mathews (1966), Turoff (1965), and others. For example, Mathews has pointed out that both angular velocity data and computer models occasionally yield inward motions, especially at the inner edge of a ring. (Note Figure 2!)

Finally, there exist a number of planetaries that present special problems of interest. The conspicuous ansae of NGC 7009 (the "Saturn" nebula) move outward at a velocity close to the value one would predict from a linear extrapolation of the inner region velocities. The "rim" of certain planetaries near the galactic plane moves outwards at a lower velocity than one might predict by linear extrapolation, suggesting that the rim is caused by a piling up of material resulting from the interaction of the expanding nebula with the interstellar medium.

Lastly we mention the comet-like condensations on the inner edge of the Helix nebula, NGC 7293. The three brightest condensations move outwards with a velocity of $0''.88 \pm 0''.44/\text{century}$, and if we take the distance of the nebula to be 100 pc, as the parallax data suggest, this angular velocity corresponds to a linear velocity of only 4.2 ± 2.1 km/s. Recently, Vorontsov-Velyaminov (1968) predicted that the outward velocities of these knots, accelerated by the stellar wind, should be high, perhaps close to 100 km/s. Such a velocity is clearly far too large for consideration.

In the following paper, Professor Menzel will comment further on these interesting features in NGC 7293.

REFERENCES

- Bohuski, T.J., Smith, M.G., and Weedman, D.W. 1970, *Ap. J.*, 162, 27.
- Campbell, W., and Moore, J.H. 1918, *Pub. Lick Obs. Bull.*, 13, 75.
- Carranza, G., Courtès, G. and Louise, R. 1968, in *Planetary Nebulae*, ed. D.E. Osterbrock and C.R. O'Dell (New York: Springer Verlag), p. 249.
- Chudovicheva, O.N. 1964, *Izv. Pulkovo Obs.*, 23, 154.
- Courtès, G. 1960, *Ann. Astrophys.*, 23, 155.
- Davies, L.B., Ring, J. and Selby, M.J. 1964, *M.N.*, 128, 399.
- Fabry, C. and Buisson, H. 1911, *Ap. J.*, 33, 406.
- Latypov, A.A. 1957, *Pub. Astron. Obs. Tashkent* (2), 5, 31.
- Liller, M. and Liller, W. 1968, in *Planetary Nebulae*, ed. D.E. Osterbrock and C.R. O'Dell (New York: Springer Verlag), p. 38.
- Liller, M.H., Welther, B.L. and Liller, W. 1966, *Ap. J.*, 144, 280.
- Liller, W. 1957, *P.A.S.P.*, 69, 511.
- Mathews, W.G. 1966, *Ap. J.*, 143, 173.
- Menzel, D.H. 1926, *P.A.S.P.*, 38, 295.
- Minkowski, R. 1965, *Numerical Data and Functional Relationships in Science and Technology*, ed. H.H. Voigt (Berlin: Springer Verlag) Group VI, 1, 566.
- Münch, G. 1968, in *Planetary Nebulae*, ed. D.E. Osterbrock and C.R. O'Dell (New York: Springer Verlag), p. 259.
- Osterbrock, D.E., Miller, J.S. and Weedman, D.W. 1966, *Ap. J.*, 145, 697.
- Pičmiš, P. 1971, private communication.
- Shklovsky, I.S. 1956, *A. J.* (U.S.S.R.), 33, 222, 315.
- Smith, Haywood, Jr. 1971, *Astron. J.*, 76, 193.
- Turoff, M. 1965, *A Computer Model for Planetary Nebulae* (Ph. D. Thesis, Brandeis University).
- Vaughan, A.H., Jr. 1967, *Ann. Rev. of Astr. and Ap.*, 5, 139.
- Vorontsov-Velyaminov, B.A. 1968, in *Planetary Nebulae*, ed. D.E. Osterbrock and C.R. O'Dell (New York: Springer Verlag), p. 256.
- Weedman, D.W. 1968, *Ap. J.*, 153, 49.
- Wilson, O.C. 1950, *Ap. J.*, 111, 279.
- Wilson, O.C. 1958, *Rev. Mod. Phys.*, 30, 1025.

FILAMENTARY STRUCTURE OF PLANETARY NEBULAE

Donald H. Menzel

Harvard College Observatory

The largest and presumably the nearest of all planetary nebulae is NGC 7293, often referred to as the Helical Nebula in Aquarius. Various determinations have been made of its distance. I shall adopt the value of 60 parsecs as representative. The observed angular radius of the outer ring, 400", thus leads to a value of 24,000 Astronomical Units or 3.6×10^{17} cm for the true radius.

A remarkable feature of this nebula (see Figure 1), first discovered by Walter Baade, is the filamentary structure of the inner portion (see *Sky and Telescope*, 13, 302, 1954). These filaments are cometary in appearance, each with a well-defined "head" and with a "tail" stretching radially away from the nuclear star.

B. A. Vorontsov-Velyaminov (1967) and G. A. Gurzadian (1967) have both briefly discussed this filamentary structure. They have also noted the existence of condensations or "clots" on the inner end of the radial filament. Gurzadian points out a possible analogy between the nebular structure and the interaction of the solar wind with the heads of comets.

In most models of planetary nebulae, the gaseous envelope is regarded as a uniform, continuous shell, presumably ejected from the star by some type of nova action. The shell, expanding indefinitely, eventually dissipates into space and vanishes.

Alternatively, in this paper I plan to investigate various properties of a model planetary structure composed of some large number, N , of orbiting structures resembling comets, whose tails are responsible for the filamentary structure. The orbits, I shall suppose, are elliptical. The periods would be of the order 4×10^6 years. I further assume that this shell probably originated long ago, perhaps as condensations from nova ejecta. Alternatively, the structures may simply be debris left over from the original contraction of a large mass of gas into a star.



Figure 1. NGC 7293 planetary nebula in Aquarius. Photographed in red light; 200-inch photograph. (Hale Observatories)

I am fully aware that C. T. Daub (1963), G. B. Field (1965), and S. Sofia (1966) have concluded that such condensations cannot form. Since the observations speak for themselves, I feel that some special conditions, not envisaged in the assumed initial conditions, are able to produce condensations. Magnetic fields may well be the missing link in the evolutionary process.

Certain data relating to the nebula and nucleus are relevant. For the hotter range of nuclear stars, application of the Zanstra-Menzel theory gives a minimum surface temperature for the nuclear star. Most of the stellar radiation lies in the far ultraviolet, where it can ionize hydrogen atoms. Of this energy, one-fourth can appear as radiation in the visible spectral range. The remainder goes to produce Lyman α . The total energy of the nebula, in the visible region, therefore will be

$$B_n = A\sigma \frac{T^4}{4} \quad (1)$$

where T is the surface temperature and A the area of the star. The apparent brightness of the nuclear star will be, by Planck's law,

$$B_s = A \frac{2\pi h}{c^2} \int \frac{\nu^3 d\nu}{e^{h\nu/kT} - 1} \quad (2)$$

$$\sim A \frac{2\pi kT}{c^2} \int \nu^2 d\nu = A 2\pi c kT \left(\frac{1}{\lambda_1^3} - \frac{1}{\lambda_2^3} \right),$$

where λ_1 and λ_2 represent the wavelengths of the short- and long-wave limits of plate sensitivity. The approximation is valid because $h\nu/kT \ll 1$ for the photo-visual region. Let m_n and m_s be the observed apparent magnitude of nebula and star. Then the ratio of brightnesses

$$B_n/B_s = (2.512)^{m_s - m_n}. \quad (3)$$

Let

$$F = \left(\frac{1}{\lambda_1^3} - \frac{1}{\lambda_2^3} \right) = 1.5 \times 10^{13} \quad (4)$$

for $\lambda_1 = 3500\text{\AA}$ and $\lambda_2 = 5000\text{\AA}$.

The foregoing equations thus lead to

$$\begin{aligned} T^3 &= \frac{8\pi k c F}{3\sigma} (2.512)^{m_s - m_n} \\ &= 9.2 \times 10^{12} (2.512)^{m_s - m_n}. \end{aligned} \quad (5)$$

For NGC 7293, $m_n = 7.5$ and $m_s = 13.5$. Hence we obtain, as the stellar temperature, the value of

$$T = 6 \times 10^4 \text{ } ^\circ\text{K} . \quad (6)$$

This figure is a minimum; it will be greater if the nebula does not completely absorb the radiation beyond the Lyman limit.

The absolute magnitude of the nuclear star is about 9.6. Elementary calculations show that the nuclear star is very small, perhaps even smaller than the Earth. This means that despite the star's high surface temperature, the effective temperature of the surrounding nebula cannot be raised by direct absorption of its radiation. The effective black-body temperature that a star can produce varies inversely as the square root of the distance from its center. Hence the effective T of the Sun at a distance of 1 A.U. is about 425°K . At a distance of only 1000 A.U., a small fraction of the diameter attributed to NGC 7293, the effective temperature would be only 13°K , a value far too small to melt or vaporize the icy structure of an ordinary comet. For the nuclear star of NGC 7293, this figure would increase by perhaps a factor of 10. But again, it appears that the comet-like structures cannot be ordinary comets of the solar-system variety.

To estimate the density of NGC 7293, let us compare it with NGC 7662, for which the data are well known (Table 1). The quantity $\Delta m/\text{sq min}$ represents the quantity applied to m_n to give the surface brightness H_n , in magnitudes per square minute of arc:

$$\Delta m/\text{sq min} = 2.5 \log \pi + 5 \log A''/60 \quad (7)$$

and

$$H_n = m_n + \Delta m/\text{sq min} . \quad (8)$$

TABLE 1

NGC	R"	$R \times 10^{-17}$ cm	dist, pc	m_n	$\Delta m/\text{sq min}$	H_n
7662	8	1.43	1200	8.7	-3.11	5.6
7293	400	3.6	60	7.5	+5.4	12.9

The difference of 7.3 magnitudes in surface brightness between NGC 7662 and NGC 7293 corresponds to a ratio of 832, which agrees well with the value of 600, determined observationally by H. D. Curtis (1918).

Let us determine the electron density of the nebula from equation (13) given by Menzel and Aller (1941):

$$N_e = 1.84 \times 10^4 T^{3/4} \exp(-x_4/2) (2.512)^{-H_\beta/2} (Rb_4)^{1/2} \quad (9)$$

wherein T now represents the electron temperature, H_β the surface brightness of the nebula in the light of the second member of the Balmer series, b_4 the dimensionless factor describing departure of the gas from thermodynamic equilibrium at temperature T (Menzel 1937), and

$$x_4 = h\nu_4/kT = 9.8 \times 10^3/T . \quad (10)$$

From comparison with other nebulae, we may set $b_4 \sim 0.16$ and $T = 10^4$ °K. Also let

$$H_\beta = H_n + \Delta H_\beta . \quad (11)$$

Again, from other nebulae, we may take $\Delta H_\beta = 1.6$, so that $H_\beta = 14.5$. With $R = 3.6 \times 10^{17}$ cm, we thus obtain for the electron density of the nebula, $N_e = 60/\text{cm}^3$.

This figure is based on the assumption that the nebula is a homogeneous sphere. However NGC 7293 is clearly far from homogeneous. It seems to possess an outer shell consisting of two intertwined loops, in addition to the cometary condensations previously discussed. If only a fraction, ϕ , of the spherical volume contains an appreciable amount of matter, we must increase the previously-calculated electron density by a factor of $\phi^{-1/2}$.

I have estimated the apparent magnitude of the typical filament at about 16.5. Since the nebula is about nine magnitudes fainter than the filament, we should need about 4000 such filaments, if all were of the same brightness, to account for the nebular luminosity. Their dimensions on the photograph appear to be about $2'' \times 2'' \times 20''$, corresponding to a volume of some 80 sec^3 . The corresponding volume of the nebula

is about $2.7 \times 10^8 \text{ sec}^3$. The volume of the 4000 filaments would be only 3×10^5 , so that the ratio, ϕ , would be about 1/900. The mean density of the filaments would be about 30 times greater than the mean density previously calculated, or $N_e \sim 1800/\text{cm}^3$. This figure does not appear to be extreme or excessive. It is in line with or even slightly smaller than the mean electron densities for many other brighter planetaries (Menzel and Aller 1941; Liller and Aller 1954).

We have seen that radiation from the central star cannot produce appreciable heating of the nucleus of the filament. One can also show that the heating effect of the hot, tenuous electron gas is likewise negligible. The equilibrium temperature of the radiating surface will be only a few tenths of a degree absolute. How, then, are we to explain the observed filamentary structure of the nebula? Gurzadian has suggested a corpuscular stream analogous to the solar wind, but this factor, too, seems to be quantitatively insufficient.

My estimates lead to the volume of filament about $6 \times 10^{46} \text{ cm}^3$. With 1800 atoms of hydrogen per cm^3 , the total mass comes out to be some $3 \times 10^{26} \text{ g}$, a figure that agrees roughly with the slightly smaller value of $5 \times 10^{25} \text{ g}$ suggested by Vorontsov-Velyaminov, who further argues that the forces forming the radial filament must somehow derive from the nuclear star. He favors the view that the filaments represent matter ejected from the central Wolf-Rayet star. The energy source, in his opinion, lies in the original hot, expanding material.

I tend to favor a somewhat different view. If - as seems not unlikely - the total mass of the nebula greatly exceeds that of the nuclear star, the gravitational collapse of a shell consisting of gas and dust grains would also be approximately radial. The process would probably take place in the manner discussed by Prentice and ter Haar (1971), who consider the interaction of a gas cloud containing dust grains. They show how the dust grains in a fragment might fall toward the center of that fragment. The result would be a number of large condensations.

The inner edge of the luminous ring of NGC 7293 presents a peculiar appearance that has not, to my knowledge, been previously described. Ample evidence exists for the radial filamentary structure. However, the "comet heads" are no longer starlike. They look more like the heads of ordinary comets, with sharply defined, curved, inner edges, sweeping outward into hazy, stubby tails.

Could these peculiar formations, which number into the hundreds, possibly be the progenitors of the sharply defined filaments nearer the center? Might not the "tails" be the result of the well-known "tunneling effect", caused by gravitational focusing of a body falling in toward the center of the planetary? Not all of the tails are precisely radial. Some have considerable inclination with respect to the nuclear star, and the mass of the gravitating body could well be of the order of those of solar planets.

If one assumes that the planetary has a mass about that of the Sun, with 4000 "comets", the individual masses could prove to be 5×10^{29} g. The figures are uncertain and speculative, but they do at least suggest that here we may have a true planetary nebula, a solar system in the making.

In passing one may note that the nebulosity probably does not contain any large quantities of dust, since several external galaxies are clearly visible through it, especially near the outer boundary.

On the hypothesis that NGC 7293 may consist of large numbers of orbiting filamentary objects I have calculated the distribution of intensity from a large number, N , of such bodies randomly distributed between periastron and apastron in elliptical orbits of semi-major axis a and semi-minor axis b .

From the vis viva integral we have the equation defining the radial velocity (dr/dt) and tangential velocity $r(d\phi/dt)$ of an orbiting comet:

$$\left(\frac{dr}{dt}\right)^2 + r^2\left(\frac{d\phi}{dt}\right)^2 = GM\left(\frac{2}{r} - \frac{1}{a}\right), \quad (12)$$

for a body at radius r ; G is the gravitational constant and M the mass of the central star. Kepler's second law prescribes that the areal velocity be constant, so that

$$\frac{1}{2} r^2 \frac{d\phi}{dt} = \frac{\pi ab}{P}, \quad (13)$$

where P is the period. Kepler's third law provides the relation, for elliptical orbits, of

$$P^2 = (2\pi)^2 a^3/GM. \quad (14)$$

Then the radial velocity will be

$$\frac{dr}{dt} = (GM)^{\frac{1}{2}} \left(\frac{2}{r} - \frac{1}{a} - \frac{b^2}{ar^2} \right)^{\frac{1}{2}} . \quad (15)$$

It is more convenient to express r in units of the semi-major axis, a . Also let the ellipticity, η , be

$$\eta = b/a . \quad (16)$$

Then equation (15) becomes:

$$\frac{dr}{dt} = \left(\frac{GM}{a^3} \right)^{\frac{1}{2}} \left(\frac{2}{r} - 1 - \frac{\eta^2}{r^2} \right)^{\frac{1}{2}} . \quad (17)$$

During the interval dt , the body will have moved through the fraction $2 dt/P$ of the half period.

$$\frac{2 dt}{P} = \frac{r dr}{\pi(2r - r^2 - \eta^2)^{\frac{1}{2}}} = p dr , \quad (18)$$

where p is the probability of finding the comet between r and $r + dr$. The factor of two enters because the comet may attain the same radius vector on either an inward or outward portion of the orbit.

Over the orbit, r ranges from r_{\max} to r_{\min} , where

$$r_{\max} = 1 + (1 - \eta^2)^{\frac{1}{2}}, \quad r_{\min} = 1 - (1 - \eta^2)^{\frac{1}{2}} . \quad (19)$$

The probability p becomes infinite for both the extreme values of r . These correspond to the two turn-around points in the radius. The infinity for apastron exceeds that for periastron by the ratio r_{\max}/r_{\min} .

Despite these infinities, the integral of the probability remains finite,

$$\int_{r_{\min}}^{r_{\max}} p \, dr = 1, \quad (20)$$

as required, since the comet must lie somewhere between the two extremes.

Consider N comets distributed randomly with respect to spherical polar coordinates θ and ϕ , but with the radial distribution as defined by equation (18). Then the average number n of comets in the volume element,

$$d\tau = r^2 \sin\theta \, dr \, d\theta \, d\phi, \quad (21)$$

will be

$$n \, d\tau = \frac{Nr^2 \sin\theta \, dr \, d\theta \, d\phi}{4\pi^2 r (2r - r^2 - \eta^2)^{\frac{1}{2}}} \quad (22)$$

whose integral over the ranges of the variables is, as required,

$$\int n \, d\tau = N. \quad (23)$$

We suppose that the brightness of an individual object varies as Cr^{-k} . For convenience in calculation, we adopt the value $k = 4$, usually employed for solar-system comets. The total brightness, B , of the shell follows from the integral

$$B = \int \frac{nC}{r^k} \, d\tau = \frac{NC(3 - \eta^2)}{2\eta^5}. \quad (24)$$

Spherical coordinates are inconvenient for expressing the apparent distribution over the plane of the sky. Cartesian or cylindrical coordinates may be used, with the z-axis directed along the line of sight. We therefore replace the spherical volume element by:

$$d\tau = r^2 \sin\theta \, dr \, d\theta \, d\phi = dx \, dy \, dz = \rho \, d\rho \, d\psi \, dz \quad , \quad (25)$$

for cylindrical coordinates ρ, ψ, z . We must also make the substitution

$$r^2 = x^2 + y^2 + z^2 = \rho^2 + z^2 \quad . \quad (26)$$

As before, the units of length are expressed in terms of a .

The surface brightness H depends on an integration along the z coordinate.

$$H = \frac{\eta^5 B}{\pi^2 (3-\eta^2)} \int \frac{dz}{(\rho^2+z^2)^{(k+1)/2} \left[2(\rho^2+z^2)^{1/2} - (\rho^2+z^2) - \eta^2 \right]^{1/2}} \quad . \quad (27)$$

Since the integrand is an even function of z , we introduce a factor of 2 and integrate over only positive values of z . Let

$$\rho^2 + z^2 = \omega^2 \quad . \quad (28)$$

Then the integral becomes

$$H = \frac{\eta^5 B}{\pi^2 (3-\eta^2)} \int_{\omega_{\min}}^{\omega_{\max}} \frac{d\omega}{\omega^k (\omega^2 - \rho^2)^{1/2} (2\omega - \omega^2 - \eta^2)^{1/2}} \quad (29)$$

with

$$\omega_{\max} = 1 + \sqrt{1 - \eta^2} = \alpha \quad (30)$$

and

$$\omega_{\min} = \left\{ \begin{array}{l} 1 - \sqrt{1 - \eta^2} = \beta \\ \rho \end{array} \right\} \text{whichever is greater.} \quad (31)$$

The quantities α and β are respectively the apastron and periastron distances.

I have not been able to find a general expression for the integral (29). However, a satisfactory approximation can be developed. First of all, factor the radicals in the denominator to obtain

$$(\omega + \rho)(\omega - \rho)(\omega - \beta)(\alpha - \omega), \quad (32)$$

which has two singularities, one at $\omega = \alpha$, the upper limit, and the second at either β or ρ , by (31). This confluence of roots introduces a difficulty, although the integrals for $\rho = 0$ and $\rho \gg \beta$ are easily obtained. To derive an approximate expression, we proceed as follows

$$(\omega - \rho)(\omega - \beta) = \omega^2 - (\rho + \beta)\omega + \beta\rho \quad (33)$$

$$\sim \omega^2 - (\rho + \beta)\omega = \omega \left[\omega - (\rho + \beta) \right]$$

whose singularity at $\rho + \beta$ we now adopt for the lower limit. We may then write the integral (29) in the approximate form:

$$H = \frac{\eta^5 B}{\pi^2 (3 - \eta^2)} \int_{\beta + \rho}^{\alpha} \left[\frac{\omega}{\omega + \rho} \right]^{\frac{1}{2}} \frac{d\omega}{\omega^{k+1} (\alpha - \omega)^{\frac{1}{2}} (\omega - \rho - \beta)^{\frac{1}{2}}}. \quad (34)$$

For the factor in brackets, we adopt a mean value, $F(\rho)$, taken over the range from ρ to α , as follows:

$$F(\rho) = \frac{\int_{\rho}^{\alpha} \left[\frac{\omega}{\omega + \rho} \right]^{\frac{1}{2}} d\omega}{\int_{\rho}^{\alpha} d\omega} =$$

$$\frac{\sqrt{\alpha^2 + \rho\alpha} + \sqrt{2\rho} + \rho \ln[\sqrt{\rho}(\sqrt{2} + 1) / (\sqrt{\alpha + \rho} + \sqrt{\alpha})]}{(\alpha - \rho)}$$

(35)

This is a slowly changing function of ρ . One readily finds, by the standard method of removing indeterminacy, that

$$F(0) = 1, \text{ and } F(\alpha) = 1/\sqrt{2} \quad (36)$$

$$H = \frac{\eta^5 B F(\rho)}{(3 - \eta^2)} \frac{35(2 + \rho)^4 - 120(2 + \rho)^2(\eta^2 + \alpha\rho) + 48(\eta^2 + \alpha\rho)^2}{128(\eta^2 + \alpha\rho)^{\frac{3}{2}}}$$

(37)

From this equation we may calculate the distribution of surface brightness as a function of ρ (see Table 2). The details depend markedly on our choice of η . The smaller the ellipticity, the greater will be the theoretical increase of brightness toward the center of the nebula, marked by the nuclear star.

This increase, however, results from the assumption that the brightness of the individual comets

TABLE 2
RELATIVE SURFACE BRIGHTNESS H OF PLANETARY NEBULAE

η^2	$\rho = 0$	0.2	0.4	0.6	0.8	1.0	1.2	1.4	1.6	1.8	2.0
0	--	36,800	1,830	306	92.8	38.3	21.2	11.4	7.43	5.28	4.00
0.2	65,200	5,040	542	129	61.8	21.3	14.0	7.27	5.02	3.74	2.95
0.4	23,200	1,160	213	64.8	26.9	13.8	9.28	5.53	4.05	3.8	2.63
0.6	2,880	369	95.3	36.0	17.5	10.1	7.62	4.88	3.82	3.17	--
0.8	564	138	51.5	25.2	14.9	10.1	8.56	6.07	5.12	--	--
1.0	128	84.6	51.2	32.5	38.3	--	--	--	--	--	--

varies as r^{-4} . One would expect the orbiting media to become highly ionized toward the central star. The gas would then be expected to radiate in entirely different wavelengths.

It is tempting to suggest that the broad emission bands of Wolf-Rayet stars, many of which comprise planetary nuclei, arise from comets near perihelion passage. The broadening would then result from the high orbital velocities at that position.

One may readily extend the elementary comet-shell model developed in this paper to cover a range of orbits of different semi-major axes and eccentricities. I would not go so far as to argue that the comet shell postulated by Oort is analogous to those in the planetary nebulae. But the postulated radii are not very different.

I wish to acknowledge the help and suggestions generously given by W. Liller and F. L. Whipple.

REFERENCES

- Curtis, H.D. 1918, *Pub. Lick. Obs.*, 13, 55.
Daub, C.T. 1963, *Ap. J.*, 137, 185.
Field, G.B. 1965, *Ap. J.*, 142, 531.
Gurzadian, G.A. 1967, *Planetary Nebulae, I.A.U. Symposium 34*, eds. D. Osterbrock and C.R. O'Dell (Dordrecht, Holland: Reidel Publishing Co.), p. 450.
Liller, W. and Aller, L.H. 1954, *Ap. J.*, 120, 48.
Menzel, D.H. 1937, *Ap. J.*, 85, 330.
Menzel, D.H. and Aller, L.H. 1941, *Ap. J.*, 93, 195.
Prentice, A.J.R. and ter Haar, D. 1971, *M.N.R.A.S.*, 151, 177.
Sofia, S. 1966, *Ap. J.*, 145, 84.
Vorontsov-Velyaminov, B.A. 1967, *Soviet Astronomy A.-J.*, 12, 389.



